The Dissertation Committee for John Michael Napier Cormack certifies that this is the approved version of the following dissertation:

Plane Nonlinear Shear Waves in Relaxing Media

Committee:

Mark F. Hamilton, Supervisor

Michael C. Downer

Michael R. Haberman

Kyle S. Spratt

Preston S. Wilson

Plane Nonlinear Shear Waves in Relaxing Media

by

John Michael Napier Cormack

DISSERTATION

Presented to the Faculty of the Graduate School of

The University of Texas at Austin

in Partial Fulfillment

of the Requirements

for the Degree of

DOCTOR OF PHILOSOPHY

THE UNIVERSITY OF TEXAS AT AUSTIN

August 2019

To my parents.

Acknowledgments

My time at The University of Texas at Austin has been a blast, and would not have been so if it weren't for the many people that I have had the honor and pleasure to know and to work with over the last five years.

First and foremost I have to thank Professor Mark Hamilton for being the best advisor that I could have asked for. His passion for acoustics and dedication to students are unrivaled in my experience.

Thanks is also owed to the other members of my dissertation committee, Drs. Michael Downer, Michael Haberman, Kyle Spratt, and Preston Wilson for their helpful comments on the content of this dissertation, not to mention their guidance over the course of my time here.

I'd like to thank all of the fellow graduate students, former and current, whose time at UT overlapped with mine, but sufficient space does not exist to list them all. Special gratitude is owed to Jay Johnson for being the other half of the Acoustics incoming class of 2014, and to Gabe Venegas and Ben Treweek for sharing with me the experience of preparing for and taking the qualifying exams. Finally, it could only be an egregious understatement to attempt to describe how indebted I am to Katrina Ramirez-Meyers for the years of guidance and support.

While in the Walker Department of Mechanical Engineering and the

Applied Research Laboratories, I had the honor of working on several fun and enlightening projects in addition to my dissertation research, including those with the Austin Student Chapter of the Acoustical Society of America, Profs. Michael Haberman and Carolyn Seepersad, Clint Morris, Thomas Muir, and Charles Tinney. It was also a pleasure to work with Prof. Christophe Schram of the von Karman Institute for Fluid Dynamics during his brief time in Austin.

Lastly, I need to thank my family. My parents, Anna and Alastair, to whom this work is dedicated, first suggested to me that acoustics might be a fun topic to study. My sister Fiona has been a fantastic role model and source of inspiration as we tackled graduate school at the same time.

This work was supported by several fellowships: the Applied Research Laboratories Chester M. McKinney Graduate Fellowship in Acoustics, the John M. Stemmons Endowed Fellowship in Engineering, the Elizabeth L. and Russell F. Hallberg Foundation Graduate Fellowship in Engineering Acoustics, a Graduate School Scholarship, and the Graduate School Continuing Fellowship, each from The University of Texas at Austin.

John M. Cormack

Plane Nonlinear Shear Waves in Relaxing Media

John Michael Napier Cormack, Ph.D.
The University of Texas at Austin, 2019

Supervisor: Mark F. Hamilton

This dissertation investigates plane nonlinear shear wave motion in a material that possesses a single relaxation mechanism. Derivations that employ three common yet separate descriptions of viscoelasticity are followed to arrive at the same mathematical model for a nonlinear and relaxing medium. The model is then used to obtain a single wave equation for linearly polarized particle motion, and two coupled wave equations for elliptically polarized particle motion. The resulting wave equations account for cubic nonlinearity and viscoelasticity in the form of a single relaxation mechanism. Progressive wave solutions are obtained from a Burgers-type evolution equation, thereby illustrating competition between nonlinearity and viscoelasticity in the wave motion. Energy loss due to relaxation is found insufficient to prevent the occurrence of multivalued solutions of the evolution equation when the wave amplitude is sufficiently large, thus indicating that the model is lacking essential physics in those cases. Multivalued solutions are prevented by employing weak shock theory in the obtained analytical solution for a step shock, or by introducing shear viscosity when solving the evolution equation numerically.

A coordinate transformation is employed that allows simulation of waveform evolution up to and beyond the point of waveform overturning, which permits determination of the parameter space in which multivalued solutions exist. The analysis is also applied to nonlinear shear waves in media characterized by attenuation that is proportional to frequency raised to some power. Finally, standing nonlinear shear waves are investigated by developing an augmented Duffing equation that describes the nonlinear response of a shear wave resonator near its lowest resonance. Both linearly and elliptically polarized motions are described with analytical implicit solutions of the augmented Duffing equation.

Table of Contents

List of Figures

Chapter 1

Introduction

Soft elastic materials such as rubber and soft tissue possess small shear moduli, resulting in shear wave speeds on the order of 1 m/s. The small shear moduli of these materials facilitate the generation of shear deformations with large shear strains, potentially of order unity, necessitating the consideration of *nonlinear elastic* effects in the subsequent motion.

At the same time, materials such as rubber and soft tissue have a complex internal structure. For example, soft tissue is composed at the microscale of a dense, irregular mesh of various cells and tissues. Strain energy associated with deformation of these materials contributes to rearrangement of the internal micro-structure, the complex dynamics of which can occur over many time scales. On the macroscale, these processes cumulatively manifest as *viscoelasticity*, for which the material response to deformation or applied stress is rate-dependent and results in energy loss.

This dissertation is a study of the combined effects of nonlinear elasticity and viscoelasticity on the propagation of plane shear waves in soft elastic media. The particular type of viscoelasticity considered is known as stress relaxation, which has the benefit of a simple mathematical representation that

lends itself to analytical treatment. This work borrows heavily from the study of nonlinear acoustic waves in relaxing fluids, for which the mathematics are very similar, the difference being that leading-order nonlinearity is cubic for plane shear waves, whereas it is quadratic for compressional waves. The aim of this dissertation is to both quantitatively and qualitatively describe ways that viscoelasticity, in the form of stress relaxation, affects the motion of plane shear waves of finite-amplitude.

1.1 Background

1.1.1 Shear waves in soft tissue

The principle motivation behind this work is the use of shear waves for material characterization, in particular the mechanical characterization of soft tissue. It is known that the health of soft tissue is correlated with its shear stiffness. For example, cirrhotic liver is stiffer than healthy liver, and a breast tumor is stiffer than the healthy tissue surrounding it. While manual palpation has been used for centuries as a diagnostic tool, in the 1990s a technique known as *shear wave elastography* began to develop in which shear wave propagation in soft tissue, observed using conventional ultrasound imaging techniques, is used to infer the shear stiffness of the tissue in order to identify regions of healthy and unhealthy tissue (see, e.g., the review by Sarvazyan et al. [1]). In practice, shear waves used for elastography may be generated using the acoustic radiation force produced by a high-intensity sound beam [1], or alternatively, characteristics of the noisy ambient shear wave field can be used

to infer the shear modulus of the medium [2].

Attempts have been made recently to exploit the nonlinear shear modulus as a diagnostic metric, a technique known as *nonlinear elastography*. The most common technique used for nonlinear elastography is the measurement of the shear wave speed as a function of the magnitude of pre-stress of a material, and is known as acoustoelastography [3]. Use of acoustoelastography has revealed the nonlinear shear modulus to be a promising identifier of regions of unhealthy tissue, for example in the detection of breast tumors [4].

It is well known that shear waves in soft tissue are subject to viscoelastic effects; see the review by Carstensen and Parker [5]. As of yet, however, tissue models used for nonlinear elastography do not account for the viscoelasticity of the medium. It is therefore of interest to those in the field of nonlinear material characterization of soft solids, such as nonlinear elastography, to understand the interaction of nonlinear and viscoelastic effects in the propagation of shear waves.

1.1.2 Propagation of nonlinear shear waves

While the study of the propagation of acoustic waves of finite amplitude dates back to Euler in 1759 [6], the study of nonlinear shear waves began more recently. Gol'dberg [7] was the first, in 1961, to investigate the nonlinear propagation of elastic waves in an isotropic solid, demonstrating that leading order nonlinear effects in plane shear wave propagation are cubic, compared to the leading order quadratic nonlinearity for compressional waves. Lee-Bapty and

Crighton [8] studied in detail a modified version of the Burgers equation that describes the evolution of progressive plane waves in a medium with purely cubic nonlinearity, and they developed the corresponding weak shock theory (see also Naugolnykh and Ostrovsky [9] for weak shock relations for progressive plane waves subject to cubic nonlinearity). Extensions of the Fubini and Fay solutions to describe the spectral evolution of an initially monochromatic waveform in a medium with cubic nonlinearity were derived by Gusev and Makov [10].

Measurements of nonlinear waveform distortion and shock formation in a plane shear wave were published first by Catheline et al. [11] in 2003. They excited a plane shear wave of 100 Hz and transverse particle velocity amplitude 0.6 m/s in a tissue-mimicking gel phantom with a shear wave speed of 1.6 m/s. The wave thus had a very large acoustic Mach number (ratio of particle velocity amplitude to shear wave speed) of 0.375, and exhibited significant nonlinear distortion, including shock formation. Their measurements, presented in Fig. 1.1, confirmed that nonlinearity in the plane shear wave is purely cubic, as the nonlinearly generated harmonics were only odd multiples of the fundamental. Dispersion was negligible in their phantom. Furthermore, the reported value of the nonlinear shear modulus inferred from their measurement was on the order of kilopascals, the same order of magnitude as the linear shear modulus. In contrast, elastic constants associated with compressive deformations in tissue-like materials are of the same order as those for water, e.g., on the order of gigapascals.

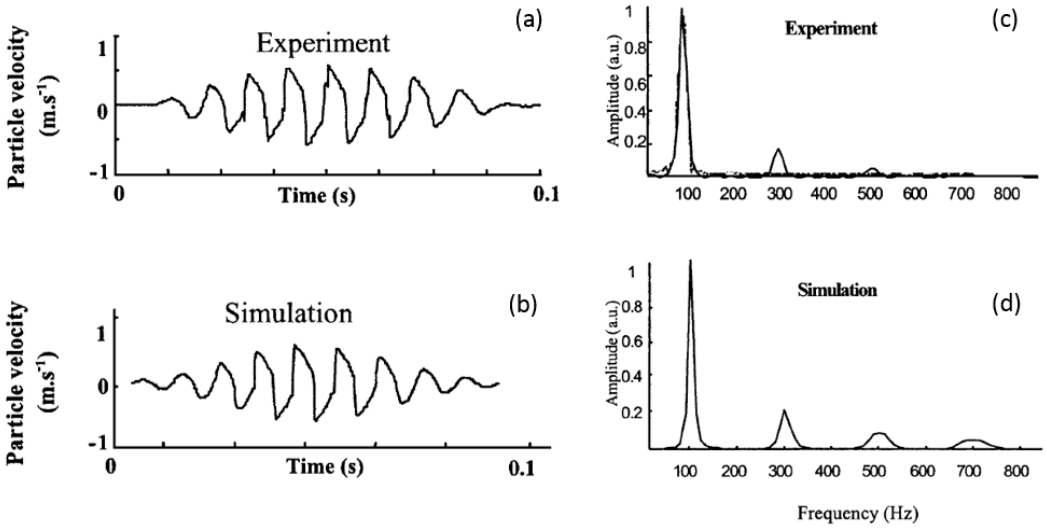

Figure 1.1: (a) Measurement and (b) simulation of a shear waveform containing shocks. Plots (c) and (d) show the harmonic content of the measured and simulated waveforms in (a) and (b), respectively. Figure 1.1 is adapted from Figs. 2 and 3 of Catheline et al. [11].

The vast difference in the order of magnitude of the nonlinear elastic constants for shear deformations compared to compressive deformations motivated Hamilton et al. [12] to develop a formulation of the strain energy density up to fourth order in strain that is specific to incompressible materials such as soft tissue and rubber. Zabolotskaya et al. [13] subsequently used that formulation for the strain energy density to derive an expression for the shear wave coefficient of nonlinearity in an incompressible material. They also considered the effects of viscous absorption (attenuation but no dispersion) and presented solutions for third harmonic generation from a time-harmonic source. Using an acoustoelastographic technique along with the expression of Zabolotskaya et al. for harmonic generation by a plane wave in a viscous medium, Rénier et

al. [14] were able to measure independently the three elastic constants in the strain energy expansion of Hamilton et al. for agar gelatin samples, demonstrating that they are all of the same order of magnitude.

Nonlinear shear waves have also been studied in the context of shear wave beams. Zabolotskaya [15] was the first to obtain a parabolic equation for diffracting elastic waves in an isotropic solid, showing that shear wave beams are subject to quadratic as well as cubic nonlinearity. Spratt et al. [16] investigated the effect that diffraction and quadratic nonlinearity have on the propagation of shear wave beams with various polarizations. Wochner et al. [17] studied the interaction of diffraction and cubic nonlinearity in the propagation of shear wave beams.

1.1.3 Linear and nonlinear waves in relaxing media

Rayleigh [18] was the first to speculate that something like a relaxation process could influence the propagation of a sound wave; in particular he postulated that some energy in the sound wave could go to the rotation of molecules (as opposed to translation), thus contributing to attenuation of the sound wave. Einstein [19] later discussed acoustic propagation in a reacting mixture of two gases, attempting to develop a method for measuring the rate of the chemical reaction. He noted that the frequency of the sound wave would affect the extent to which acoustic energy was used for the chemical reaction, and would therefore affect the attenuation of the acoustic wave and the compressibility of the gas. The classical phenomenological model for

acoustic wave motion in a relaxing fluid was developed by Mandel'shtam and Leontovich [20], a condensed description of which in the English language is given by Landau and Lifshitz [21].

Following their initial pioneering work in nonlinear optics, R. V. Khokhlov and his students in Moscow turned their attention in the early 1960s to nonlinear acoustic wave motion in a relaxing fluid. The first investigation of nonlinear acoustic wave motion in a relaxing fluid was by Polyakova et al. [22], who obtained an analytical solution for propagation of a pressure jump. Soluyan and Khokhlov [23] soon afterwards presented further results for periodic acoustic waves of finite amplitude in a relaxing fluid. The most common modern application of nonlinear acoustic wave propagation in a relaxing fluid is to sonic boom propagation through the atmosphere [24], as air exhibits two distinct relaxation mechanisms in the audible frequency range [25].

The study of shear wave propagation in relaxing media is a recent development. Carstensen and Parker present a good discussion of various linear viscoelastic models for tissue in shear and the motivation behind them [5]. It is common in the biomedical community to represent viscoelastic materials using a configuration of lumped-element springs and dampers, such as the Maxwell and Voigt models [26]. The particular lumped element configuration that accounts for simple stress relaxation is known as the Standard Linear Solid model or Zener model. Asbach et al. [27] found good agreement between measured shear wave speed and attenuation with that predicted by a linear Zener model in both healthy and unhealthy liver tissue in the 20–60 Hz

range. Recently, Yengul et al. [28] reported measurements of a torsional shear wave resonator formed from a tissue-mimicking gel, showing that the material response corresponded to a linear Zener model in the 1–100 Hz range. The only previous study of nonlinear shear waves in a relaxing material appears to be the investigation carried out by Andreev et al. [29] in 2011, who numerically and experimentally studied the nonlinear response of a shear wave resonator formed from plastisol, a type of soft rubber. They found that in the linear limit the plastisol behaved according to a linear Zener model in the 30–300 Hz frequency range, and then compared their measurements to numerical simulations based on a nonlinear Zener material model.

1.2 Outline of the dissertation

This dissertation is divided roughly into three parts: development of the material model for plane shear deformations in a relaxing solid (Chapter 2), analysis of progressive shear waves of finite amplitude in a relaxing medium (Chapters 3 and 4), and the analysis of nonlinear standing shear waves (Chapter 5). In each chapter, analyses are presented that illustrate the competition between nonlinearity and relaxation. Furthermore, in each chapter (except for Chapter 4), applications of the derived solutions for measurement of nonlinear and viscoelastic parameters are presented and discussed.

In Chapter 2 a model for plane shear waves in a nonlinear, relaxing material is developed following three approaches: a method common to biomechanics that employs a nonlinear Zener lumped-element configuration, the

internal variable approach of Mandel'shtam and Leontovich common to linear and nonlinear acoustics, and a three-dimensional tensor description of viscoelasticity. Various solutions and representations of the resulting constitutive relation are presented that illustrate the effects of nonlinearity and viscoelasticity. Nonlinear shear wave equations that account for relaxation are presented for the cases of linearly and elliptically polarized particle motion. Extension of the material model to multirelaxing media and diffracting beams is discussed.

Chapter 3 is concerned with progressive nonlinear shear wave motion in a relaxing material. An evolution equation similar to Lee-Bapty and Crighton's modified Burgers equation is derived and subsequently solved in a number of ways that demonstrate the competition between nonlinearity and relaxation in progressive wave motion. In particular, analytical solutions are obtained for the profile of a steady step shock and for harmonic generation in radiation from a time-harmonic source. The limiting cases of waves with very low or very high source frequency are discussed, with a weak shock theory solution developed in the high-frequency case.

Chapter 4 is an investigation of the mathematical phenomenon of waveform overturning, in which solutions of the evolution equation for progressive plane shear waves may possess three or more values at the same point in time and space. A coordinate transformation that enables numerical simulation of multivalued waveforms, first developed by Hammerton and Crighton to investigate overturning of nonlinear acoustic waves in a relaxing fluid [30, 31], is extended to the case of nonlinear shear waves. The formulation is used

to determine the critical source amplitude above which waveform overturning will occur as a function of the source frequency of an initially sinusoidal shear wave, and also the distance from the source at which overturning first occurs when this critical amplitude is exceeded. Thus the parameter space in which multivalued solutions of the evolution equation derived in Chapter 3 exist is mapped out numerically.

Nonlinear and relaxation effects on standing shear waves are the topic of Chapter 5. The nonlinear shear wave equation developed in Chapter 2 is approximated using a normal mode expansion, thereby reducing the full wave equation to one or more ordinary differential equations that are augmented forms of the Duffing equation. An implicit expression for the amplitude-dependent frequency response of the resonator for excitation near the lowest resonance frequency is obtained from the augmented Duffing equation. Subharmonic generation is considered in the case where the excitation frequency is near the second resonance frequency. When the particle motion of the resonator is elliptically polarized, approximate solutions of two coupled augmented Duffing equations are obtained that illustrate effects due to coupling of the transverse displacement components that arises from nonlinearity.

Derivations that are necessary to include in the dissertation, but would be distracting in the main text, are included in Appendices A and C, which cover weak shock theory and Hammerton and Crighton's coordinate transformation, respectively. An amusing historical anecdote that is relevant to Chapter 4 is detailed in Appendix B. Finally, an analysis of overturning of

nonlinear shear waves that parallels Chapter 4, but for a material that exhibits power-law attenuation, is presented in Appendix D.

Chapter 2

Material Models for Soft, Relaxing Media

Elastic materials such as soft tissue and rubber are made up of many entangled chains of molecules. This complex internal structure results in stretching and subsequent rearranging of the molecules in response to an applied stress or strain, with the response of the material taking place over many different time scales. These materials are called *viscoelastic*; the material response to deformation results in both the loss and storage of elastic energy. Due to the complex internal structure of these materials, it is necessary to develop mathematical models that account for the macroscale effects of the rearrangement and interaction of the molecules that make up the material on the microscale.

Furthermore, soft tissue and rubber possess small shear moduli, resulting in a low shear wave speed, on the order of meters per second. Thus these materials facilitate the generation of shear strains, or equivalently shear waves with acoustic Mach number, on the order of unity. A complete mathemati-

Selected material from this chapter was previously published in J. M. Cormack and M. F. Hamilton, "Plane nonlinear shear waves in relaxing media," *J. Acoust. Soc. Am.* **143**, 1035–1048 (2018), which appears as Ref. [32] in this dissertation. Contributions from JMC include conception and analysis of the material models and equations of motion, and writing of the article.

cal model of such a material that accounts for elastic nonlinearity as well as viscoelasticity is therefore of great interest to those that study the nonlinear elasticity of materials like soft tissue and rubber. In this chapter a mathematical material model for pure shear deformations is developed that accounts for nonlinearity up to third order in strain, and viscoelasticity with simple stress relaxation.

In this work it is assumed that viscoelastic effects are small and on the same order as nonlinear effects. Thus terms in the model equations that represent a combination of nonlinearity and viscoelasticity will be excluded as negligible. Nonlinearity in shear wave motion is described in Sec. 2.1 in the lossless case. Viscoelastic effects are incorporated later on in the derivation in Sec. 2.2, where stress relaxation is modeled using three commonly used approaches. A lumped-element representation, an approach typically used in the modeling of soft tissues that is convenient for visualization, is detailed in Sec. 2.2.1. Section 2.2.2 begins with a general stress-strain relation that is augmented with an internal rate-dependent state variable, a procedure common to linear and nonlinear acoustics. These two approaches are valid only in the one-dimensional case of linearly polarized plane shear waves. A three-dimensional material model for elliptically polarized particle motion is developed in Sec. 2.2.3 by determining the appropriate form of a stress relaxation tensor for plane shear wave motion. A discussion and interpretation of the mathematical material model is given in Sec. 2.3. The chapter is concluded in Sec. 2.4 by presenting a nonlinear shear wave equation that is obtained

from the material model and includes cubic nonlinearity and relaxation. In the case of elliptically polarized motion there are two coupled nonlinear wave equations.

2.1 Nonlinearity

The strain energy density in an isotropic solid may be expanded to fourth order in particle displacement as [12]

$$\begin{aligned}\mathcal{E} = \mu I_2 + \left(\frac{1}{2}K - \frac{1}{3}\mu\right) I_1^2 + \frac{1}{3}AI_3 + BI_1I_2 + \frac{1}{3}CI_1^3 \\ + EI_1I_3 + FI_1^2I_2 + GI_2^2 + HI_1^4,\end{aligned} \tag{2.1}$$

where μ is the shear modulus, K is the bulk modulus, A, B, C, E, F, G, and H are higher-order elastic constants, and $I_1 = E_{ii}$, $I_2 = E_{ij}E_{ji}$, and $I_3 = E_{ij}E_{jk}E_{ki}$ are invariants of the Lagrangian strain tensor,

$$E_{ij} = \frac{1}{2}\left(\frac{\partial u_i}{\partial x_j} + \frac{\partial u_j}{\partial x_i} + \frac{\partial u_l}{\partial x_i}\frac{\partial u_l}{\partial x_j}\right), \tag{2.2}$$

where u_i is particle displacement in direction x_i[1]. For soft, nearly incompressible elastic media, for example soft tissue, for which $\mu/K = O(10^{-5})$ [1, 11], the strain energy density may instead be expressed as [12]

$$\mathcal{E} = \mu I_2 + \tfrac{1}{3}AI_3 + DI_2^2\,, \tag{2.3}$$

which depends only on the three elastic constants μ, A, and D, which are all of the same order of magnitude in value. The first Piola-Kirchhoff stress tensor

[1]In the definitions of the invariants and Eq. (2.2), and for the remainder of the dissertation, Einstein's index notation is used to describe tensor expressions. Repeated indices represent a summation over the repeated index, e.g., $I_1 = E_{ii} = E_{11} + E_{22} + E_{33}$.

is obtained from the strain energy density using

$$\sigma_{ij} = \frac{\partial \mathcal{E}}{\partial(\partial u_i/\partial x_j)}. \tag{2.4}$$

The particular cases of deformation associated with plane shear waves are illustrated in Fig. 2.1. The particle displacement is confined to the plane perpendicular to the direction of wave propagation, and consists in general of two vector components. When the two components of the particle motion are in phase, particle trajectories in the y-z plane trace out a straight line, and the wave is called *linearly polarized*. On the other hand, when a phase difference exists between the two components of the motion, particle trajectories in the y-z plane are closed loops and the wave is *elliptically polarized*.

For a linearly polarized plane shear wave in which u (with index suppressed) is particle displacement perpendicular to the propagation direction x, the resulting relation for the shear stress σ accounting for nonlinearity at leading order is

$$\sigma = \mu\left[1 + \frac{2}{3}\beta\left(\frac{\partial u}{\partial x}\right)^2\right]\frac{\partial u}{\partial x}\,, \tag{2.5}$$

where β is the coefficient of nonlinearity. The form of β depends on which expansion of the strain energy density is used to describe the medium. For general isotropic solids Eq. (2.1) leads to [17]

$$\beta = \frac{3}{4\mu}\left(K + \frac{4}{3}\mu + A + 2B + 2G\right) - \frac{3}{4\mu}\frac{\left(K + \frac{4}{3}\mu + \frac{1}{2}A + B\right)^2}{K + \frac{1}{3}\mu}, \tag{2.6}$$

whereas for soft elastic media Eq. (2.3) yields [13]

$$\beta = \frac{3}{2}\left(1 + \frac{\frac{1}{2}A + D}{\mu}\right). \tag{2.7}$$

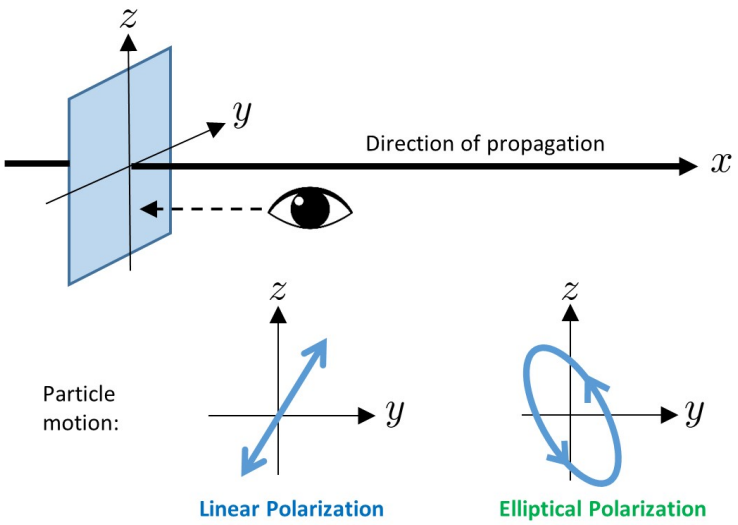

Figure 2.1: Illustration of particle motion in plane shear waves with linear or elliptical polarization.

Elliptically polarized plane shear waves have particle motion with two components that are both perpendicular to the direction of propagation:

$$\mathbf{u} = u_y(x)\mathbf{e}_y + u_z(x)\mathbf{e}_z. \tag{2.8}$$

In this case there are two contributing components of the stress tensor, which are determined from Eq. (2.4) to be

$$\sigma_{yx} = \mu\frac{\partial u_y}{\partial x} + \frac{2}{3}\beta\mu\frac{\partial u_y}{\partial x}\left[\left(\frac{\partial u_y}{\partial x}\right)^2 + \left(\frac{\partial u_z}{\partial x}\right)^2\right], \tag{2.9}$$

$$\sigma_{zx} = \mu\frac{\partial u_z}{\partial x} + \frac{2}{3}\beta\mu\frac{\partial u_z}{\partial x}\left[\left(\frac{\partial u_y}{\partial x}\right)^2 + \left(\frac{\partial u_z}{\partial x}\right)^2\right]. \tag{2.10}$$

Equations (2.9) and (2.10) show clearly the coupling between the two components of the particle motion due to nonlinearity of the deformation.

By considering nonlinearity independently from viscoelasticity, we have been able to determine the form of the stress-strain relation and the coefficient of nonlinearity β in terms of constants in the strain energy density expansion. These expressions for the lossless and nonlinear stress-strain relation are augmented to account for stress relaxation in Sec. 2.2.

2.2 Relaxation

In this section the stress-strain relation is obtained for a relaxing and nonlinear medium three separate ways. The approaches are common to the analysis of wave motion in viscoelastic fluids and solids, and each illustrates the mechanics from a different perspective.

2.2.1 Nonlinear Zener body representation

A method for depicting viscoelastic materials that is convenient for visualization and is common in the field of biomechanics is the use of lumped-element models for one-dimensional shear deformations. Two common configurations are depicted in Fig. 2.2; Fig. 2.2(a) shows a Kelvin-Voigt body, which is used to represent materials that exhibit classical viscous losses [32], and Fig. 2.2(b) depicts the configuration that will be analyzed here and is known as a nonlinear Zener model, or sometimes as the standard solid model. The lower arm in both Figs. 2.2(a) and 2.2(b) accounts for nonlinear elasticity with a modulus that depends on the shear deformation $\epsilon = \partial u/\partial x$ according to $\mu_1(\epsilon) = \mu_0(1 + \frac{2}{3}\beta\epsilon^2)$. The stress across the lower arm is thus $\sigma_1 = \mu_1(\epsilon)\epsilon$,

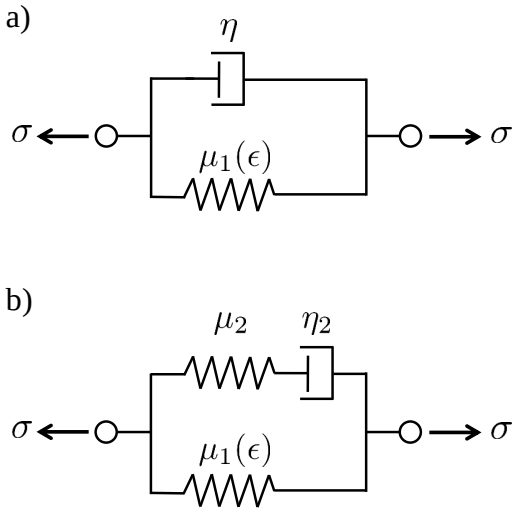

Figure 2.2: Lumped-element representation of a nonlinear elastic medium (a) with classical viscosity (b) with relaxation. The system in (b) is the one analyzed in this work.

which corresponds to the lossless nonlinear constitutive relation presented in Eq. (2.5). Linear elements in the upper arm in Fig. 2.2(b) introduce relaxation via the elastic modulus μ_2 and shear viscosity η_2, such that the stress across the upper arm is $\sigma_2 = \mu_2\epsilon_{2\mu} = \eta_2\dot{\epsilon}_{2\eta}$.

The individual stresses and deformations are related as $\sigma = \sigma_1 + \sigma_2$ and $\epsilon = \epsilon_{2\mu} + \epsilon_{2\eta}$, and therefore the total stress σ is related to the total deformation ϵ according to

$$\frac{\eta_2}{\mu_2}\frac{\partial\sigma}{\partial t} + \sigma = \frac{\eta_2}{\mu_2}\frac{\partial}{\partial t}\left[\mu_1(\epsilon)\epsilon\right] + \mu_1(\epsilon)\epsilon + \eta_2\frac{\partial\epsilon}{\partial t}\,. \tag{2.11}$$

This stress-strain relation may be rearranged into a more standard and convenient notation by introducing the constants $t_r = \eta_2/\mu_2$ and $\mu_\infty = \mu_0 + \mu_2$,

yielding

$$\left(\sigma - \mu_0\epsilon - \frac{2}{3}\beta\mu_0\epsilon^3\right) + t_r\frac{d}{dt}\left(\sigma - \mu_\infty\epsilon - \frac{2}{3}\beta\mu_0\epsilon^3\right) = 0, \tag{2.12}$$

or

$$\left(1 + t_r\frac{d}{dt}\right)\left(\sigma - \mu_0\epsilon - \frac{2}{3}\beta\mu_0\epsilon^3\right) = m\mu_0 t_r\frac{d\epsilon}{dt}, \tag{2.13}$$

where the *relaxation strength* is defined by

$$m = \frac{\mu_2}{\mu_0} = \frac{\mu_\infty - \mu_0}{\mu_0}. \tag{2.14}$$

It is clear from Eq. (2.12) that the response can be separated into two regimes: low frequency or slowly varying motions for which $t_r|d/dt| \ll 1$ and the linear shear modulus is given by μ_0, and high frequency or rapidly varying motions for which $t_r|d/dt| \gg 1$ and the linear shear modulus is given by μ_∞. The subscripts 0 and ∞ thus correspond to the value of the linear shear modulus at zero and infinite frequency respectively. This interpretation is expanded on in Secs. 2.2.2 and 2.3.1–2.3.3.

A medium characterized by classical viscous losses may be modeled using the lumped-element configuration shown in Fig. 2.2(a). To obtain Fig. 2.2(a) from Fig. 2.2(b) the linear stiffness μ_2 is replaced by a rigid link, i.e., the limit $\mu_2 \to \infty$ is taken. Taking that limit in Eq. (2.11) results in the same nonlinear stress-strain relation used by Zabolotskaya et al. [13] in their Sec. V where $\eta = \eta_2$. In Eq. (2.13) the limit $\mu_2 \to \infty$ corresponds to the simultaneous limits $t_r \to 0$ and $mt_r \to \eta/\mu_0$.

2.2.2 Internal state variable formulation

An alternative approach for determining the stress-strain relation in a nonlinear relaxing material is through the expansion of a general state equation. This approach was first presented by Mandel'shtam and Leontovich [20] to describe sound absorption in liquids, and is traditional in nonlinear acoustics literature [33]. In particular it is the approach used by Polyakova et al. [22] in the first investigation of nonlinear acoustic wave propagation in a relaxing fluid.

One can determine the dependence of stress on deformation for a monorelaxing elastic medium by asserting that for one-dimensional motion the stress depends on some additional state variable ξ as well as the deformation ϵ such that

$$\sigma = \sigma\left(\epsilon,\, \xi\right). \tag{2.15}$$

The new state variable ξ accounts for an arbitrary inelastic property of the medium, the perturbation of which returns the state variable to its equilibrium value $\xi_0(\epsilon)$ according to the rate equation

$$\frac{d\xi}{dt} = -\frac{\xi - \xi_0(\epsilon)}{t_r}. \tag{2.16}$$

We will later make use of the value of $\xi_0(\epsilon)$ in a quiet medium that is undisturbed by a wave: $\xi_0(\epsilon_0) = \xi_{00}$, which is a constant.

In the atmosphere, for example, the variable ξ accounts for vibrational energy of diatomic molecules such as oxygen or nitrogen, and in the ocean it accounts for concentrations of boric acid or magnesium sulfate. Because air

and seawater both exhibit two relaxation processes, they are termed *multirelaxing media*, and in both cases Eq. (2.15) would require two additional state variables to account for each relaxation process, ξ_1 and ξ_2, each with their own rate equations defined by $\xi_{01}(\epsilon)$, $t_{r,1}$, $\xi_{02}(\epsilon)$, and $t_{r,2}$. See Blackstock [25] for further details on the relaxation mechanisms in air and seawater. Extensions to multirelaxing media are discussed further in Sec. 2.3.5 below.

Equation (2.15) is now expanded in a Taylor series to cubic order in the deformation and first order in the perturbation of ξ:

$$\sigma(\epsilon,\xi) = \sigma_0 + \left(\frac{\partial\sigma}{\partial\epsilon}\right)_{\xi_0}\epsilon + \frac{1}{6}\left(\frac{\partial^3\sigma}{\partial\epsilon^3}\right)_{\xi_0}\epsilon^3 + \left(\frac{\partial\sigma}{\partial\xi}\right)_{\epsilon_0}(\xi-\xi_0), \tag{2.17}$$

where $\sigma_0 = 0$ (no pre-stress), $\epsilon_0 = 0$ (no pre-strain), and subscripts on partial derivatives indicate the value of the corresponding quantity at which the derivative is evaluated. Because particle motion in a plane shear wave is perpendicular to the propagation direction, symmetry requires that $(\partial^2\sigma/\partial\epsilon^2)_{\xi_0} = 0$, and therefore quadratic terms are absent from the constitutive relation. An alternative expansion is obtained by taking ξ_{00}, instead of $\xi_0(\epsilon)$ as in Eq. (2.17), as the reference value of ξ [34]:

$$\sigma(\epsilon,\xi) = \sigma_0 + \left(\frac{\partial\sigma}{\partial\epsilon}\right)_{\xi_{00}}\epsilon + \frac{1}{6}\left(\frac{\partial^3\sigma}{\partial\epsilon^3}\right)_{\xi_{00}}\epsilon^3 + \left(\frac{\partial\sigma}{\partial\xi}\right)_{\epsilon_0}(\xi-\xi_{00}). \tag{2.18}$$

The expansion in Eq. (2.17) represents motion of the material that occurs slowly enough that the internal variable ξ is allowed sufficient time to relax and remains at the equilibrium value ξ_0, and so $(\partial\sigma/\partial\epsilon)_{\xi_0} = \mu_0$ is identified as the *equilibrium modulus*, thus labeled because the internal state of

the material is always in equilibrium. On the other hand, Eq. (2.18) represents motion that occurs so rapidly that the internal variable ξ may not relax and is confined to values near the unperturbed value ξ_{00}. Therefore $(\partial\sigma/\partial\epsilon)_{\xi_{00}} = \mu_\infty$ is labeled the *frozen modulus* because in this case the internal state of the material is frozen in time. The two moduli μ_0 and μ_∞ are sometimes also referred to as the relaxed and unrelaxed moduli, respectively, for example in geophysics.

A relation between the equilibrium and frozen moduli is obtained from Eqs. (2.17) and (2.18) by first expanding ξ_0 about ϵ_0: $\xi_0(\epsilon) = \xi_{00} + (\partial\xi_0/\partial\epsilon)_{\epsilon_0}\epsilon$. This expansion is substituted into Eq. (2.17), yielding

$$\sigma(\epsilon,\xi) = \left[\left(\frac{\partial\sigma}{\partial\epsilon}\right)_{\xi_0} - \left(\frac{\partial\sigma}{\partial\xi}\right)_{\epsilon_0}\left(\frac{\partial\xi_0}{\partial\epsilon}\right)_{\epsilon_0}\right]\epsilon + \frac{1}{6}\left(\frac{\partial^3\sigma}{\partial\epsilon^3}\right)_{\xi_0}\epsilon^3 + \left(\frac{\partial\sigma}{\partial\xi}\right)_{\epsilon_0}(\xi-\xi_{00}). \tag{2.19}$$

Comparison of the linear order coefficients of ϵ in Eqs. (2.18) and (2.19), and recognizing that the difference between the nonlinear terms is negligible, results in the relation

$$\left(\frac{\partial\sigma}{\partial\epsilon}\right)_{\xi_0} = \left(\frac{\partial\sigma}{\partial\epsilon}\right)_{\xi_{00}} + \left(\frac{\partial\sigma}{\partial\xi}\right)_{\epsilon_0}\left(\frac{\partial\xi_0}{\partial\epsilon}\right)_{\epsilon_0}. \tag{2.20}$$

To obtain a stress-strain relation, the time derivative of Eq. (2.18) is taken and Eq. (2.16) is used to replace $\dot{\xi}$ with $-(\xi-\xi_0)/t_r$, yielding

$$\frac{d\sigma}{dt} = \left(\frac{\partial\sigma}{\partial\epsilon}\right)_{\xi_{00}}\frac{d\epsilon}{dt} + \frac{1}{6}\left(\frac{\partial^3\sigma}{\partial\epsilon^3}\right)_{\xi_0}\frac{d\epsilon^3}{dt} - \frac{1}{t_r}\left(\frac{\partial\sigma}{\partial\xi}\right)_{\epsilon_0}(\xi-\xi_0). \tag{2.21}$$

The final result is obtained by adding $\sigma + t_r(d\sigma/dt)$ using Eqs. (2.17) and

(2.21):

$$\left(\sigma - \mu_0\epsilon - \frac{2}{3}\beta\mu_0\epsilon^3\right) + t_r\frac{d}{dt}\left(\sigma - \mu_\infty\epsilon - \frac{2}{3}\beta\mu_0\epsilon^3\right) = 0. \tag{2.22}$$

The linear shear moduli are given by

$$\mu_0 = \left(\frac{\partial\sigma}{\partial\epsilon}\right)_{\xi_0}, \tag{2.23}$$

$$\mu_\infty = \left(\frac{\partial\sigma}{\partial\epsilon}\right)_{\xi_{00}} \tag{2.24}$$

$$= \left(\frac{\partial\sigma}{\partial\epsilon}\right)_{\xi_0} - \left(\frac{\partial\sigma}{\partial\xi}\right)_{\epsilon_0}\left(\frac{\partial\xi_0}{\partial\epsilon}\right)_{\epsilon_0}, \tag{2.25}$$

where Eq. (2.20) has been used. After comparison with Eq. (2.12) the coefficient of nonlinearity is identified as

$$\beta = \frac{1}{4\mu_0}\left(\frac{\partial^3\sigma}{\partial\epsilon^3}\right)_{\xi_0}. \tag{2.26}$$

Equations (2.23) and (2.25) offer an alternative means of expressing the relaxation strength m defined by Eq. (2.14):

$$m = -\left(\frac{\partial\epsilon}{\partial\sigma}\right)_{\xi_0}\left(\frac{\partial\sigma}{\partial\xi}\right)_{\epsilon_0}\left(\frac{\partial\xi_0}{\partial\epsilon}\right)_{\epsilon_0}. \tag{2.27}$$

Landau and Lifshitz [21] assert that $\mu_\infty > \mu_0$ by deriving an equivalent viscosity parameter in the frequency domain, and also note that the same conclusion follows from Le Chatelier's principle that any internal processes must act to reduce the stress. Thus it is concluded from Eq. (2.25) that $(\partial\sigma/\partial\xi)_{\epsilon_0}$ and $(\partial\xi_0/\partial\epsilon)_{\epsilon_0}$ must have opposite signs. From Eq. (2.3) it follows that $(\partial\epsilon/\partial\sigma)_{\xi_0} > 0$. Thus Eq. (2.27) reveals that the inequality $m > 0$ is required.

Equation (2.27) may be connected directly to the lumped-element model in Fig. 2.2(b). Because $\mu_2\epsilon_{2\mu} = \eta_2\dot{\epsilon}_{2\eta}$ and $\epsilon = \epsilon_{2\mu} + \epsilon_{2\eta}$, the deformation of the damper satisfies the rate equation

$$\frac{d\epsilon_{2\eta}}{dt} = -\frac{\epsilon_{2\eta} - \epsilon}{\eta_2/\mu_2}. \tag{2.28}$$

Comparison with Eq. (2.16) reveals that the internal state variable for the lumped-element model in Fig. 2.2(b) is $\xi = \epsilon_{2\eta}$, the equilibrium value is $\xi_0 = \epsilon$, and the relaxation time is $t_r = \eta_2/\mu_2$; therefore $(\partial\xi_0/\partial\epsilon)_{\epsilon_0} = 1$. Since the stress across the lumped-element system is $\sigma = \mu_1\epsilon + \mu_2\epsilon_{2\mu} = (\mu_1 + \mu_2)\epsilon - \mu_2\epsilon_{2\eta}$ it follows that $(\partial\sigma/\partial\xi)_{\epsilon_0} = -\mu_2$. Substituting these values, along with Eq. (2.23), into Eq. (2.27) yields the result $m = \mu_2/\mu_0$, which is the expression for the relaxation strength given by Eq. (2.14).

2.2.3 Relaxation tensor

The lumped-element representation and state equation methods used to model the material response in Secs. 2.2.1 and 2.2.2, respectively, are convenient when considering one-dimensional motion that can be described using scalar functions. In order to describe elliptically polarized plane wave motion in a relaxing elastic material, a tensor description of the viscoelastic material response is necessary.

According to the memory hypothesis, the instantaneous stress in a material is due to the complete history of the strain [35]. The elastic component of the stress that reacts instantaneously to changes in strain may be separated

without loss of generality from the viscous component that depends on the strain history. The stress tensor is thus written as

$$\sigma_{ij} = \bar{\sigma}_{ij} + \bar{\sigma}'_{ij}, \tag{2.29}$$

where $\bar{\sigma}_{ij}$ and $\bar{\sigma}'_{ij}$ are the elastic and viscous stresses, respectively, and they are both Piola-Kirchoff stresses. The elastic stress $\bar{\sigma}_{ij}$ is found from Eq. (2.4) as in Sec. 2.1. The viscous stress $\bar{\sigma}'_{ij}$ will now be determined. The derivation begins with a general expression for the viscous Cauchy stress[2] τ'_{ij}, which is simplified by considering the specific deformation of pure shear. The viscous Piola-Kirchhoff stress is then determined from the Cauchy stress with the formula $\bar{\sigma}'_{ij} = (\det \mathbf{F})\tau'_{ik}(F^{-T})_{kj}$, where $F_{ij} = \delta_{ij} + \partial u_i/\partial x_j$ is the deformation gradient.

The viscous part of the stress may be written as a convolution integral [35]:

$$\tau'_{ij} = \int_{-\infty}^{t} G_{ijkl}(t - t') \frac{\partial e_{kl}}{\partial t'} \, dt' \tag{2.30}$$

where τ'_{ij} is the viscous (Cauchy) stress tensor. In Eq. (2.30), e_{kl} is the infinitesimal (linearized) strain tensor,

$$e_{kl} = \frac{1}{2} \left(\frac{\partial u_k}{\partial x_l} + \frac{\partial u_l}{\partial x_k} \right), \tag{2.31}$$

[2] A Cauchy stress tensor represents forces in the material frame, or current configuration, with relation to areas in the material frame. It is necessarily symmetric. The first Piola-Kirchhoff stress tensor, however, relates forces in the material frame to areas in the reference configuration, and is in general not symmetric. The desired form of the stress tensor is the first Piola-Kirchhoff form, as that is the form that appears in the relation we will use for conservation of momentum in the material frame, Eq. (2.68) in Sec. 2.4.

which is used here instead of the finite strain tensor E_{kl} given by Eq. (2.2) in order to be consistent with the assumption that viscoelastic effects are as small as nonlinear effects. The fourth order tensor G_{ijkl} is referred to as the *relaxation tensor*. For an isotropic and homogeneous material the relaxation tensor can be described completely by two scalar functions of time:

$$G_{ijkl}(t) = \left[\Lambda(t) - \frac{2}{3}g(t)\right]\delta_{ij}\delta_{kl} + g(t)\left(\delta_{ik}\delta_{jl} + \delta_{il}\delta_{jk}\right). \tag{2.32}$$

Plane shear wave motion is volume conserving, so there will be no compressive, or dilatational, strain. Therefore the first term on the right-hand side of Eq. (2.32) may be neglected and what remains of the relaxation tensor is described completely by the scalar function $g(t)$:

$$G_{ijkl}(t) = g(t)\left(\delta_{ik}\delta_{jl} + \delta_{il}\delta_{jk}\right). \tag{2.33}$$

For a plane elliptically polarized shear wave with particle displacement given by Eq. (2.8), the only nonzero components of τ'_{ij} have $i \neq j$ and $kl = yx$, zx, xy, or xz in Eq. (2.30), and therefore there are only four possible components of the stress:

$$\tau'_{yx} = \tau'_{xy} = \int_{-\infty}^{t} g(t-t')\frac{\partial \epsilon_y}{\partial t'}\,dt', \tag{2.34}$$

$$\tau'_{zx} = \tau'_{xz} = \int_{-\infty}^{t} g(t-t')\frac{\partial \epsilon_z}{\partial t'}\,dt', \tag{2.35}$$

where $\epsilon_i = \partial u_i/\partial x$.

The Piola-Kirchhoff stress $\bar{\sigma}'_{ij}$ in Eq. (2.29) is obtained from the Cauchy stress τ'_{ij} using the formula given after Eq. (2.29). For this special case of

deformation, transformation of the stress tensor does not alter the nonzero components of τ'_{ij} and consequently the two contributing components of $\bar{\sigma}'_{ij}$ are

$$\bar{\sigma}'_{yx} = \int_{-\infty}^{t} g(t-t') \frac{\partial \epsilon_y}{\partial t'} \, dt', \tag{2.36}$$

$$\bar{\sigma}'_{zx} = \int_{-\infty}^{t} g(t-t') \frac{\partial \epsilon_z}{\partial t'} \, dt'. \tag{2.37}$$

In order for the viscous stress tensor to account for a single relaxation mechanism, we make the choice

$$g(t) = m\mu_0 e^{-t/t_r}, \tag{2.38}$$

where m and μ_0 are as before, so that

$$\bar{\sigma}'_{yx} = m\mu_0 \int_{-\infty}^{t} e^{-(t-t')/t_r} \frac{\partial \epsilon_y}{\partial t'} \, dt', \tag{2.39}$$

$$\bar{\sigma}'_{zx} = m\mu_0 \int_{-\infty}^{t} e^{-(t-t')/t_r} \frac{\partial \epsilon_z}{\partial t'} \, dt'. \tag{2.40}$$

Combination of Eqs. (2.9), (2.10), (2.29), (2.39), and (2.40) yields

$$\sigma_{yx} = \mu_0 \epsilon_y + \frac{2}{3}\beta\mu_0\epsilon_y(\epsilon_y^2 + \epsilon_z^2) + m\mu_0 \int_{-\infty}^{t} e^{-(t-t')/t_r} \frac{\partial \epsilon_y}{\partial t'} \, dt', \tag{2.41}$$

$$\sigma_{zx} = \mu_0 \epsilon_z + \frac{2}{3}\beta\mu_0\epsilon_z(\epsilon_y^2 + \epsilon_z^2) + m\mu_0 \int_{-\infty}^{t} e^{-(t-t')/t_r} \frac{\partial \epsilon_z}{\partial t'} \, dt'. \tag{2.42}$$

Equations (2.41) and (2.42) are rearranged into a form consistent with Eqs. (2.12) and (2.22) by employing the mathematical identity

$$f(t) = \left(\frac{1}{t_r} + \frac{\partial}{\partial t} \right) \int_{-\infty}^{t} f(t') e^{-(t-t')/t_r} \, dt', \tag{2.43}$$

where $f(t)$ is any function, and is identified as $\epsilon_{y,z}$ in Eqs. (2.41) and (2.42):

$$\sigma_{yx} - \mu_0\epsilon_y - \frac{2}{3}\beta\mu_0\epsilon_y(\epsilon_y^2 + \epsilon_z^2) + t_r\frac{\partial}{\partial t}\left[\sigma_{yx} - \mu_\infty\epsilon_y - \frac{2}{3}\beta\mu_0\epsilon_y(\epsilon_y^2 + \epsilon_z^2)\right] = 0, \tag{2.44}$$

$$\sigma_{zx} - \mu_0\epsilon_z - \frac{2}{3}\beta\mu_0\epsilon_z(\epsilon_y^2 + \epsilon_z^2) + t_r\frac{\partial}{\partial t}\left[\sigma_{zx} - \mu_\infty\epsilon_z - \frac{2}{3}\beta\mu_0\epsilon_z(\epsilon_y^2 + \epsilon_z^2)\right] = 0. \tag{2.45}$$

Clearly Eqs. (2.44) and (2.45) reduce to the stress-strain relations given by Eq. (2.12) and (2.22) for the case of linear polarization when either $u_y = 0$ or $u_z = 0$. Otherwise, each relation is identical to the case of linearly polarized particle motion, but with the addition of extra nonlinear terms that account for coupling between the two components of the transverse motion.

In the case of linearly polarized motion when $\epsilon_y = \epsilon$ and $\epsilon_z = 0$, the relaxation function may be connected to the internal variable formulation from Sec. 2.2.2 as follows. Integration of Eq. (2.16) yields

$$\xi = \int_{-\infty}^{t} e^{-(t-t')/t_r}\frac{\xi_0(\epsilon)}{t_r}\,dt'. \tag{2.46}$$

Substitution of the expansion of ξ_0 given after Eq. (2.19) and taking a time derivative yields

$$\dot{\xi} = \frac{1}{t_r}\int_{-\infty}^{t} e^{-(t-t')/t_r}\left(\frac{\partial\xi_0}{\partial\epsilon}\right)_{\epsilon_0}\frac{d\epsilon}{dt'}\,dt'. \tag{2.47}$$

Comparison of Eqs. (2.17) and (2.29) reveals that $\bar{\sigma}' = (\partial\sigma/\partial\xi)_{\epsilon_0}(\xi - \xi_0) = -t_r(\partial\sigma/\partial\xi)_{\epsilon_0}\dot{\xi}$. Substitution into that relation for $\bar{\sigma}'$ of the expression for $\dot{\xi}$ in

Eq. (2.47) and comparison with Eq. (2.36) results in

$$-\left(\frac{\partial\sigma}{\partial\xi}\right)_{\epsilon_0}\left(\frac{\partial\xi_0}{\partial\epsilon}\right)_{\epsilon_0}\int_{-\infty}^{t} e^{-(t-t')/t_r}\frac{d\epsilon}{dt'}\,dt' = \int_{-\infty}^{t} g(t-t')\frac{d\epsilon}{dt'}\,dt', \qquad (2.48)$$

from which the relaxation function is identified as

$$g(t) = -\left(\frac{\partial\sigma}{\partial\xi}\right)_{\epsilon_0}\left(\frac{\partial\xi_0}{\partial\epsilon}\right)_{\epsilon_0} e^{-t/t_r}. \qquad (2.49)$$

Substitution of the definition of m given in Eq. (2.27) yields $g(t) = m\mu_0 e^{-t/t_r}$, which is identical to the definition of $g(t)$ given by Eq. (2.38).

2.3 Discussion of the material model

The form of Eq. (2.12) or (2.22) lends itself to an interpretation of the constitutive relation for a nonlinear, relaxing material as the superposition of two lossless nonlinear Hooke's laws, one which has linear shear modulus μ_0 and dominates for slow deformations when $t_r d/dt \ll 1$, and the other which has linear shear modulus $\mu_\infty = (1+m)\mu_0$ that dominates for rapid deformations when $t_r d/dt \gg 1$. Taken as a whole, however, each constitutive relation represents a lossy material for which the shear modulus is rate dependent. The behavior of the material is explored in this section: a frequency domain approach is used in Sec. 2.3.1, and time domain solutions are presented in Secs. 2.3.2–2.3.4. Modeling choices made in the derivations are discussed in Sec. 2.3.5. Finally, extension of the model to multirelaxing media and multidimensional motion is discussed in Sec. 2.3.6.

2.3.1 Complex shear modulus

In the linear case, a common way to represent a viscoelastic material is in the frequency domain through the *complex modulus* $\widetilde{\mu}(\omega) = \mu'(\omega) + j\mu''(\omega)$, where ω is the frequency, and μ' and μ'' are called the *storage modulus* and *loss modulus*, respectively. The relations $\sigma = \sigma_\omega e^{j\omega t}$ and $\epsilon = \epsilon_\omega e^{j\omega t}$ are substituted into Eq. (2.12) with $\beta = 0$, yielding

$$\sigma_\omega = \frac{\mu_0 + j\omega t_r \mu_\infty}{1 + j\omega t_r} \epsilon_\omega. \tag{2.50}$$

With the complex shear modulus defined by

$$\widetilde{\mu} = \frac{\sigma_\omega}{\epsilon_\omega} \tag{2.51}$$

$$= \frac{\mu_0 + j\omega t_r \mu_\infty}{1 + j\omega t_r}, \tag{2.52}$$

the storage and loss moduli become

$$\mu' = \frac{\mu_0 + \omega^2 t_r^2 \mu_\infty}{1 + \omega^2 t_r^2}, \qquad \mu'' = \frac{m\omega t_r \mu_0}{1 + \omega^2 t_r^2}, \tag{2.53}$$

where $m = (\mu_\infty - \mu_0)/\mu_0$ is the relaxation strength as before. The complex modulus in Eq. (2.52) may also be represented in terms of the magnitude $|\widetilde{\mu}|$ and loss factor $\eta = \mu''/\mu'$:

$$|\widetilde{\mu}| = \mu_0 \left[\frac{1 + (1+m)^2 \omega^2 t_r^2}{1 + \omega^2 t_r^2} \right]^{1/2}, \qquad \eta = \frac{m\omega t_r}{1 + (1+m)\omega^2 t_r^2}. \tag{2.54}$$

Equations (2.53) and (2.54) reduce for materials that possess values of the relaxation strength m that are much less that unity such that $\mu' = |\widetilde{\mu}|$ and $\mu'' = \eta$ in that case.

Physical interpretation of Eqs. (2.54) is as follows: for a sinusoidal applied strain with $\epsilon(t) = \epsilon_0 \sin \omega t$, the effective shear modulus at frequency ω is the magnitude $|\widetilde{\mu}|$ and the loss factor is related to the difference in phase ϕ between the stress and the strain by $\phi = \tan^{-1} \eta$. The phase ϕ also corresponds to the angle of the complex modulus in Eq. (2.52), $\phi = \angle \widetilde{\mu}$. Thus the stress is given in the time domain by $\sigma(t) = |\widetilde{\mu}|\epsilon_0 \sin(\omega t + \phi)$. This representation of the complex modulus is used in the time-domain example in Sec. 2.3.3 to describe the stress response to a sinusoidal strain that is applied at $t = 0$, and is extended to nonlinear motion in Sec. 2.3.4.

The storage modulus, loss modulus, and phase difference, plotted against frequency in Fig. 2.3, offer insight into the frequency dependence of the material response. At very low frequencies ($\omega t_r \ll 1$) Eqs. (2.53) reduce to $\mu' = \mu_0$ and $\mu'' = m\mu_0 \omega t_r$; the storage modulus is constant with frequency and the loss modulus increases proportionally to frequency. The phase difference at low frequencies is small and increases proportionally to frequency. At very high frequencies ($\omega t_r \gg 1$) Eqs. (2.53) reduce to $\mu' = \mu_\infty$, $\mu'' = m\mu_0/(\omega t_r)$; the storage modulus is again constant with frequency, but with a different value [larger; recall the discussion following Eq. (2.26)], and the loss modulus decreases in proportion to frequency. The phase difference is again small and decreases in proportion to frequency. At intermediate frequencies ($\omega t_r \approx 1$) the storage modulus increases smoothly from μ_0 to μ_∞. The loss modulus and phase difference increase from low frequencies to a peak value at $\omega t_r = 1$ and $\omega t_r = (1 + m)^{-1/2}$, respectively, and then decrease with increasing fre-

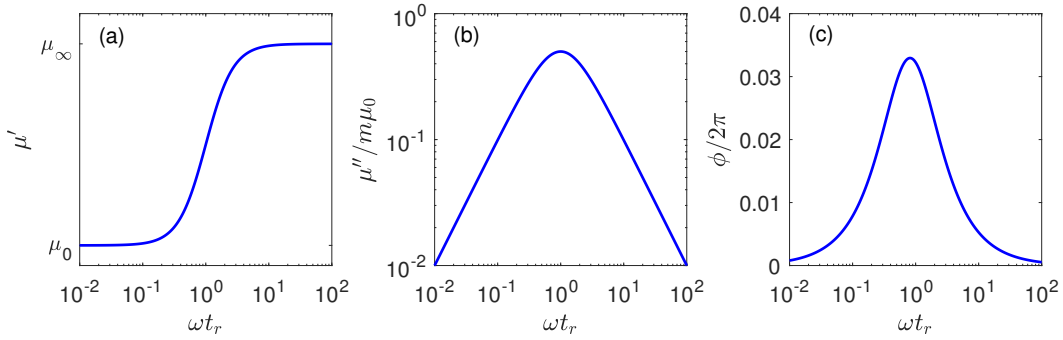

Figure 2.3: (a) Storage and (b) loss moduli, and (c) phase difference ($m = 0.5$) between stress and strain as functions of frequency.

quency. Frequency dependence of the effective shear modulus $|\widetilde{\mu}|$ and loss factor η are qualitatively similar to that of the storage modulus and loss modulus, respectively. In Chapter 3 the storage and loss moduli are related to the frequency-dependent shear wave speed $c(\omega)$ and attenuation coefficient $\alpha(\omega)$ for a progressive wave.

In σ-ϵ space, time harmonic motion is a closed loop that encloses a finite area because of the phase difference between the stress and the strain, indicating that the process is irreversible and results in energy loss. The work W done on the material during one cycle of harmonic motion is the energy lost per cycle, and is found from the closed contour integral $W = \oint \sigma \, d\epsilon$, which can be evaluated as

$$W = \int_0^{2\pi/\omega} \sigma \frac{d\epsilon}{dt} \, dt = \int_0^{2\pi/\omega} |\widetilde{\mu}| \epsilon_0 \sin(\omega t + \phi) \times \omega \epsilon_0 \cos \omega t \, dt \tag{2.55}$$

$$= \pi |\widetilde{\mu}| \epsilon_0^2 \sin \phi. \tag{2.56}$$

The energy lost per cycle is thus proportional to the phase difference ϕ, which

achieves a maximum value at the frequency given by $\omega t_r = (1+m)^{-1/2}$. For materials with $m \ll 1$, the relation $|\widetilde{\mu}| \sin\phi \simeq \mu''$ holds, and the energy lost per cycle can be expressed in terms of the loss modulus as $W = \pi\mu''\epsilon_0^2$.

The motion described after Eqs. (2.54), for which the energy loss per cycle is given by Eq. (2.56), is used in rheometry measurements to determine the viscoelastic properties of a material. During such an experiment, the phase difference between the stress and an applied strain is monitored as a function of frequency. For a relaxing material, the frequency $\omega_{W,\mathrm{Rh}}$ at which the phase difference is maximum is

$$\omega_{W,\mathrm{Rh}} = \frac{1/t_r}{\sqrt{1+m}}. \tag{2.57}$$

The value of the phase difference at its maximum is $\phi_{\max} = \tan^{-1}[\eta(\omega_{W,\mathrm{Rh}})]$, where

$$\eta(\omega_{W,\mathrm{Rh}}) = \frac{m}{2\sqrt{1+m}}. \tag{2.58}$$

In addition to rheometry techniques, other methods that use progressive wave propagation or resonance techniques can be used to determine the viscoelastic properties of a material sample. Progressive wave propagation and resonance techniques are discussed in Chapters 3 and 5, respectively. The frequency of interest, where maximum energy loss occurs, is given by $\omega_{W,\mathrm{Prog}} = 1/t_r$ for a progressive wave, and by $\omega_{W,\mathrm{Res}} = t_r^{-1}(1+m)^{-3/4}$ for the standing waves in Chapter 5.

2.3.2 Response to applied step strain

An illustration of the effect of viscoelasticity in the time domain is the stress response to an applied step strain, for which the deformation is defined by

$$\epsilon = \epsilon_0 H(t), \tag{2.59}$$

where $H(t) = 1$ for $t > 0$ and $H(t) = 0$ otherwise. Substitution into Eq. (2.12) and use of the relations $\epsilon^3 = \epsilon_0^3 H(t)$, $\dot{\epsilon} = \epsilon_0 \delta(t)$ where $\delta(t) = \dot{H}(t)$ is the Dirac delta function, and $\frac{d}{dt}[\epsilon^3] = \epsilon_0^3 \delta(t)$ results in a first-order linear ordinary differential equation in $\sigma(t)$ that can be integrated in a straightforward way to obtain

$$\sigma = \left[\mu_0 \epsilon_0 \left(1 + m e^{-t/t_r}\right) + \frac{2}{3}\beta \mu_0 \epsilon_0^3\right] H(t). \tag{2.60}$$

The stress response to a step strain given by Eq. (2.60) is presented in Fig. 2.4 for three values of the applied step strain. It illustrates, in a different way than the complex modulus, the rate, or frequency dependence, of the material response. Upon application of the strain, the stress immediately takes on a value of $\sigma(0^+) = \mu_\infty \epsilon_0 + \frac{2}{3}\beta \mu_0 \epsilon_0^3$ and then subsequently relaxes to a value of $\sigma(\infty) = \mu_0 \epsilon_0 + \frac{2}{3}\beta \mu_0 \epsilon_0^3$ at a rate determined by the relaxation time t_r. Thus for a deformation that occurs slowly compared to the relaxation time t_r, the material has ample time to adjust, resulting in the softer equilibrium shear modulus μ_0. For rapid deformations such as the onset of the step strain or a high-frequency oscillation, the material has no time to adjust to the deformation and relax, resulting in the stiffer frozen modulus μ_∞.

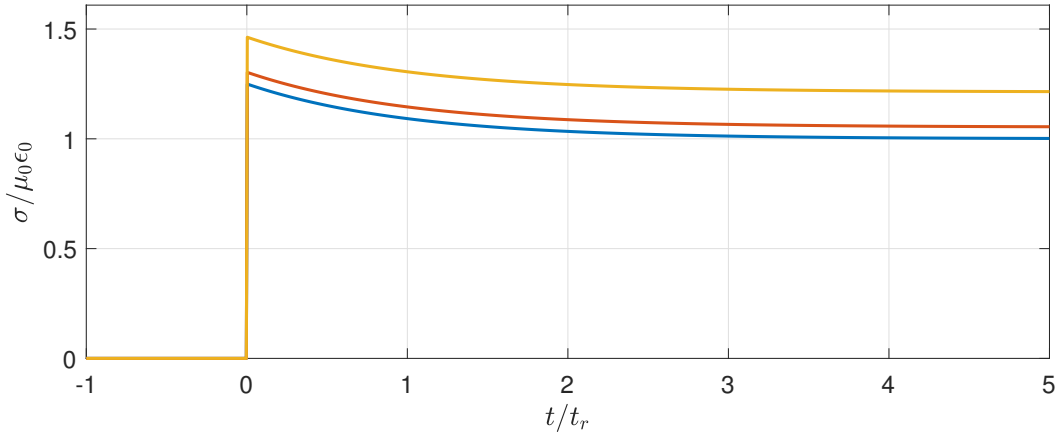

Figure 2.4: Shear stress in the material in response to an applied step strain for which $\epsilon(t) = \epsilon_0 H(t)$. Blue, red, and orange curves correspond to strain amplitudes ϵ_0 of 0 (linear theory), 0.2, and 0.4, respectively. The relaxation strength in each case is $m = 0.25$. A value of $\beta = 2$ is assumed.

The nonlinear solution in Eq. (2.60) and the curves in Fig. 2.4 demonstrate competition between relaxation and nonlinearity, which is a recurring theme in this dissertation. The transient term accounts for relaxation and has a magnitude determined by the relaxation strength m, and the nonlinear term accounts for finite amplitude effects and has a magnitude proportional to $\beta\epsilon_0^2$. The competition between the terms can be quantified by the dimensionless ratio $\delta = 3m/2\beta\epsilon_0^2$, which is large if relaxation dominates or small if nonlinearity dominates. The ratio δ is equal to ∞ (linear theory), 4.69, and 1.17 for the blue, red, and orange curves, respectively, in Fig. 2.4, indicating that relaxation is dominant in the responses represented by the blue and red curves, whereas the orange curve corresponds to the case where nonlinearity affects the response about as much as relaxation. A similar ratio D is used

in Chapter 3 to quantify competition between relaxation and nonlinearity in the propagation of a progressive wave, in particular a steady shock front [see Eq. (3.24)].

2.3.3 Response to transient sinusoid

An illustration that combines the frequency and time domain aspects of the effects of relaxation on the material response from Secs. 2.3.1 and 2.3.2 is the stress response to a sinusoidal strain that is applied at $t = 0$. In this case the deformation is given by

$$\epsilon(t) = \epsilon_0 H(t) \sin \omega t. \tag{2.61}$$

Substitution of Eq. (2.61) into Eq. (2.12) as in Sec. 2.3.2 and ignoring nonlinearity results in an ordinary differential equation that can be integrated to obtain the stress response:

$$\sigma(t) = \epsilon_0 \left[-\mu'' e^{-t/t_r} + |\widetilde{\mu}| \sin(\omega t + \phi) \right] H(t), \tag{2.62}$$

where the loss modulus μ'' is the second of Eqs. (2.53), and $|\widetilde{\mu}|$ and $\phi = \tan^{-1} \eta$ are the magnitude and phase of the complex modulus given by Eqs. (2.54). The two terms in square brackets in Eq. (2.62) are the transient and steady-state responses, respectively. The transient term is proportional to the loss modulus and decays at a rate determined by the relaxation time; it is only significant for intermediate frequencies ($\omega t_r \approx 1$) and during the time interval $0 < t < t_r$. The steady-state term, as discussed after Eqs. (2.54), is the time-domain representation of the complex modulus presented in Eqs. (2.54): the

effective shear modulus at frequency ω is the magnitude $|\widetilde{\mu}|$, and the phase difference ϕ between the stress and the applied strain is given by the arctangent of the loss factor η. The energy lost per cycle in the steady state is given by Eq. (2.56), and is only significant at intermediate frequencies when the phase difference is near its maximum.

In each plot of Fig. 2.5 the applied strain given by Eq. (2.61), the stress response given by Eq. (2.62), and the transient part of the stress given by $\sigma_{\rm tr} = -\epsilon_0 \mu'' e^{-t/t_r}$ are represented by the dashed black, solid blue, and dotted black curves, respectively. Figure 2.5(a) reveals that at low frequencies ($\omega t_r \ll 1$) the stress is very nearly in phase with the applied strain and the effective shear modulus is the equilibrium modulus $|\widetilde{\mu}| \approx \mu_0$; the stress has ample time to adjust and stay in equilibrium throughout the motion. The transient part of the stress is very small in amplitude in this case due to the small value of the loss modulus at low frequencies, and it decays rapidly compared to the period of the motion. At the intermediate frequency depicted in Fig. 2.5(b), the stress and strain are out of phase and the effective shear modulus is in the range $\mu_0 < |\widetilde{\mu}| < \mu_\infty$; the stress in this case increases initially with the strain, but has just begun to relax by the time the strain reaches its initial peak at $\omega t = \pi/2$, resulting in a phase difference between the stress and strain that persists out to steady state. The transient part of the stress is most apparent in Fig. 2.5(b) because the maximum of the loss modulus occurs at this frequency ($\omega t_r = 1$). Finally, at high frequencies ($\omega t_r \gg 1$) Fig. 2.5(c) illustrates that the stress and strain are in phase and the effective

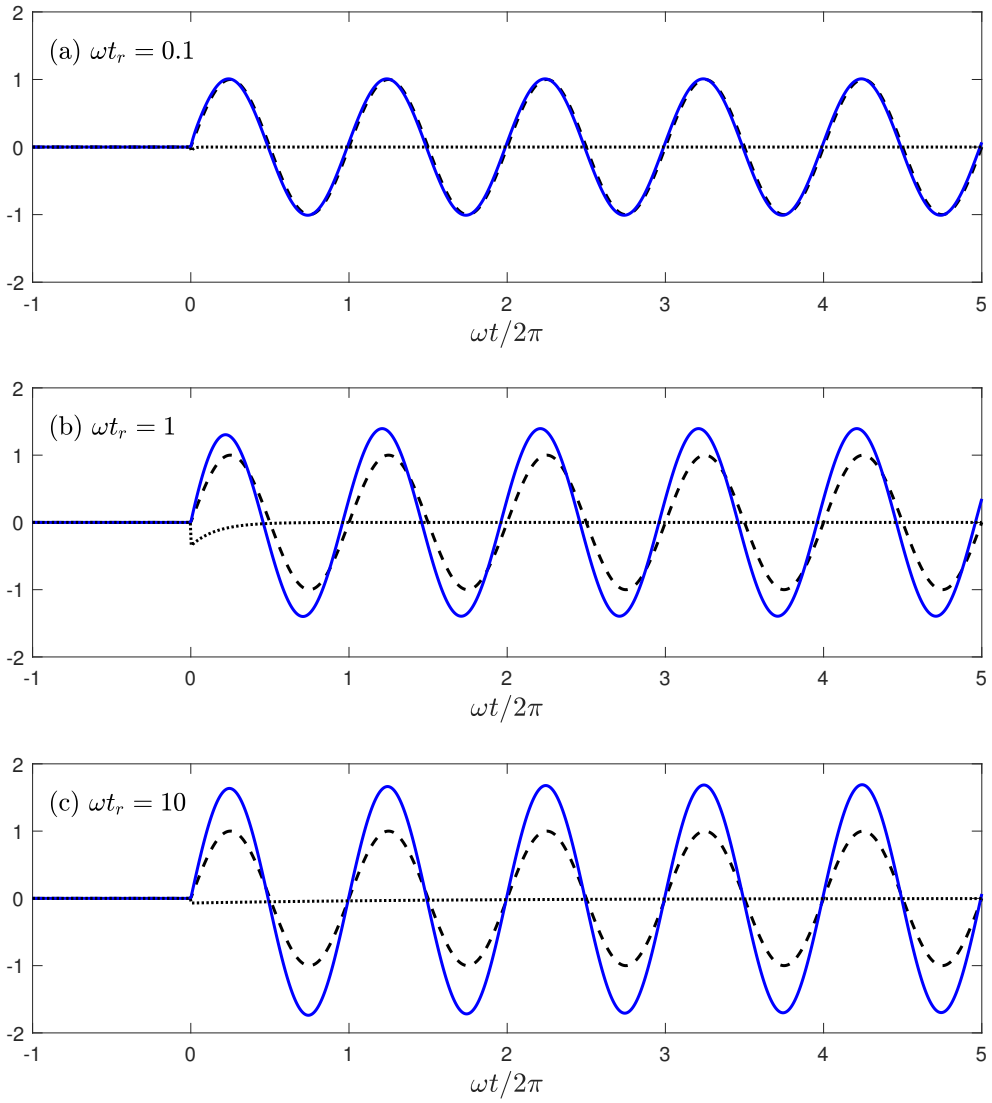

Figure 2.5: Stress response to an applied strain that is a sinusoid beginning at $t = 0$. (a) Low frequency, (b) intermediate frequency, and (c) high frequency cases. In each plot the black dashed, solid blue, and black dotted curves represent the applied strain ϵ/ϵ_0, the stress response $\sigma/\mu_0\epsilon_0$, and the transient part of the stress response $\sigma_{\rm tr}/\mu_0\epsilon_0 = -(\mu''/\mu_0)e^{-t/t_r}$, respectively. The relaxation strength is $m = 0.7$ for all cases.

shear modulus is the frozen modulus $|\widetilde{\mu}| \approx \mu_\infty$, because the stress does not have time to relax during the rapidly varying motion. The transient part of the stress in this case decays slowly compared to the period of the motion, but is not significant due to the small value of the loss modulus at high frequencies.

2.3.4 Nonlinear response to sinusoid

By ignoring transient effects and retaining nonlinear terms in a derivation similar to that of Eq. (2.62), an expression for the steady-state stress response to a finite-amplitude, sinusoidal applied strain is obtained. Such an expression is useful for determining the coefficient of nonlinearity from a rheological experiment. Substitution of the applied strain given by Eq. (2.61) into Eq. (2.12), including nonlinearity, integrating the resulting differential equation, and ignoring transient terms results in the steady-state solution for the stress response:

$$\sigma(t) = |\widetilde{\mu}|\epsilon_0 \sin(\omega t + \phi) + \frac{2}{3}\beta\mu_0\epsilon_0^3 \sin\omega t - \frac{1}{6}\beta\mu_0\epsilon_0^3 \sin 3\omega t. \tag{2.63}$$

The first term on the right-hand side of Eq. (2.63) is the linear steady-state response and the last two terms are due to the finite amplitude of the deformation. The second term is an additional term at the drive frequency ω that accounts for a finite-amplitude adjustment of the amplitude of the response and the phase difference between the stress and the strain. The amplitude-dependent effective shear modulus $|\widetilde{\mu}|_\beta$ and phase difference ϕ_β are

$$|\widetilde{\mu}|_\beta = |\widetilde{\mu}| + \frac{2}{3}\beta\mu_0\epsilon_0^2 + O(\epsilon_0^3), \qquad \phi_\beta = \tan^{-1}\left[\frac{m\omega t_r}{1 + (1+m)\omega^2 t_r^2 + \frac{2}{3}\beta\epsilon_0^2}\right]. \tag{2.64}$$

The third term on the right-hand side of Eq. (2.63) represents the response at 3ω. The measured amplitude of the response at three times the drive frequency may be used to determine the coefficient of nonlinearity using the relation

$$\sigma_{3\omega} = -\frac{1}{6}\beta\mu_0\epsilon_0^3. \tag{2.65}$$

The nonlinear solution for the stress response in Eq. (2.63) therefore offers a means to experimentally determine the nonlinear and viscoelastic properties of a material using rheological techniques. Progressive wave and resonance methods for determining these material properties are identified in Chapters 3 and 5, respectively.

2.3.5 Discussion of modeling choices

As stated in the first paragraph of this chapter, the complex internal structure of soft tissue and rubber makes modeling at the microscale level implausible. Thus in order to obtain a useful model, physical modeling choices must be made as to how to represent the macroscale behavior of the material. Those choices that are made in Sec. 2.2 are identified and discussed in this section.

It is assumed that effects due to viscoelasticity are small and on the same order as nonlinear effects. This choice manifests in each of the three derivations in Sec. 2.2. In the lumped-element model in Sec. 2.2.1 the assumption is enforced by restricting the stiffness μ_2 and damper η_2 to be linear elements. This results in the the same nonlinear term appearing in both

parenthesized expressions in Eq. (2.12). For the state variable expansion in Sec. 2.2.2, the assumption of weak viscoelasticity allowed us to expand only to first order in deviations of ξ, and also to ignore combinations of terms such as the difference between $(\partial^3\sigma/\partial\epsilon^3)_{\xi_0}\epsilon^3$ and $(\partial^3\sigma/\partial\epsilon^3)_{\xi_{00}}\epsilon^3$ in Eqs. (2.17) and (2.18). Finally, in the approach employing a relaxation tensor in Sec. 2.2.3, assuming a linear relation between viscous stress and strain allowed for several simplifications that resulted in the simple forms of Eqs. (2.39) and (2.40) for the components of the viscous stress tensor.

In Sec. 2.2.1, the choice of how to represent the viscoelasticity of the material was made up front by representing the material with the specific lumped-element configuration of a nonlinear Zener body. Other combinations of springs and dampers in either parallel or series result in their own constitutive relations. Several lumped-element configurations are commonly used to represent soft tissue in shear [26]; see especially the recent review by Carstensen and Parker [5]. Other types of viscoelasticity have been modeled using lumped-element configurations that are fractal [36], contain fractional elements [37], or are based on a generalized Maxwell body [38]. The generalized Maxwell body is also a representation of a material that exhibits multiple relaxation mechanisms [39].

The material model was chosen in Sec. 2.2.2 by introducing Eq. (2.16) to explicitly define the behavior of the internal variable. The rate equation chosen for Eq. (2.16) is the simplest analytical representation of an internal variable that requires a finite time to react to a change in the state of the ma-

terial; it can be interpreted as a first-order expansion in the rate of change $\dot{\xi}$ of the internal variable when the deviation $\xi - \xi_0$ is small [21]. A viscoelastic material that exhibits a different kind of stress relaxation could be modeled using another choice of rate equation for the internal variable instead of Eq. (2.16), such as a power-law, which would result in a different stress-strain relation. Equation (2.16) is commonly used to represent molecular relaxation of motion in gases when used in conjuction with acoustical models.

Finally, the model of stress relaxation considered in Sec. 2.2.3 was developed by choosing the relaxation function $g(t)$ to be given by Eq. (2.38). As is Eq. (2.16), Eq. (2.38) is the simplest analytical form that the relaxation function can take to represent a material that requires a finite time to react to an applied stress or strain, and other manifestations of stress relaxation would be modeled by a different choice for the function $g(t)$. There are few restrictions on the behavior of the relaxation function, apart from being real-valued and bounded for all t. Causality requires that $g(t) = 0$ for $t < 0$, which is taken into account by the integration limits in Eq. (2.30). The relaxation function is seen to be equivalent to the step response given above in Eq. (2.60) after the elastic contribution is subtracted out, which introduces additional restrictions, namely $g(0^+) < \infty$ and $g(t \to \infty) = 0$. Furthermore, most materials exhibit a so-called *fading memory* for which the magnitude of the relaxation function and of its derivative are monotonically decreasing functions of time [35]. Holm and Holm [39] provide a good description of the relationship between relaxation functions and lumped-element configurations

for viscoelastic media.

2.3.6 Extensions of the model

A material with a different response than the stress relaxation described above is often modeled using a spectrum of relaxation processes. As discussed after Eq. (2.16), air and sea water both exhibit two separate relaxation mechanisms. Also, materials that are characterized by power-law attenuation such as soft tissue and marine sediment can be modeled as multirelaxing materials [40]. The lumped-element model developed in Sec. 2.2.1 may be augmented to account for multiple relaxation mechanisms by adding an additional linear spring-damper combination in parallel with the upper arm in Fig. 2.2(b) for each additional relaxation mechanism, thereby creating a generalized Maxwell model [39]. As discussed after Eq. (2.16) in Sec. 2.2.2, multiple relaxation mechanisms can be included in the state equation by introducing an additional internal state variable and corresponding rate equation for each relaxation mechanism:

$$\sigma = \sigma(\epsilon, \xi_1, \xi_2, \cdots), \qquad \dot{\xi}_i = -(\xi_i - \xi_{i0})/t_{r,i}. \tag{2.66}$$

In the relaxation tensor approach of Sec. 2.2.3, the relaxation function $g(t)$ for a multirelaxing material is a summation of decaying exponentials, one for each relaxation mechanism:

$$g(t) = m_1\mu_0 e^{-t/t_{r,1}} + m_2\mu_0 e^{-t/t_{r,2}} + \cdots, \qquad m_i > 0. \tag{2.67}$$

All three modeling approaches offer unique insights into the internal behavior of a relaxing material, and are all illustrative in the case of a monorelaxing medium. However, the algebraic manipulations required to derive a stress-strain relation for a multirelaxing material from a generalized Maxwell representation or from an expansion of a state equation are cumbersome, whereas the relaxation function given by Eq. (2.67) is straightforward to implement in the convolution form of the constitutive relation.

The models developed and discussed in this chapter are for the special one-dimensional case of plane wave motion, a very simple kind of deformation for which the scalar lumped-element and state variable expansion derivations can be used to obtain the stress-strain relation, as in Secs. 2.2.1 and 2.2.2, respectively, and for which the relaxation tensor can be simplified significantly, as in Sec. 2.2.3. Incorporating the effects of viscoelasticity into multidimensional motion such as a diffracting shear wave beam requires the development of a relaxation tensor as in Sec. 2.2.3. However, not all of the simplifications used in Sec. 2.2.3 for plane waves apply in this case. For example, there are more components of the viscous stress tensor for a diffracting beam than those given in Eqs. (2.34) and (2.35).

2.4 Plane nonlinear shear wave equations

This chapter is concluded with the presentation of equations of motion for the material, which are nonlinear shear wave equations. Conservation of

momentum requires that

$$\rho \frac{\partial^2 u_i}{\partial t^2} = \frac{\partial \sigma_{ij}}{\partial x_j}, \tag{2.68}$$

where ρ is the density of the material, and the relationship between stress σ_{ij} and particle displacement u_i is given by Eq. (2.12) or (2.22) for linearly polarized plane waves, or Eqs. (2.44) and (2.45) for elliptically polarized plane waves. In each case the stress and strain are functions of only one spatial variable, and so evaluation of the right-hand side of Eq. (2.68) is straightforward. For linearly polarized waves, substitution of Eq. (2.12) or (2.22) into Eq. (2.68) and rearranging results in a single nonlinear wave equation:

$$\left(1 + t_r \frac{\partial}{\partial t}\right) \left[\frac{\partial^2 u}{\partial t^2} - c_0^2 \frac{\partial^2 u}{\partial x^2} - \frac{2}{3}\beta c_0^2 \frac{\partial}{\partial x}\left(\frac{\partial u}{\partial x}\right)^3\right] = m t_r c_0^2 \frac{\partial^3 u}{\partial x^2 \partial t}, \tag{2.69}$$

where $c_0 = \sqrt{\mu_0/\rho}$ is identified as the low-frequency limit of the shear wave speed. In the limit of $t_r \to \infty$ the high-frequency limit of the shear wave speed is identified as $c_\infty = \sqrt{\mu_\infty/\rho} = c_0\sqrt{1+m}$. The relaxation strength may then be expressed in terms of the high and low frequency limits of the shear wave speed:

$$m = \frac{c_\infty^2 - c_0^2}{c_0^2}. \tag{2.70}$$

The expression in square brackets on the left-hand side of Eq. (2.69), when set equal to zero, is identical to the lossless nonlinear shear wave equation derived by Zabolotskaya et al. [13], who present several solutions for the cases of no losses and also when classical thermoviscous losses are included. Equa-

tion (2.69) may be written in a form similar to Eq. (2.12):

$$\left[\frac{\partial^2 u}{\partial t^2} - c_0^2\frac{\partial^2 u}{\partial x^2} - \frac{2}{3}\beta c_0^2\frac{\partial}{\partial x}\left(\frac{\partial u}{\partial x}\right)^3\right] + t_r\frac{\partial}{\partial t}\left[\frac{\partial^2 u}{\partial t^2} - c_\infty^2\frac{\partial^2 u}{\partial x^2} - \frac{2}{3}\beta c_0^2\frac{\partial}{\partial x}\left(\frac{\partial u}{\partial x}\right)^3\right] = 0, \tag{2.71}$$

which explicitly shows again that a relaxing material can be described as the superposition of two lossless material models with different shear moduli, or in this case shear wave speeds. When taken as a whole, Eq. (2.71) represents a material with energy loss due to an effective elastic modulus that depends on deformation rate.

In the case of elliptically polarized plane wave motion, Eqs. (2.44) and (2.45) are used in Eq. (2.68), resulting in two coupled nonlinear wave equations:

$$\left(1 + t_r\frac{\partial}{\partial t}\right)\left\{\frac{\partial^2 u_y}{\partial t^2} - c_0^2\frac{\partial^2 u_y}{\partial x^2} - \frac{2}{3}\beta c_0^2\frac{\partial}{\partial x}\left[\left(\frac{\partial u_y}{\partial x}\right)^3 + \frac{\partial u_y}{\partial x}\left(\frac{\partial u_z}{\partial x}\right)^2\right]\right\} = mt_r c_0^2\frac{\partial^3 u_y}{\partial x^2 \partial t}, \tag{2.72}$$

$$\left(1 + t_r\frac{\partial}{\partial t}\right)\left\{\frac{\partial^2 u_z}{\partial t^2} - c_0^2\frac{\partial^2 u_z}{\partial x^2} - \frac{2}{3}\beta c_0^2\frac{\partial}{\partial x}\left[\left(\frac{\partial u_z}{\partial x}\right)^3 + \frac{\partial u_z}{\partial x}\left(\frac{\partial u_y}{\partial x}\right)^2\right]\right\} = mt_r c_0^2\frac{\partial^3 u_z}{\partial x^2 \partial t}. \tag{2.73}$$

The expressions in braces in Eqs. (2.72) and (2.73), when set equal to zero, are the coupled nonlinear wave equations in a lossless material, as presented by Zabolotskaya et al. [13] along with several solutions.

The remainder of this dissertation consists of solutions of Eqs. (2.69)–(2.73). Progressive wave motion in Chapters 3 and 4 is limited to the analysis

of linearly polarized plane waves in order to focus the discussion on the effects of relaxation on nonlinear shear wave motion. Elliptically polarized plane waves are analyzed in Chapter 5 for the case of standing waves, where the response of a shear wave resonator to elliptical driving motion is investigated.

Chapter 3

Plane Progressive Nonlinear Shear Waves

In this chapter the propagation of plane progressive shear waves in a nonlinear and relaxing material is investigated. A *progressive wave* is a disturbance that propagates in one direction and transports energy in that direction. Progressive waves do not interact with boundaries or other waves. On the other hand, *standing waves* that consist of forward and backward traveling waves of equal amplitude do not result in a net transport of energy. Standing waves are the topic of Chapter 5. Furthermore, analyses in this chapter are limited to shear waves with particle motion that is linearly polarized in order to focus the discussion on the competition between nonlinearity and relaxation in progressive wave motion. Plane nonlinear progressive shear waves with elliptically polarized particle motion are discussed by Zabolotskaya et al. [13].

A simplified version of the nonlinear wave equation presented in Sec. 2.4 for progressive wave motion is derived in Sec. 3.1. The resulting equation is termed an *evolution equation* because it describes the evolution of a time wave-

Selected material from this chapter was previously published in J. M. Cormack and M. F. Hamilton, "Plane nonlinear shear waves in relaxing media," *J. Acoust. Soc. Am.* **143**, 1035–1048 (2018), which appears as Ref. [32] in this dissertation. Contributions from JMC include derivation of equations of motion, derivation and validation of solutions, and writing of the article.

form, in a reference frame moving at the small signal shear wave speed, during propagation away from the source in a nonlinear and relaxing medium. An exact solution of the evolution equation for the profile of a steady step disturbance is derived in Sec. 3.2. In Sec. 3.3 numerical solutions are presented for the evolution of an initially sinusoidal waveform that develops shocks. Limiting forms of the evolution equation in the cases of weak nonlinearity, low frequencies, and high frequencies are presented in Sec. 3.4, with solutions presented for third harmonic generation and shock front propagation in the cases of weak nonlinearity and high frequency motion, respectively.

3.1 Evolution equation

A simplified model for progressive wave propagation in a nonlinear, relaxing medium is obtained from the full nonlinear wave equation presented in Sec. 2.4, rewritten here for convenience,

$$\left(1 + t_r \frac{\partial}{\partial t}\right) \left[\frac{\partial^2 u}{\partial t^2} - c_0^2 \frac{\partial^2 u}{\partial x^2} - \frac{2}{3}\beta c_0^2 \frac{\partial}{\partial x}\left(\frac{\partial u}{\partial x}\right)^3\right] = m t_r c_0^2 \frac{\partial^3 u}{\partial x^2 \partial t}, \tag{3.1}$$

by introducing the retarded time τ and slowly varying length scale x_1 [13]:

$$\tau = t - x/c_0, \qquad x_1 = \epsilon_0^2 x, \tag{3.2}$$

where $\epsilon_0 = v_0/c_0 \ll 1$ is a typical acoustic Mach number and v_0 is a characteristic particle velocity amplitude for the wave. For a progressive wave, the Mach number is also equivalent to the strain amplitude of the wave. The significance of the slowly varying length scale is that changes in the waveform

during propagation due to nonlinearity or relaxation take place over a distance of several wavelengths, and so the parameter ϵ_0 is used here as a small scaling parameter. The derivation then consists of transforming Eq. (3.1) into the (τ, x_1) coordinate system. To be consistent with the fourth order expansion of the strain energy density used in Sec. 2.1, only terms up to $O(\epsilon_0^3)$ are retained in the evolution equation. The assumption that effects due to relaxation are small and on the same order as nonlinear effects is enforced by introducing the restriction that the relaxation strength is small, i.e., $m = O(\epsilon_0)$, from which it follows that the relaxation strength may be expressed as $m = 2(c_\infty - c_0)/c_0$ to lowest order in $c_\infty - c_0$.

Transformation of the time and space derivatives into the moving reference frame and slowly varying length scale yields

$$\frac{\partial}{\partial t} = \frac{\partial}{\partial \tau}, \qquad \frac{\partial}{\partial x} = \epsilon_0^2 \frac{\partial}{\partial x_1} - \frac{1}{c_0}\frac{\partial}{\partial \tau}. \tag{3.3}$$

With the use of Eqs. (3.3), terms in Eq. (3.1) become, to leading order in ϵ_0,

$$\frac{\partial^2 u}{\partial t^2} - c_0^2 \frac{\partial^2 u}{\partial x^2} = 2\epsilon_0^2 c_0 \frac{\partial^2 u}{\partial x_1 \partial \tau}, \tag{3.4}$$

$$\frac{2}{3}\beta c_0^2 \frac{\partial}{\partial x}\left(\frac{\partial u}{\partial x}\right)^3 = \frac{2}{3}\frac{\beta}{c_0^2}\frac{\partial}{\partial \tau}\left(\frac{\partial u}{\partial \tau}\right)^3, \tag{3.5}$$

$$m t_r c_0^2 \frac{\partial^3 u}{\partial x^2 \partial t} = m t_r \frac{\partial^3 u}{\partial \tau^3}. \tag{3.6}$$

Substitution of Eqs. (3.3)–(3.6) into Eq. (3.1) and rearranging yields

$$\left(1 + t_r \frac{\partial}{\partial \tau}\right)\left[\epsilon_0^2 \frac{\partial^2 u}{\partial x_1 \partial \tau} - \frac{1}{3}\frac{\beta}{c_0^3}\frac{\partial}{\partial \tau}\left(\frac{\partial u}{\partial \tau}\right)^3\right] = \frac{m t_r}{2c_0}\frac{\partial^3 u}{\partial \tau^3}. \tag{3.7}$$

The final dimensional form of the evolution equation is obtained by reinstating x for x_1 and introducing the particle velocity $v = \partial u/\partial\tau$, yielding

$$\left(1 + t_r \frac{\partial}{\partial\tau}\right)\left(\frac{\partial v}{\partial x} - \frac{\beta}{c_0^3} v^2 \frac{\partial v}{\partial\tau}\right) = \frac{m t_r}{2c_0} \frac{\partial^2 v}{\partial\tau^2}. \tag{3.8}$$

Equation (3.8) is the desired evolution equation for plane progressive shear waves in a nonlinear and relaxing medium, and it is the main result of this section. The second parenthesized expression in Eq. (3.8), when set equal to zero, is identical to the evolution equation derived by Zabolotskaya et al. [13] for plane nonlinear shear waves in a lossless medium. The first parenthesized expression on the left-hand side and the term on the right-hand side account for relaxation, and are identical to the corresponding terms in the evolution equation for plane compressional waves in a relaxing fluid [22, 41].

The form of the evolution equation in Eq. (3.8) is convenient for both analytical and computational analysis of progressive waves, as well as for physical interpretation. The retarded time scale places the wave in a reference frame that translates along with the wave at the equilibrium wave speed c_0, thereby avoiding the need for a spatial propagator term such as e^{-jkx} in analytical solutions and reducing the necessary computational domain size of numerical solutions. Use of the slowly varying length scale results in Eq. (3.8) having only a single first-order spatial derivative, allowing one to rewrite the evolution equation in the following form:

$$\frac{\partial v}{\partial x} = \frac{\beta}{c_0^3} v^2 \frac{\partial v}{\partial\tau} + \frac{m}{2c_0} \int_{-\infty}^{\tau} e^{-(\tau-\tau')/t_r} \frac{\partial^2 v}{\partial\tau'^2}\, d\tau', \tag{3.9}$$

where the mathematical identity in Eq. (2.43) has been used. The left-hand side of Eq. (3.9) represents change in the wave profile during propagation through the medium, and terms on the right-hand side account for the processes that affect the evolution of the waveform, namely nonlinearity and relaxation. The form of the evolution equation presented in Eq. (3.9) lends itself to numerical solutions, as an algorithm based on operator splitting is easily implemented beginning with Eq. (3.9); see, for example, the algorithm of Cleveland et al. [41] for simulation of nonlinear acoustic waves in a relaxing fluid, a modified version of which is used to obtain the simulated results presented in Sec. 3.3.

3.1.1 Attenuation and dispersion

Energy loss due to the phase difference between stress and strain that is a consequence of relaxation is discussed in Chapter 2, with the energy loss per cycle during time-harmonic excitation given by Eq. (2.56). For a progressive wave, energy loss due to this phase difference manifests as a frequency-dependent attenuation of the wave amplitude with propagation distance. Because the effective shear modulus of the material is also frequency dependent, the attenuation is accompanied by a frequency-dependent wave speed, which is known as *dispersion*. Relations for the attenuation and dispersion resulting from relaxation for progressive waves with $m \ll 1$ are obtained by ignoring the nonlinear term in Eq. (3.8) and substituting $v = v_\omega(x)e^{j\omega\tau}$:

$$\frac{dv_\omega}{dx} + \widetilde{\alpha} v_\omega = 0, \qquad \widetilde{\alpha} = \frac{m\omega^2 t_r}{2c_0(1 + j\omega t_r)}. \tag{3.10}$$

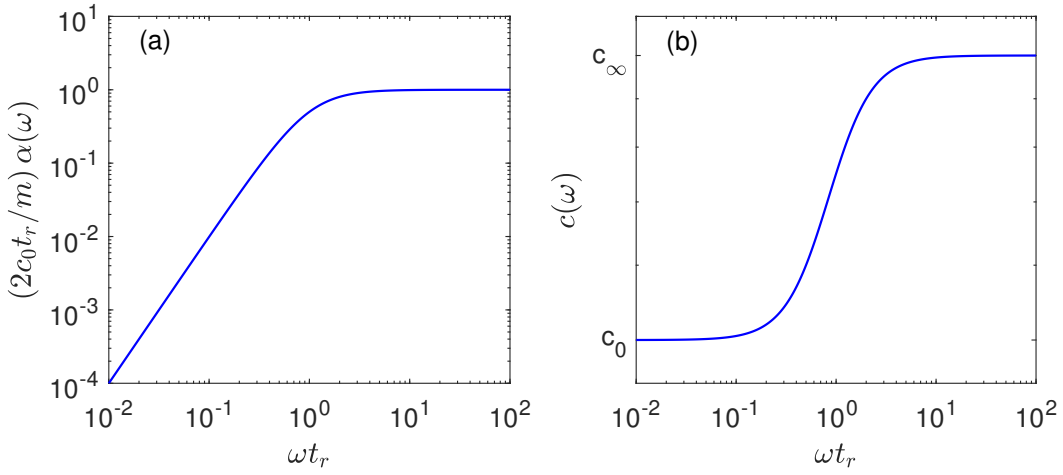

Figure 3.1: Frequency dependence of (a) attenuation coefficient and (b) phase speed for a relaxing material.

Solutions of the first of Eqs. (3.10) are of the form $v_\omega(x) \propto e^{-\widetilde{\alpha}x}$, and thus linear solutions of Eqs. (3.8) at frequency ω are $v(x,\tau) \propto e^{-\widetilde{\alpha}x}e^{j\omega\tau}$. The attenuation coefficient $\alpha(\omega)$ and phase speed $c(\omega)$ are defined as

$$\alpha(\omega) = \frac{m\omega^2 t_r}{2c_0(1+\omega^2 t_r^2)}, \tag{3.11}$$

$$c(\omega) = c_0\left[1 + \frac{m\omega^2 t_r^2}{2(1+\omega^2 t_r^2)}\right], \tag{3.12}$$

in terms of which the exponential $e^{-\widetilde{\alpha}x}e^{j\omega\tau}$ is expressed as

$$\exp\left[-\widetilde{\alpha}x + j\omega\left(t - \frac{x}{c_0}\right)\right] = \exp\big[-\alpha(\omega)x\big]\exp\left[j\omega\left(t - \frac{x}{c(\omega)}\right)\right]. \tag{3.13}$$

The amplitude of a signal with frequency ω thus decreases with distance at a rate given by the attenuation coefficient $\alpha(\omega)$, and the phase speed of the signal is given by $c(\omega)$.

The frequency dependencies of the attenuation and phase speed in Eqs. (3.11) and (3.12) are shown in Fig. 3.1. At low frequencies corresponding

to $\omega t_r \ll 1$, Eqs. (3.11) and (3.12) reduce to $\alpha(\omega) \simeq m\omega^2 t_r/2c_0$ and $c(\omega) \simeq c_0$, respectively; the material exhibits the same viscoelastic behavior as a medium that is characterized by classical viscous losses: attenuation that increases as frequency squared and a constant phase speed. At high frequencies corresponding to $\omega t_r \gg 1$, Eqs. (3.11) and (3.12) reduce to $\alpha(\omega) \simeq m/2c_0 t_r$ and $c(\omega) \simeq c_0(1 + m/2)$; both attenuation and phase speed are constant with frequency. At intermediate frequencies ($\omega t_r \approx 1$) both the attenuation coefficient and phase speed increase monotonically with frequency. The magnitudes of both the attenuation and the dispersion are determined by the relaxation strength m, and because the attenuation coefficient α must be a positive quantity, the restriction $m > 0$ is reinforced by Eq. (3.11).

The attenuation and phase speed can be directly related to the storage and loss moduli derived in Sec. 2.3.1. Comparison of Eqs. (2.53) and (3.11) reveals the relation

$$\alpha\lambda = \frac{\pi\mu''}{\mu_0}, \tag{3.14}$$

where $\lambda = \omega/2\pi c_0$ is the shear wavelength. With Eq. (3.14) written as $\alpha\lambda = \lambda/l_\alpha$, where $l_\alpha = 1/\alpha$ is the attenuation length, it is seen that the loss modulus is a measure of the number of wavelengths that a wave will propagate before attenuating in amplitude by a factor of $1/e$. The quantity $\alpha\lambda$ is commonly referred to as the inverse quality factor Q^{-1} and is used in geophysics literature to describe progressive wave attenuation. Finally, the phase speed is related

to the storage modulus by squaring Eq. (3.12), yielding

$$\left(\frac{c}{c_0}\right)^2 = 1 + \frac{m\omega^2 t_r^2}{1+\omega^2 t_r^2}, \qquad m \ll 1 \tag{3.15}$$

$$= \frac{\mu'}{\mu_0}. \tag{3.16}$$

3.1.2 Dimensionless form

Rearrangement of Eq. (3.8) into a dimensionless form is convenient for carrying out subsequent calculations, and also yields insight into competition between the physical processes that affect waveform evolution. The following dimensionless parameters are chosen:

$$V = \frac{v}{v_0}, \qquad X = \frac{x}{x_{\text{sh}}}, \qquad \theta = \omega\tau, \qquad \theta_r = \omega t_r. \tag{3.17}$$

The particle velocity v is scaled by a characteristic amplitude v_0, propagation distance x by the plane wave shock formation distance $x_{\text{sh}} = c_0^3/\beta\omega v_0^2$ for an initially sinusoidal waveform with amplitude v_0 in a lossless medium, and the time scale τ and relaxation time t_r are both scaled by a characteristic frequency ω. Substitution of Eqs. (3.17) into Eq. (3.8) results in

$$\left(1 + \theta_r \frac{\partial}{\partial\theta}\right)\left(\frac{\partial V}{\partial X} - V^2\frac{\partial V}{\partial\theta}\right) = D\theta_r \frac{\partial^2 V}{\partial\theta^2}, \tag{3.18}$$

where the constant $D = mc_0^2/2\beta v_0^2$ is the scaled relaxation strength. The corresponding dimensionless form of Eq. (3.9) is

$$\frac{\partial V}{\partial X} = V^2\frac{\partial V}{\partial\theta} + D\int_{-\infty}^{\theta} e^{-(\theta-\theta')/\theta_r}\frac{\partial^2 V}{\partial\theta'^2}\,d\theta', \tag{3.19}$$

which shows clearly the role played by the parameter D as a metric of competition between relaxation and nonlinearity. By virtue of the scaling parameters in Eqs. (3.17), one has $V = O(1)$ and $\partial/\partial\theta = O(1)$ so that the first term on the right-hand side of Eq. (3.19), which accounts for nonlinearity, is $O(1)$. Similarly, the integral in the second term on the right-hand side of Eq. (3.19) is $O(1)$, so that the second term, which accounts for relaxation, is $O(D)$. Therefore when $D \gg 1$ the second term dominates the first and relaxation effects control waveform evolution. Conversely, the first term dominates the second when $D \ll 1$, so that nonlinear effects dictate waveform evolution in that case.

3.2 Step shock

A solution of Eq. (3.18) is obtained for a step disturbance propagating into an undisturbed medium with $V = 0$ and possessing amplitude $V = 1$ far behind the wavefront. Such a waveform is stationary (i.e., $\partial V/\partial X = 0$) in the time frame $\psi = \theta + X/3$ [9], in terms of which Eq. (3.18) becomes

$$\frac{1}{3}\left(\frac{d}{d\psi} + \theta_r \frac{d^2}{d\psi^2}\right)\left(V - V^3\right) = D\theta_r \frac{d^2V}{d\psi^2}\,. \tag{3.20}$$

Equation (3.20) is integrated directly to obtain

$$\left(\frac{1}{3} - D - V^2\right)\theta_r \frac{dV}{d\psi} + \frac{1}{3}\left(V - V^3\right) = \text{const.} \tag{3.21}$$

The conditions far ahead of the wavefront are $dV/d\psi = 0$ and $V = 0$, and far behind the wavefront they are $dV/d\psi = 0$ and $V = 1$, and therefore the integration constant must be zero. The ordinary differential equation in

Eq. (3.21) is solved by separating variables:

$$\frac{3D-1+3V^2}{V-V^3}dV = \frac{d\psi}{\theta_r}. \tag{3.22}$$

Integration of the right-hand side of Eq. (3.22) is straightforward. The left-hand side is first expanded using partial fractions,

$$\frac{3D-1+3V^2}{V-V^3} = \frac{3D-1}{V} + \frac{(3D+2)V}{1-V^2}, \tag{3.23}$$

which is easily integrated. The final result is the implicit solution for the wave profile of a steady jump transition in a nonlinear, relaxing medium with cubic nonlinearity:

$$\psi = \theta_r \ln\left[\frac{V^{3D-1}}{(1-V^2)^{(3/2)D+1}}\right] + \psi_0\,. \tag{3.24}$$

The new integration constant ψ_0, which merely translates the solution relative to the coordinate ψ, is set equal to zero in what follows. Equation (3.24) is similar to the solution obtained by Polyakova et al. [22] for a steady shock wave in a relaxing fluid with quadratic nonlinearity.

In general, Eq. (3.24) cannot be inverted analytically to obtain the desired explicit solution $V(\psi)$. However, for $D \gg 1$, which indicates that nonlinearity is weak in comparison with relaxation ($\beta v_0^2/c_0^2 \ll m/2$), Eq. (3.24) can be inverted to obtain

$$V \simeq \frac{\exp(\psi/3D\theta_r)}{\sqrt{1+\exp(2\psi/3D\theta_r)}}\,, \qquad D \gg 1\,. \tag{3.25}$$

This solution describes a step shock with nominal dimensionless rise time $\psi_{\text{rise}} = 3D\theta_r$ (or dimensional rise time $t_{\text{rise}} = 3Dt_r \gg t_r$), and is equivalent to

the solution presented by Crighton [42] for a step shock in a viscous medium with cubic nonlinearity. The quantity $D\theta_r$ plays the role of a dimensionless viscous attenuation parameter in Eq. (3.25). In this case the limit of $D \gg 1$ corresponds to the low-frequency limit discussed after Eq. (3.12) because the rise time of the shock is much greater than the relaxation time.

Shown in Fig. 3.2(a) is a comparison of Eqs. (3.24) (solid curve) and (3.25) (dashed curve) for $D = 1$. Even though the strong inequality $D \gg 1$ is not satisfied, apart from a slight advance in phase the approximate solution captures the wave profile reasonably well. For $D > 5$ (not shown) the curves are nearly indistinguishable.

For $D < 1/3$, which indicates that nonlinearity is strong in comparison with relaxation ($\beta v_0^2/c_0^2 > 3m/2$), Eq. (3.24) describes a multivalued waveform. Shown in Fig. 3.2(b) is the solution for the critical value $D = 1/3$, for which an infinite slope appears at the leading edge of the wavefront at $\psi = 0$. For smaller values of D the unphysical multivalued solution can be corrected using weak-shock theory as follows.

Immediately behind the shock, which is modeled as a discontinuity, the propagation speed is the quantity c_∞ obtained in the high-frequency limit because of the rapid change in the waveform at the shock [43]. From the weak-shock relations for cubic nonlinearity given in [9] one obtains

$$\frac{dx_{\rm sh}}{dt} = \left(\frac{1}{c_\infty} - \frac{\beta v_{\rm sh}^2}{3c_0^3} \right)^{-1}, \tag{3.26}$$

where $x_{\rm sh}$ and $v_{\rm sh}$ are the position of the shock along the propagation axis and

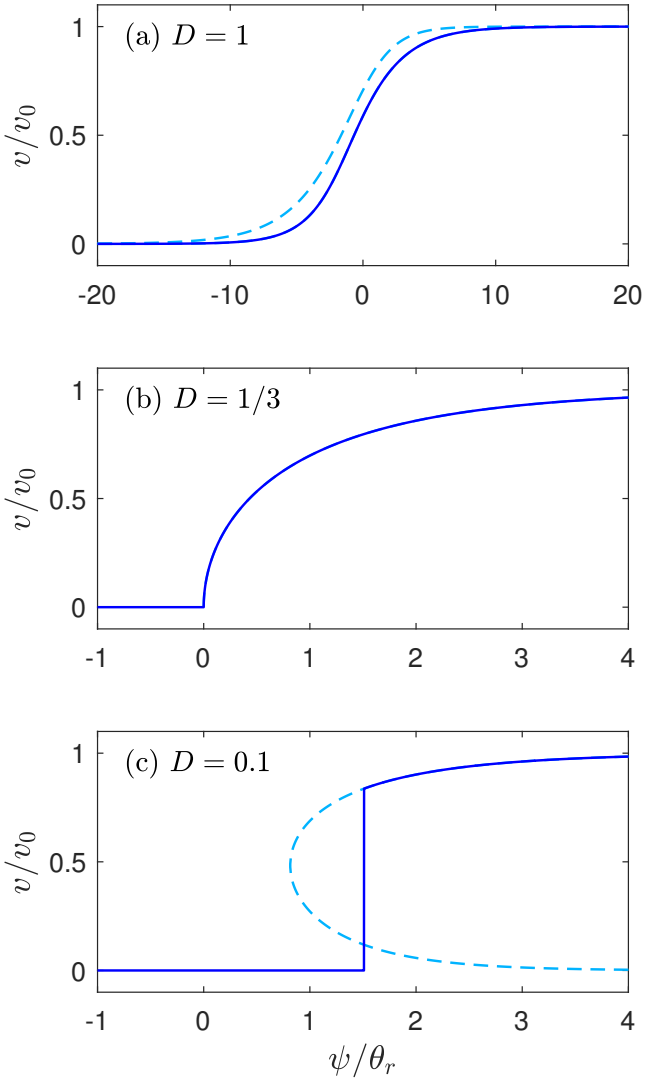

Figure 3.2: Solutions for a step shock in a relaxing medium for different values of D. (a) $D = 1$, solid curve obtained using Eq. (3.24) with $\psi_0 = 0$ and dashed curve obtained using the asymptotic relation given by Eq. (3.25). (b) $D = 1/3$, the critical value below which a multivalued solution is predicted by Eq. (3.24). (c) $D = 0.1$, vertical solid line inserted according to Eq. (3.29) based on weak-shock theory to correct the multivalued portion of the dashed waveform predicted by Eq. (3.24).

particle velocity amplitude at the shock, respectively. The shock must also be stationary relative to the retarded time ψ. The speed at which the reference frame translates is obtained by setting $d\psi = d\theta + dX/3 = 0$:

$$\left(\frac{dx}{dt}\right)_{\psi} = \left(\frac{1}{c_0} - \frac{\beta v_0^2}{3c_0^3}\right)^{-1}. \tag{3.27}$$

Equating $dx_{\rm sh}/dt$ and $(dx/dt)_\psi$ after substituting $c_\infty \simeq c_0(1 + m/2)$ yields an expression for the shock amplitude $v_{\rm sh}$. To leading order in the relaxation strength m the shock amplitude is, in dimensionless form,

$$V_{\rm sh} = \sqrt{1 - 3D}\,, \qquad D \le 1/3\,, \tag{3.28}$$

where $V_{\rm sh} = v_{\rm sh}/v_0$. The arrival time of the shock $\psi_{\rm sh}$ is obtained by substituting Eq. (3.28) into Eq. (3.24):

$$\psi_{\rm sh}/\theta_r = -\tfrac{1}{2}\ln\left[(1-3D)^{1-3D}(3D)^{2+3D}\right]\,, \qquad D \le 1/3\,, \tag{3.29}$$

where we have set $\psi_0 = 0$ as before. The result $\psi_{\rm sh} = 0$ is obtained for the critical value $D = 1/3$, which identifies the location of the leading edge of the wavefront in Fig. 3.2(b).

The dashed curve shown in Fig. 3.2(c) for $D = 0.1$ is the multivalued solution obtained from Eq. (3.24). The location of the vertical solid line representing the shock is determined by Eq. (3.29), which yields $\psi_{\rm sh}/\theta_r = 1.51$, and the corresponding shock amplitude is given by Eq. (3.28), which yields $V_{\rm sh} = 0.837$.

In general, the waveforms in Fig. 3.2 are qualitatively the same as those for a step shock in a relaxing fluid with quadratic nonlinearity [22].

3.3 Evolution of an initially sinusoidal waveform

In order to illustrate the combined effects of nonlinearity and relaxation for a periodic waveform, numerical simulations were performed using the algorithm described in [41] following minor modification to account for cubic nonlinearity. In order to stabilize shocks that develop in the waveform, a term that accounts for classical viscous losses is added to Eq. (3.18) so that the equation to be solved numerically in this section is

$$\left(1+\theta_r\frac{\partial}{\partial\theta}\right)\left(\frac{\partial V}{\partial X}-V^2\frac{\partial V}{\partial\theta}-A\frac{\partial^2 V}{\partial\theta^2}\right)=D\theta_r\frac{\partial^2 V}{\partial\theta^2}, \tag{3.30}$$

where the dimensionless viscous attenuation parameter is $A = \alpha_{\rm tv}x_{\rm sh}$ and $\alpha_{\rm tv} = \eta\omega^2/2\rho c_0^3$ is the viscous attenuation coefficient [13]; see also Sec. 2.2.1. Shown in the first row of Fig. 3.3 are simulated shear waveforms at $X = 3$ (solid curves) for an initially sinusoidal waveform $V = \sin\theta$ at $X = 0$ (dashed curves) in a viscous medium [Fig. 3.3(a)] and a relaxing medium [Fig. 3.3(b)]. The waveforms in Fig. 3.3(a) were obtained from Eq. (3.30) with $D = 0$ and $A = 10^{-3}$. This value of A is sufficiently small that for propagation out to $X = 3$ the simulations are in agreement with weak-shock theory; that is, the effect of viscosity is negligible except at the shocks, which resemble discontinuities on the scale of the periodicity of the waveform. The waveforms in Fig. 3.3(b) were obtained from Eq. (3.30) with $D = 0.25$, $\theta_r = 1$, and $A = 10^{-3}$. Because the value of D is sufficiently small for shock formation to occur (see Chapter 4), the viscous loss term in Eq. (3.30) is needed in order to simulate results that agree with weak-shock theory.

The waveform in Fig. 3.3(a) for a shear wave in a viscous medium exhibits the characteristic distortion reported elsewhere [8, 9, 13, 17, 11], most notably the appearance of two shocks per period. The waveform in Fig. 3.3(b) for a shear wave in a relaxing medium exhibits rounding of the waveform just behind each shock, similar to that which occurs for compressional waves in

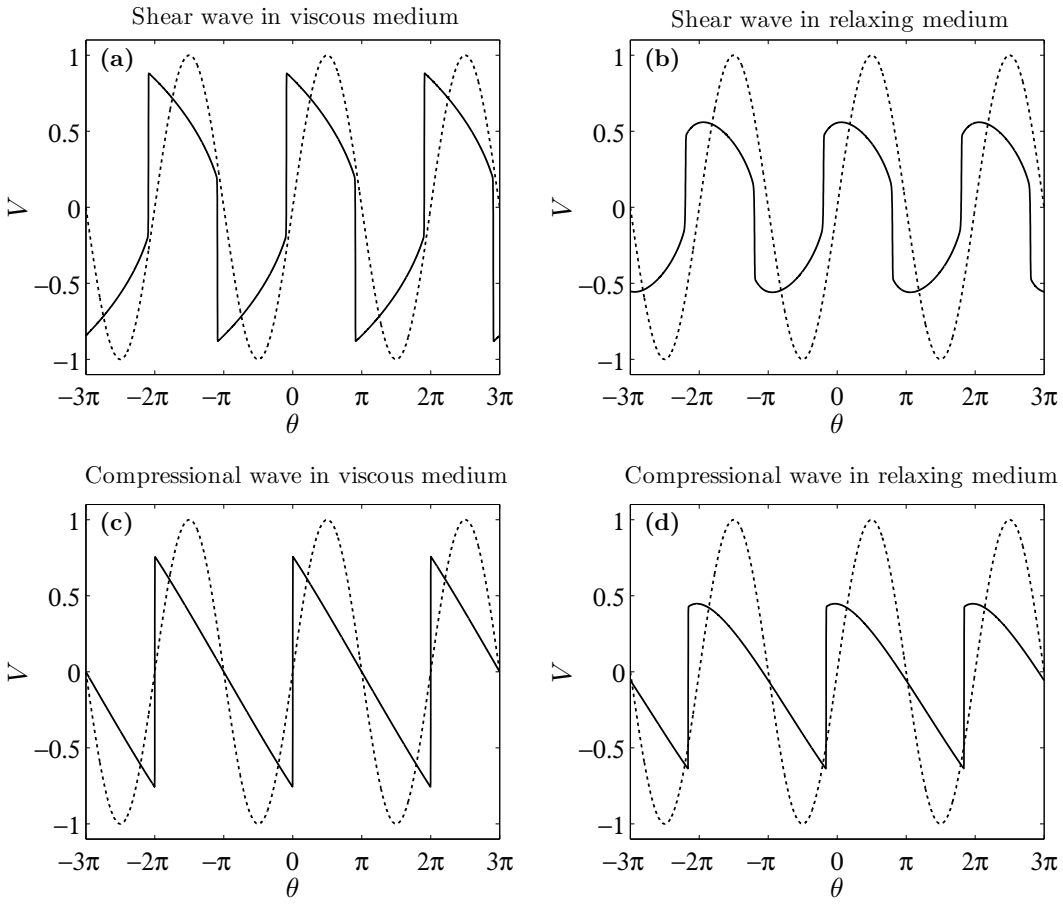

Figure 3.3: Numerical simulation of initially sinusoidal waveform at $X = 0$ (dashed curves) out to $X = 3$ (solid curves) for a shear wave (upper row) and a compressional wave (lower row) in a viscous medium (left column) and in a relaxing medium (right column).

relaxing fluids. Note that the nonlinear shear waveform remains symmetric, i.e., $V(X, \theta + \pi) = -V(X, \theta)$ for all X, even in a relaxing medium. This relation applies to any Fourier series containing only odd harmonics regardless of their amplitudes and phases.

For comparison, Figs. 3(c) and (d) in the lower row repeat Figs. 3(a) and (b) in the upper row but for quadratic nonlinearity, e.g., for compressional waves in a fluid. Propagation in a viscous fluid, Fig. 3.3(c), was simulated by solving Eq. (3.30) with V^2 replaced by V in the first term on the right-hand side and with $D = 0$ and $A = 10^{-3}$. To simulate propagation in a relaxing fluid, Fig. 3.3(d), the same modified form of Eq. (3.30) as used for Fig. 3.3(c) was solved, but with D replaced by $D' = mc_0/2\beta v_0$ [41], and with the same parameter values used as in Fig. 3.3(b): $D' = 0.25$, $\theta_r = 1$, and $A = 10^{-3}$. As for the simulation of shear waves in a relaxing medium, viscous loss is utilized in Eq. (3.30) to account for shock formation.

3.4 Limiting cases

Three limiting cases of Eq. (3.18) are developed in this section. The case of weak nonlinearity is examined in Sec. 3.4.1, where a solution for harmonic generation in the field generated by a time harmonic source is presented. A Kortweg-de Vries (KdV) equation is obtained from Eq. (3.18) in Sec. 3.4.2 in the limit of low frequency wave motion. Finally, an exact solution is obtained for the approximate form of Eq. (3.18) in the limit of very high frequency motion in Sec. 3.4.3.

3.4.1 Weak nonlinearity

When nonlinearity is weak compared to relaxation, i.e., $D \gtrsim 1$, small deviations from the linear solution may be determined by considering third-harmonic generation in the field generated by a harmonic source. Let the source condition be $V(\theta, 0) = \sin\theta = \mathrm{Im}\{e^{j\theta}\}$ and assume a solution of the form

$$V = V_1 + V_3, \qquad |V_1| \gg |V_3|, \tag{3.31}$$

where the fundamental and third harmonic are expressed as

$$V_1 = \mathrm{Im}\{\widetilde{V}_1(X)e^{j\theta}\} = \frac{1}{2}\widetilde{V}_1(X)e^{j\theta} - \text{c.c.}, \tag{3.32}$$

$$V_3 = \mathrm{Im}\{\widetilde{V}_3(X)e^{j3\theta}\} = \frac{1}{2}\widetilde{V}_3(X)e^{j3\theta} - \text{c.c.}, \tag{3.33}$$

and c.c. denotes the complex conjugate. Substitution of Eqs. (3.32) and (3.33) into Eq. (3.18) following the method of successive approximations yields two ordinary differential equations for the complex amplitudes:

$$\frac{d\widetilde{V}_1}{dX} + \zeta_1\widetilde{V}_1 = 0, \qquad \widetilde{V}_1(0) = 1, \tag{3.34}$$

$$\frac{d\widetilde{V}_3}{dX} + \zeta_3\widetilde{V}_3 = \frac{j}{4}\widetilde{V}_1^3, \qquad \widetilde{V}_3(0) = 0, \tag{3.35}$$

where

$$\zeta_n = \widetilde{\alpha}(n\omega)x_{\mathrm{sh}} = \frac{n^2 D\theta_r}{1 + jn\theta_r} = \frac{n^2 D\theta_r}{1 + n^2\theta_r^2} - j\frac{n^3 D\theta_r^2}{1 + n^2\theta_r^2}, \tag{3.36}$$

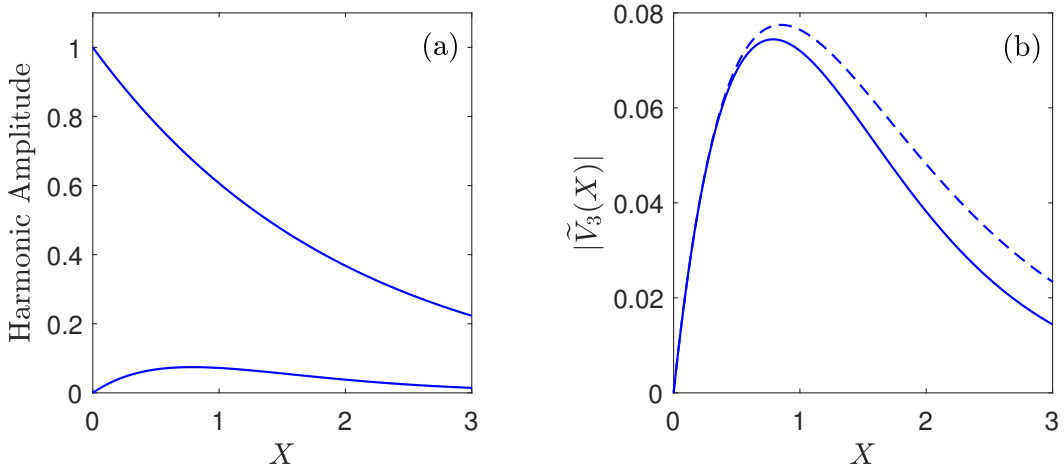

Figure 3.4: Harmonic amplitudes in the field generated by a time harmonic source with $D = 1$ and $\theta_r = 1$. (a) Fundamental and third harmonic amplitudes given by Eqs. (3.37) and (3.38), respectively. (b) Third harmonic amplitude with (solid) and without (dashed) dispersion.

and $\widetilde{\alpha}$ is given by the second of Eqs. (3.10). The differential equations are solved sequentially to obtain

$$\widetilde{V}_1 = e^{-\zeta_1 X}, \tag{3.37}$$

$$\widetilde{V}_3 = \frac{j}{4}\frac{e^{-3\zeta_1 X} - e^{-\zeta_3 X}}{\zeta_3 - 3\zeta_1}. \tag{3.38}$$

These solutions may be compared with those for second-harmonic generation in a monorelaxing fluid [44].

The amplitudes of the fundamental and third harmonic are presented in Fig. 3.4(a) for parameter values of $D = 1$ and $\theta_r = 1$, which correspond to a source amplitude that results in relatively weak nonlinearity [see Eq. (3.25) and Fig. 3.2(a)] and a frequency for which there is a relatively significant difference in the phase speeds for the fundamental and third harmonic. While the

amplitude at the source frequency is monotonically decreasing with distance, the amplitude of the third harmonic initially increases close to the source as energy is transfered from the fundamental into the third harmonic because of nonlinearity. Farther from the source, the third harmonic amplitude reaches a peak value as attenuation effects dominate those of nonlinearity. Following this peak, both harmonic amplitudes decrease monotonically.

Dispersion is relatively weak in a relaxing medium compared to attenuation, and so a relatively simple analytical estimate of the distance at which the maximum amplitude of the third harmonic occurs for weak nonlinearity may be obtained by ignoring dispersion altogether, which is equivalent to ignoring the imaginary part of Eq. (3.36). Doing so yields the following approximation of the distance at which the third harmonic achieves its maximum amplitude:

$$X_3 \simeq \frac{\ln(\zeta_3^r/3\zeta_1^r)}{\zeta_3^r - 3\zeta_1^r}, \tag{3.39}$$

where $\zeta_n^r = \mathrm{Re}\{\zeta_n\} = n^2 D\theta_r/(1+n^2\theta_r^2)$. This approximation agrees to within 10% of the result obtained when dispersion is included by retaining the imaginary part of ζ_n in Eq. (3.36). Third harmonic amplitudes are plotted with and without dispersion taken into account in Fig. 3.4(b). The effect of dispersion is a reduction in efficiency of nonlinear energy transfer to the third harmonic, resulting in the solid curve lying underneath the dashed curve in Fig. 3.4 for all X.

Measurement of third harmonic generation can be used to determine the nonlinear and viscoelastic material properties of a material. Equations (3.37)–

(3.39) provide the necessary set of relations for inferring D, θ_r, and β from measurements of the evolution of the fundamental and third harmonic fields. Such a measurement has been reported for a material characterized by classical viscous losses [14].

3.4.2 Low frequency waves

Asymptotic forms of the model equation are obtained at low and high frequencies by first rewriting Eq. (3.18) as

$$\frac{\partial V}{\partial X} - V^2 \frac{\partial V}{\partial \theta} = D\theta_r L_R \frac{\partial^2 V}{\partial \theta^2}, \tag{3.40}$$

where $L_R = (1 + \theta_r \, \partial_\theta)^{-1}$ is a linear operator and $\partial_\theta \equiv \partial/\partial\theta$. In terms of dimensional quantities one has $\theta_r \partial_\theta = t_r \partial_\tau$, and therefore this quantity represents the ratio of the relaxation time to the characteristic time scale of the waveform. For a sinusoidal waveform $\theta_r \partial_\theta$ thus corresponds to ωt_r, and for a pulse which decays exponentially as e^{-t/t_0} it corresponds to t_r/t_0.

At very low frequencies relative to the relaxation time, i.e., $O(\theta_r \partial_\theta) \ll 1$, the operator L_R may be expanded as

$$L_R = 1 - \theta_r \partial_\theta + O[(\theta_r \partial_\theta)^2], \tag{3.41}$$

and Eq. (3.40) becomes, up to $O[(\theta_r \partial_\theta)^2]$,

$$\frac{\partial V}{\partial X} - V^2 \frac{\partial V}{\partial \theta} = D\theta_r \frac{\partial^2 V}{\partial \theta^2} - D\theta_r^2 \frac{\partial^3 V}{\partial \theta^3}, \qquad O(\theta_r \partial_\theta) \ll 1. \tag{3.42}$$

The first term on the right-hand side of Eq. (3.42) is a viscous loss term with dimensionless attenuation coefficient $D\theta_r$. The second term results in dispersion equivalent to that described by the Kortweg–de Vries (KdV) equation.

3.4.3 High frequency waves

At very high frequencies relative to the relaxation time, i.e., $O(\theta_r\partial_\theta) \gg 1$, the operator L_R may be expanded as

$$\begin{aligned} L_R &= (\theta_r\partial_\theta)^{-1}\left[1 + (\theta_r\partial_\theta)^{-1}\right]^{-1} \\ &= (\theta_r\partial_\theta)^{-1} - (\theta_r\partial_\theta)^{-2} + O\left[(\theta_r\partial_\theta)^{-3}\right], \end{aligned} \tag{3.43}$$

where the antiderivatives ∂_θ^{-1}, etc., correspond to integrations. Keeping the first two terms in the expansion yields the following limiting form of Eq. (3.18) for high frequencies:

$$\frac{\partial V}{\partial X} - V^2\frac{\partial V}{\partial \theta} = D\frac{\partial V}{\partial \theta} - \frac{D}{\theta_r}V, \qquad O(\theta_r\partial_\theta) \gg 1. \tag{3.44}$$

The first term on the right-hand side of Eq. (3.44) shifts the reference phase speed from c_0 at low frequencies to c_∞ at high frequencies. The second term accounts for the frequency-independent losses that are associated with relaxation at high frequencies.

The change of variables

$$Q = e^{DX/\theta_r}V, \qquad Z = \frac{1 - e^{-2DX/\theta_r}}{2D/\theta_r}, \qquad \Theta = \theta + DX \tag{3.45}$$

is applied to Eq. (3.44), thereby transforming it into the simple-wave equation,

$$\frac{\partial Q}{\partial Z} = Q^2\frac{\partial Q}{\partial \Theta}, \tag{3.46}$$

which has the implicit solution

$$Q = F\left(\Theta + ZQ^2\right), \tag{3.47}$$

where $F(\theta) = V(\theta, 0) = Q(\Theta, 0)$ is the initial waveform radiated by a source at $X = 0$. Substitution of Eqs. (3.45) into Eq. (3.47) yields the following implicit solution of Eq. (3.44):

$$V = e^{-DX/\theta_r} F\left(\theta + DX + \frac{e^{2DX/\theta_r} - 1}{2D/\theta_r} V^2\right). \tag{3.48}$$

Far from the source the stretched coordinate Z approaches a constant value:

$$Z \to \frac{\theta_r}{2D} = \frac{l_r}{2x_{\text{sh}}}, \qquad x \gg l_r, \tag{3.49}$$

where $l_r \equiv 2c_0 t_r/m$ is a relaxation length scale equal to the attenuation length at high frequencies ($l_r = 1/\alpha$, $\omega t_r \gg 1$). Thus for $x \gg l_r$ the waveform no longer distorts but only decays uniformly in amplitude. The disappearance of further nonlinear evolution of a waveform at large distances is known as waveform freezing [45].

Any solutions of the simple-wave equation (3.46) may be transformed using Eqs. (3.45) to describe plane nonlinear shear waves in a relaxing medium at high frequencies. For example, if the waveform is initially a sinusoid with $F(\theta) = \sin\theta$, then shock formation occurs at $Z = 1$, or in terms of X at

$$X_{\text{sh}} = -\frac{\ln(1 - 2D/\theta_r)}{2D/\theta_r}, \qquad \frac{D}{\theta_r} < \frac{1}{2}. \tag{3.50}$$

The shock formation distance reduces to $X_{\text{sh}} \approx 1 + D/\theta_r$ for $D \ll 1$, and it increases to infinity in the limit $D \to \theta_r/2$. At distances $X > X_{\text{sh}}$ Eq. (3.48) describes a multivalued waveform. Multivalued waveforms must be corrected using weak-shock theory. Shock formation will not occur for $D/\theta_r = x_{\text{sh}}/l_r >$

1/2. Shock formation in an initially sinusoidal shear wave in a relaxing medium is the subject of Chapter 4.

The evolution of a shock front followed by a short tail propagating into an undisturbed relaxing medium with cubic nonlinearity may be described as follows. The requirement that the transient following the shock be short, $t_{\rm pulse} \ll t_r$, is a result of the high-frequency approximation; see the discussion following Eq. (3.40). The shock amplitude as a function of propagation distance is obtained using the extension of Whitham's [46] head-shock integral to cubic nonlinearity,

$$ZQ_{\rm sh}^3 = \frac{3}{2}\int_0^{\Phi_{\rm sh}} F(\Phi)\, d\Phi, \tag{3.51}$$

which is derived in Appendix A. In Eq. (3.51), $Q_{\rm sh}$ and $\Phi_{\rm sh}$ are the values of Q and $\Phi = \Theta + ZQ^2$ at the shock, and $V(\theta, 0) = Q(\Theta, 0) = F(\theta)H(\theta)$ is the initial shape of the pulse, where $H(\theta)$ is the Heaviside step function. Evaluation of the integral in Eq. (3.51) leads to an expression relating the shock amplitude $Q_{\rm sh}$ to Z, from which one obtains $\Theta_{\rm sh} = F^{-1}(Q_{\rm sh}) - ZQ_{\rm sh}^2$ for the arrival time of the shock. Using the transforms given by Eqs. (3.45) one finds that the shock amplitude is

$$V_{\rm sh} = e^{-DX/\theta_r} Q_{\rm sh}, \tag{3.52}$$

and that the arrival time of the shock is

$$\theta_{\rm sh} = F^{-1}(e^{DX/\theta_r} V_{\rm sh}) - \frac{e^{2DX/\theta_r} - 1}{2D/\theta_r} V_{\rm sh}^2 - DX. \tag{3.53}$$

Inspection of Eq. (3.51) reveals that for large Z one obtains the proportionalities $Q_{\rm sh} \propto Z^{-1/3}$ and $\Theta_{\rm sh} \propto -Z^{1/3}$. In the far field ($X \to \infty$) Z approaches

a constant value and one obtains $V_{\rm sh} \propto e^{-DX/\theta_r}$ for the shock amplitude and $\theta_{\rm sh} \propto -DX$ for the shock arrival time.

This section concludes with application of the general weak-shock solution given by Eqs. (3.51)–(3.53) to the case of radiation of a shock followed initially by an exponential tail. Let $F(\theta) = e^{-\theta/\theta_0}$, where $\theta_0 \ll \theta_r$ (i.e., $t_0 \ll t_r$) determines the initial decay rate of the pulse. Evaluation of Eq. (3.51) yields the cubic polynomial

$$\frac{2}{3}\frac{Z}{\theta_0}Q_{\rm sh}^3 + Q_{\rm sh} - 1 = 0, \tag{3.54}$$

which may be combined with Eq. (3.52) to obtain an analytical expression for $V_{\rm sh}$:

$$V_{\rm sh} = e^{-DX/\theta_r}\left(\frac{1}{\xi} - \frac{\theta_0}{2Z}\xi\right), \tag{3.55}$$

where

$$\xi = \left[6\frac{Z^2}{\theta_0^2}\left(\sqrt{1+\frac{2}{9}\frac{\theta_0}{Z}} - 1\right)\right]^{1/3}. \tag{3.56}$$

Equation (3.53) yields

$$\theta_{\rm sh} = -\theta_0 \ln V_{\rm sh} - \frac{e^{2DX/\theta_r} - 1}{2D/\theta_r}V_{\rm sh}^2 - \left(1 + \frac{\theta_0}{\theta_r}\right)DX \tag{3.57}$$

for the shock arrival time. The pulse distorts as it propagates, increasing in duration as the shock advances. In particular, the time required for the tail to decay to $e^{-1}V_{\rm sh}$ is an increasing function of the propagation distance:

$$\theta_{\rm decay} = \theta_0\left(1 + \frac{e^{2DX/\theta_r} - 1}{2D\theta_0/\theta_r}V_{\rm sh}^2\right). \tag{3.58}$$

The $1/e$ decay time of the pulse increases due to nonlinear distortion, but use of the asymptotic relation $V_{\rm sh} \propto e^{-DX/\theta_r}$ in Eq. (3.58) reveals that it

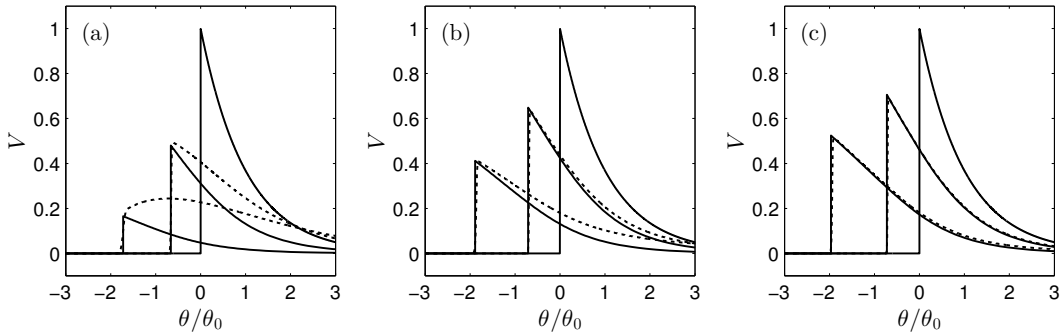

Figure 3.5: Comparison of the analytical weak-shock solution of Eq. (3.44) (solid curves) with numerical solutions of Eq. (3.30) (dashed curves) for a shock followed initially by an exponential tail at $X = 0$ as it propagates out to $X = 1$ and $X = 3$ for $D = 0.5$ and three initial pulse durations relative to relaxation time: (a) $t_0/t_r = 1$, (b) $t_0/t_r = 0.3$, and (c) $t_0/t_r = 0.1$.

approaches a constant value for large X. The constant value of the $1/e$ decay time is another illustration of waveform freezing, as the shape of the waveform no longer distorts due to nonlinearity.

Figure 3.5 compares the above analytical solution of Eq. (3.44) (solid curves) for a shock followed initially at $X = 0$ by an exponential tail with numerically simulated waveforms obtained from Eq. (3.30) at $X = 1$ and $X = 3$ (dashed curves) for several initial pulse durations $\theta_0/\theta_r = t_0/t_r$. As in Sec. 3.3, a small amount of viscous loss is necessary to stabilize the shocks so that the solutions agree with weak shock theory. Insofar as Eqs. (3.48), (3.55), and (3.57) comprise a weak-shock solution of Eq. (3.44), a more general purpose of Fig. 3.5 is to ascertain the frequency range in which Eq. (3.44) provides a good approximation of Eq. (3.18) for modeling the evolution of a transient waveform containing a shock. As shown in Fig. 3.5(a) for $t_0/t_r = 1$,

the analytical solution of Eq. (3.44) captures the amplitude and arrival time of the shock even for a pulse that has duration comparable to the relaxation time, although there is poor agreement for the tail following the shock. The better agreement at the shock than for the tail is to be expected because the shock is characterized by much more rapid motion than the tail, and Eq. (3.44) is a high-frequency approximation of Eq. (3.18). Description of the tail by the analytical solution of Eq. (3.44) becomes more accurate as t_0/t_r decreases to $t_0/t_r = 0.3$ in Fig. 3.5(b) and finally $t_0/t_r = 0.1$ in Fig. 3.5(c), which indicates good agreement out to at least $X = 3$. The convergence of the tail for $t_0/t_r \ll 1$ is consistent with the high-frequency restriction on Eq. (3.44).

Chapter 4

Overturning of an Initially Sinusoidal Shear Wave

Equation (3.8) derived in Chapter 3 for the evolution of a shear waveform in a nonlinear, relaxing medium can have solutions that are multivalued at a finite distance from the source, meaning that the model equation predicts that the wave variable possesses multiple values at the same point in time and space (see, e.g., Secs. 3.2 and 3.4.3). This phenomenon was referred to by Hammerton and Crighton [30, 31] as *waveform overturning* because of the resemblance of the multivalued solutions with the common sight of gravity waves on water that 'break.' Overturning of a nonlinear acoustic wave is a well studied process; one of the earliest encounters with overturning of an acoustic waveform occurred more than 170 years ago, the amusing story of which is documented in Appendix B.

Multivalued solutions represent a failure of the evolution equation to

---

Selected material from this chapter was previously published in J. M. Cormack and M. F. Hamilton, "Plane nonlinear shear waves in relaxing media," *J. Acoust. Soc. Am.* **143**, 1035–1048 (2018), and J. M. Cormack and M. F. Hamilton, "Overturning of nonlinear compressional and shear waves subject to power-law attenuation or relaxation," *Wave Motion* **85**, 18–33 (2019), which appear as Refs. [32] and [53], respectively, in this dissertation. Contributions from JMC include derivation of transformed equations of motion, numerical solution of those equations, validation of solutions, and writing of the article.

properly account for the underlying physics. It was Stokes [47] who first pointed out that the lossless model for acoustic waves of finite amplitude must break down at the instant of shock formation, and that viscosity limits waveform steepening such that multivalued waveforms cannot exist in real media. By accounting for viscosity and heat conduction in a fluid, Taylor [48] derived an expression for a steady shock profile for weak but finite jumps in acoustic pressure, revealing explicitly the competition between nonlinear waveform steepening and energy dissipation. "In a nutshell," observed Blackstock [6], "nonlinearity makes a wave interesting, dissipation keeps it honest." Thus waveform overturning is avoided by balancing nonlinearity with the inclusion of additional mechanisms for energy loss, such as thermoviscous absorption, in the nonlinear evolution equation, or by supplementing the model equations with weak shock theory [49]. Overturning of a nonlinear shear wave is a similar mathematical phenomenon; in the absence of dispersion it has been studied in detail using weak shock theory [9, 8].

Attenuation and dispersion due to relaxation are not always sufficient to balance nonlinear waveform steepening and prevent waveform overturning. Multivalued solutions are avoided in Chapter 3 of this dissertation by including viscous losses in Eq. (3.30) for the numerical solutions presented in Sec. 3.3, and by supplementing solutions of Eq. (3.8) using weak shock theory in Sec. 3.2 in the case of a step shock profile, and in Sec. 3.4.3 in the high frequency limit. In the cases of the step shock or a high frequency waveform, analytical solutions reveal the minimum source amplitude above which waveform overturning

occurs, and below which it does not. However, unlike Eqs. (3.24) and (3.48), no analytical solution is available for a periodic waveform in a relaxing medium with frequencies that are low or intermediate in relation to the relaxation frequency, defined as $\omega_r = 1/t_r$. In particular, and of interest here, the minimum source amplitude for shock formation in an initially sinusoidal waveform must be determined numerically.

Direct numerical solution of Eq. (3.8) cannot reliably determine conditions for the existence of multivalued solutions because numerical dispersion and dissipation introduce unavoidable inaccuracies in conventional numerical schemes, such as the finite difference algorithm used in Sec. 3.3, as the gradient becomes very large. To circumvent this impediment while studying waveform overturing of nonlinear acoustic waves in a relaxing fluid, Hammerton and Crighton [30] developed a reformulation of the evolution equation in *intrinsic coordinates* that enables accurate numerical simulation of waveform evolution up to and beyond the point at which a waveform first becomes multivalued. Using their formulation in intrinsic coordinates, Hammerton and Crighton were able to determine the minimum source amplitude of an initially sinusoidal acoustic waveform above which waveform overturning occurs at a finite distance from the source [31].

In this chapter, the approach of Hammerton and Crighton [30, 31] is applied to shear waves in a relaxing medium. The intrinsic coordinate system is introduced in Sec. 4.1, where the form of Eq. (3.19) in intrinsic coordinates is presented. A detailed derivation of the coordinate transformation and develop-

ment of the evolution equation in intrinsic coordinates is given in Appendix C. Based on numerical solutions of the evolution equation in intrinsic coordinates, the minimum source amplitude above which an initially sinusoidal shear wave in a relaxing medium will become multivalued at a finite distance from the source is determined numerically in Sec. 4.2 over a broad range of frequencies. Finally, for source amplitudes above the critical amplitude determined in Sec. 4.2, the distance from the source at which a vertical tangent first appears in the waveform, denoting the onset of overturning, is determined in Sec. 4.3.

In the limits of low and high frequencies, a relaxing material has an attenuation coefficient that is proportional to frequency raised to an exponent, i.e., $\alpha \propto \omega^{\nu}$, where $\nu = 2$ and $\nu = 0$ at low and high frequencies, respectively. So-called power-law attenuation of this kind, but with an exponent that is not necessarily an integer and is in the range $0 \leq \nu \leq 2$, has been observed for shear waves in brain tissue [50], tissue-mimicking phantoms [51], and polymers [52], for example. The corresponding analysis and results that are presented in this chapter for overturning of shear waves in a relaxing medium are presented for shear waves in a medium that exhibits power-law attenuation, and the accompanying dispersion, in Appendix D. The content of this chapter and of Appendix D can be found in Ref. [53], along with similar treatments of waveform overturning for nonlinear compressional waves in either relaxing or power-law media.

4.1 Intrinsic coordinates

The form of the evolution equation to be solved in this chapter is the dimensionless form given in Eq. (3.19), with the dimensionless quantities V, θ, and X defined in Eqs. (3.17). The intrinsic coordinates that describe a waveform $V(\theta)$ at a propagation distance X are the angle $\psi(\theta)$ of the tangent to the waveform and the corresponding arc length $s(\theta)$ along the waveform from $V(0)$ to $V(\theta)$:

$$\psi = \tan^{-1}\left(\partial V/\partial\theta\right), \qquad s = \int_0^\theta \sqrt{1 + \left(\partial V/\partial\theta\right)^2}\, d\theta\,. \tag{4.1}$$

For example, a waveform given by $V = \sin\theta$ in physical coordinates is shown in Fig. 4.1(a), and the corresponding waveform in intrinsic coordinates in Fig. 4.1(b). Evolution of the waveform is then described by $\psi(X, s)$ rather than $V(X, \theta)$. Transformation of the solution for $\psi(X, s)$ back to a particle velocity waveform is accomplished via the integrals

$$V = V_0(X) + \int_0^s \sin\psi\, ds\,, \qquad \theta = \int_0^s \cos\psi\, ds\,, \tag{4.2}$$

where $V_0(X) = V(X, 0)$. In what follows it is assumed that $V_0(X) = 0$, even in the presence of the dispersion that results from relaxation, because the source waveform is expressed only for $\theta \geq 0$ and zero-padded sufficiently that the condition $V_0(X) = 0$ is maintained throughout the simulated evolution of the waveform. If $V_0(X) \neq 0$ then an additional term appears in the evolution equation for $\psi(X, s)$ and an additional evolution equation for $V_0(X)$ is required [see Eqs. (3.10) and (3.11) in Ref. [30]].

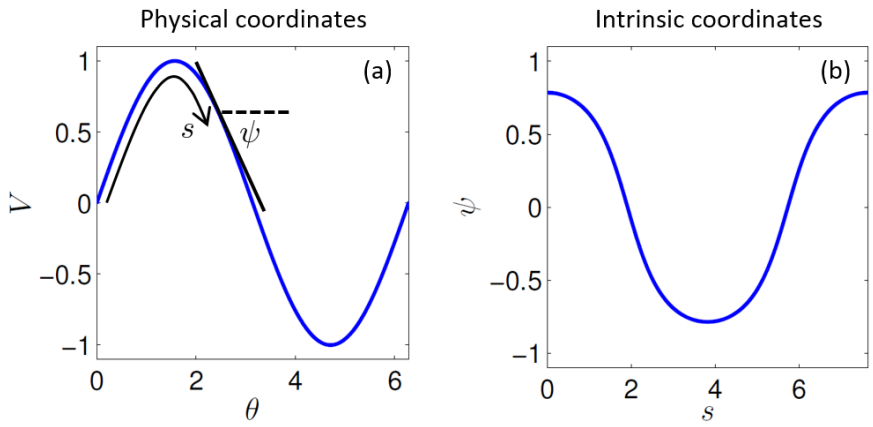

Figure 4.1: (a) A waveform given by $V = \sin\theta$ in physical coordinates, and (b) the corresponding waveform in intrinsic coordinates.

After transformation of Eq. (3.19) into intrinsic coordinates (see Appendix C for details), the evolution equation becomes

$$\frac{\partial\psi}{\partial X} = 2\sin^2\psi\int_0^s \sin\psi\,ds + 2\frac{\partial\psi}{\partial s}\int_0^s \sin\psi\cos\psi\left(\int_0^s \sin\psi(s')\,ds'\right)ds + D\left(\frac{\partial f}{\partial s} + \frac{\partial\psi}{\partial s}\int_0^s f(\psi)\frac{\partial\psi}{\partial s}\,ds\right), \tag{4.3}$$

where

$$f(\psi) = \sin\psi - \frac{1}{\theta_r}\exp\left(-\frac{1}{\theta_r}\int_0^s \cos\psi\,ds\right) \times \cos\psi\int_0^s \exp\left(\frac{1}{\theta_r}\int_0^s \cos\psi(s')\,ds'\right)\sin\psi\,ds. \tag{4.4}$$

Waveform steepening accounted for by the first two terms on the right-hand side of Eq. (4.3) is symmetric about $\psi = 0$ because the distortion is due to the cubic nonlinearity in Eq. (3.19). The last two terms in Eq. (4.3), which depend on the function $f(\psi)$ given by Eq. (4.4), are responsible for attenuation and dispersion due to relaxation.

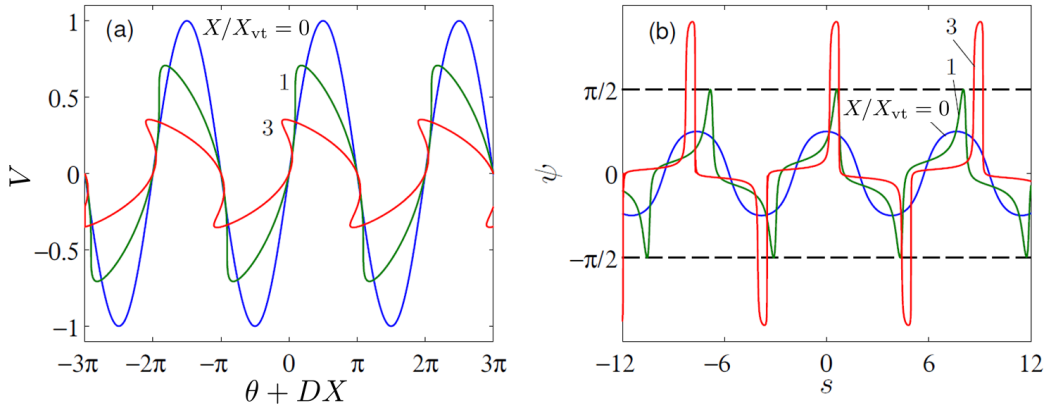

Figure 4.2: Simulation of an initially sinusoidal shear waveform in a relaxing medium with very high frequency ($\theta_r \gg 1$). (a) Physical waveforms: initial sinusoidal waveform (blue), a waveform that has developed vertical tangents (green), and a multivalued waveform that has overturned (red). (b) Corresponding waveforms in intrinsic coordinates.

An example calculation is presented in Fig. 4.2 for an initially sinusoidal shear wave with source frequency large compared to the relaxation frequency ($\theta_r \gg 1$). This case was chosen because of the availability of an implicit analytical solution, namely that presented in Eq. (3.48). A value of $D = \theta_r/4$ was chosen to ensure that waveform overturning would occur according to Eq. (3.50). The sinusoidal source waveform in physical coordinates [blue curve in Fig. 4.2(a)] is transformed into intrinsic coordinates using Eqs. (4.1), and is presented as the blue curve in Fig 4.2(b). The evolution of $\psi(X, s)$ is then determined via numerical solution of Eq. (4.3) by marching forward in X. Distorted waveforms in intrinsic coordinates are presented as the green and red curves in Fig. 4.2(b) at distances of $X/X_{\rm vt} = 1$ and 3, respectively, where

$X_{\rm vt}$ is given by Eq. (3.50). The green and red physical waveforms in Fig. 4.2(a) are recovered from those in Fig. 4.2(b) using Eqs. (4.2). Shock formation occurs at $X = X_{\rm vt}$ [green curves in Figs. 4.2(a) and 4.2(b)] when ψ achieves a value of $\pi/2$, indicating that a vertical tangent has appeared in the particle velocity waveform. At greater distances, the waveform in intrinsic coordinates has regions for which $|\psi| > \pi/2$ [red curve in Fig. 4.2(b)], corresponding to a physical waveform that is multivalued [red curve in Fig. 4.2(a)]. The waveforms in Fig. 4.2(a) are indistinguishable from the analytical solution presented in Eq. (3.48).

4.2 Critical source amplitude for waveform overturning

The criterion for waveform overturning during propagation of an initially sinusoidal plane shear wave in a relaxing medium is determined in this section via numerical solution of Eq. (4.3). Waveform overturning is characterized by the critical value of the scaled relaxation strength $D_{\rm cr}(\theta_r)$, which is the smallest value of D (largest value of v_0) for which shock formation does not occur for the source frequency given by $\theta_r = \omega t_r$, and thus the minimum (or critical) source amplitude for shock formation is given by

$$v_{\rm cr} = c_0 \sqrt{\frac{m}{2\beta D_{\rm cr}}} \,. \tag{4.5}$$

The critical source amplitude for which waveform overturning occurs at a finite distance from the source in an initially sinusoidal plane shear wave propagating in a relaxing medium is determined as follows. The source condition $V(0, \theta) =$

$\sin\theta$ is transformed into intrinsic coordinates using Eqs. (4.1) and the evolution equation in intrinsic coordinates presented in Eq. (4.3) is solved numerically by marching forward in X until either the function $|\psi|$ achieves a value of $\pi/2$, indicating that overturning has occurred, or until the maximum value of $|\psi|$ begins to decrease as the waveform propagates, indicating that attenuation and dispersion due to relaxation have kept waveform steepening in check such that the waveform remains single-valued for all X. The critical source amplitude that results in waveform overturning, if it exists, is found in this manner through iteration.

The evolution equation is solved numerically by approximating derivatives on the right-hand sides of Eqs. (4.3) and (4.4) using second-order central finite differences and by approximating integrals using Simpson's rule. The time waveform is discretized using approximately 2000 points per cycle. Marching forward in X proceeds with a first-order Euler method using a step size of approximately 5×10^{-6}.

The computed curve for $D_{\rm cr}(\theta_r)$ is presented in Fig. 4.3(a). As indicated, shock formation (or a multivalued waveform) occurs in the parameter space below the curve, and not in the parameter space above. The low- and high-frequency asymptotes shown as the dashed lines are

$$D_{\rm cr} = 1/3, \qquad \theta_r \ll 1, \tag{4.6}$$

$$= \theta_r/2, \qquad \theta_r \gg 1. \tag{4.7}$$

The high-frequency asymptote, $D_{\rm cr} = \theta_r/2$, is obtained from the analytical

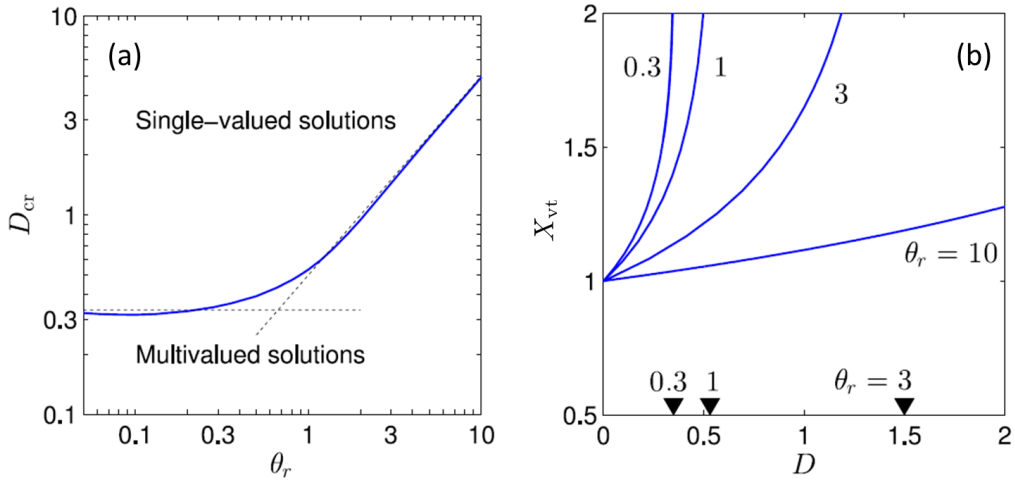

Figure 4.3: (a) Critical value of $D = mc_0^2/2\beta v_0^2$ as a function of $\theta_r = \omega t_r$ below which an initially sinusoidal shear wave radiated at frequency ω with amplitude v_0 will form a shock after propagating a finite distance, and above which shock formation does not occur. The asymptotes (dashed lines) are given by Eqs. (4.6) and (4.7). (b) Distance X_{vt} from the source at which a vertical tangent first develops in an initially sinusoidal shear waveform in a relaxing medium as a function of the scaled relaxation strength D for several values of source frequency θ_r. Triangular markers indicate the source amplitude at which X_{vt} is infinite at the given source frequency.

solution for this frequency range given by Eqs. (3.48) and (3.50).

The low-frequency asymptote, $D_{cr} = 1/3$, was deduced numerically. The fact that this critical value is the same as that for the step disturbance analyzed in Sec. 3.2 may be more than coincidence. Hammerton and Crighton [31] found analogous correspondence for a compressional wave in a relaxing fluid with quadratic nonlinearity; see also Crighton and Scott [54]. Deviation of the numerically obtained curve from the low frequency asymptote near $\theta_r = 0.1$ is also reflected in their results. A first-order correction at low frequencies can be

written as $D_{\rm cr} = 1/3 - \xi\theta_r + O(\theta_r^2)$ where ξ is a positive constant. Simulated waveforms for values of $\theta_r \lesssim 0.05$ were not obtained due to numerical difficulties when evaluating the exponentials in Eq. (4.4). Note that Hammerton and Crighton [31] plot $\Gamma = D'_{\rm cr}\theta_r$, where $D'_{\rm cr} = mc_0/2\beta v_{\rm cr}$ for a compressional wave, versus $\Omega = \theta_r$ in their Fig. 2 rather than $D_{\rm cr}$ versus θ_r as in Fig. 4.3(a) in the present work.

Referring back to Fig. 3.3(b), for which the values $D = 0.25$ and $\theta_r = 1$ were used, from Fig. 4.3(a) it is seen that shock formation is guaranteed at a finite propagation distance for $D \lesssim 1/3$ regardless of the value of θ_r. For $\theta_r = 1$ the critical value is $D_{\rm cr} \simeq 0.53$, and Eq. (4.5) indicates that the source amplitude v_0 corresponding to Fig. 4.3(b) exceeds the critical amplitude $v_{\rm cr}$ required for shock formation by approximately 45%.

At low frequencies a relaxing medium behaves approximately like a medium with viscous losses [recall Eq. (3.42)], so one might conclude that nonlinearity would always be balanced by relaxation at those frequencies and waveform overturing would never occur. However, as demonstrated by the numerically obtained waveforms in Fig. 3.5 for propagation of a shock initially followed by an exponential tail, and in particular Fig. 3.5(a), the rapid variation in the waveform that occurs at a shock is characterized by high frequencies. Attenuation and dispersion from relaxation in the high-frequency limit are unable to prevent waveform overturning, as determined in Sec. 3.4.3, and so waveform overturning occurs even for source waveforms that are initially slowly varying with respect to the relaxation time t_r. The critical source am-

plitude is larger (D_{cr} smaller) for initially low-frequency sinusoidal waveforms than for high-frequency waveforms because attenuation of the nonlinearly generated harmonics is greater relative to that of the source frequency for low frequency waveforms. Kashcheeva et al. [55] show that any attenuation law for which the attenuation coefficient increases more slowly than in proportion to frequency (i.e., $\alpha \propto \omega^1$) at the highest frequencies is insufficient to always prevent waveform overturning; relaxation has $\alpha \propto \omega^0$ at high frequencies, and so waveform overturning occurs at sufficiently high source amplitudes.

4.3 Shock formation distance

In the region of the parameter space that allows for an initially sinusoidal waveform to develop a vertical tangent at a finite distance from the source, either the model equation must be augmented to include additional mechanisms for energy loss (or conceivably dispersion) in order to ensure that the waveforms remain single-valued, or multivalued solutions must be corrected using weak-shock theory. However, even at source amplitudes for which the model equation allows for waveform overturning, the equation may still reasonably approximate the essential physics up to the distance at which the vertical tangent forms. It is therefore of interest to know the vertical-tangent formation distance whenever the critical source amplitude is exceeded.

The generalization of the shock formation distance used in this section to define the distance x_{vt} at which a vertical tangent first develops in an initially sinusoidal shear waveform in a relaxing medium is $X_{\mathrm{vt}} = x_{\mathrm{vt}}/x_{\mathrm{sh}}$,

where $x_{\rm sh} = c_0^3/\beta\omega v_0^2$ is the shock formation distance in the lossless case. The distance $X_{\rm vt}$ is plotted in Fig. 4.3(b) as a function of the relaxation strength for several source frequencies. In the lossless limit ($D = 0$) each curve approaches $x_{\rm vt} = x_{\rm sh}$. For $D > 0$ the shock formation distance increases with D as attenuation and dispersion due to relaxation partially balance waveform steepening and delay the development of vertical tangents in the waveform. The high-frequency curve with $\theta_r = 10$ is given approximately by Eq. (3.50). For lower source frequencies, the nonlinearly generated harmonics experience more attenuation compared to the fundamental, and so the shock formation distance increases more rapidly with increasing D. At values of D denoted by the triangular markers on the horizontal axis of Fig. 4.3(b), the shock formation distance at the denoted frequency is infinite; waveform overturning will not occur at values of D greater (source amplitudes lower) than the indicated value.

Referring back to Fig. 3.3(b), for which $D = 0.25$ and $\theta_r = 1$, it is seen from Fig. 4.3(b) that a vertical tangent develops in the waveform at a distance given by $X_{\rm vt} \simeq 1.24$. Beyond that distance Eq. (3.18) predicts a multivalued waveform which must be corrected by using weak shock theory, or as was done in Sec. 3.3 with numerical solutions of Eq. (3.30), by including viscous absorption in the model equation. Thus the waveform presented in Fig. 3.3(b), for which $X = 3$, contains thin shocks with a large jump in particle velocity for each shock.

Chapter 5

Nonlinear Shear Wave Resonator

In this chapter, nonlinear standing shear waves in a relaxing medium are investigated through the analysis of a shear wave resonator. The specific configuration to be considered in this chapter is depicted in Fig. 5.1. The resonator has length L, is driven by a prescribed time-harmonic acceleration at the base, and is stress free at the other end. The base and free end of the resonator are the planes perpendicular to the x axis at $x = 0$ and $x = L$, respectively. The boundary conditions are

$$\mathbf{a}(0,t) = a_0(\cos\omega t\,\mathbf{e}_y + s\sin\omega t\,\mathbf{e}_z), \qquad \frac{\partial \mathbf{u}}{\partial x}(L,t) = 0, \tag{5.1}$$

where $\mathbf{e}_i$ is the unit vector in the i direction and the parameter s defines the polarization of the drive motion. Particle motion in the resonator is *linearly polarized* for $s = 0$, *circularly polarized* for $s = 1$, and *elliptically polarized* otherwise. The resonator is formed from a nonlinear, relaxing elastic material, so the equation of motion is the nonlinear wave equation given in Eq. (2.69)

Selected material from this chapter was previously published in J. M. Cormack and M. F. Hamilton, "Plane nonlinear shear waves in relaxing media," *J. Acoust. Soc. Am.* **143**, 1035–1048 (2018), which appears as Ref. [32] in this dissertation. Contributions from JMC include derivation of equations of motion, derivation and validation of solutions, and writing of the article.

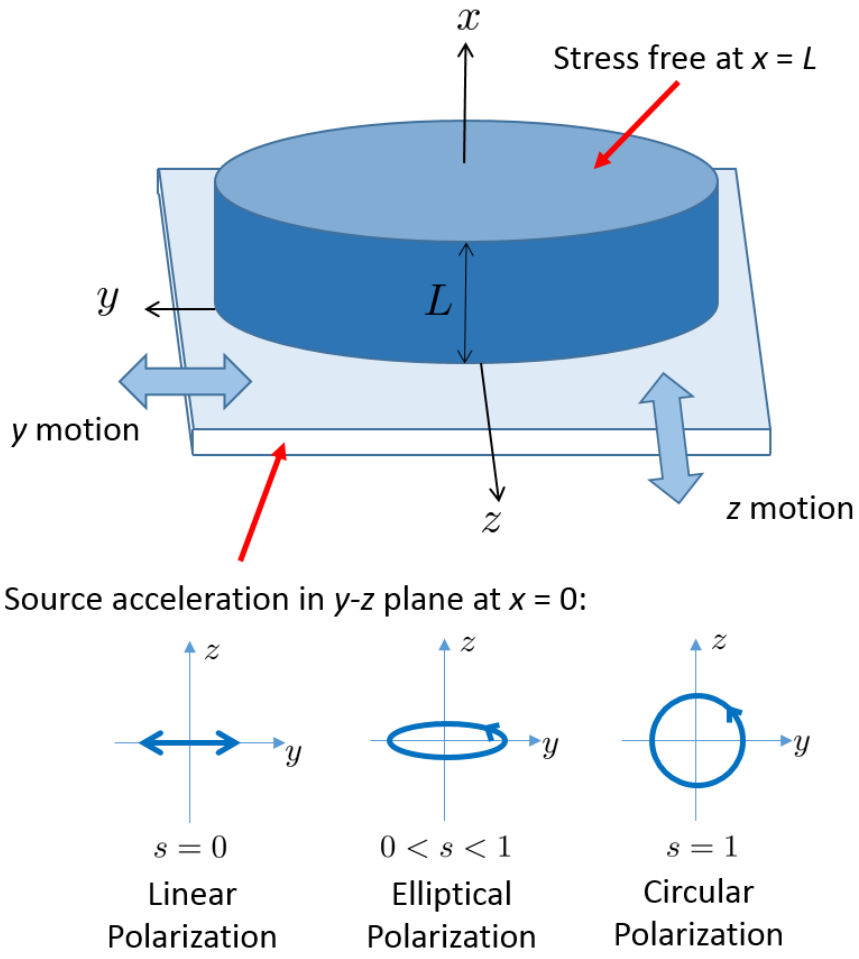

Figure 5.1: Illustration of the resonator configuration, detailing the three cases of drive motion polarization.

for linearly polarized motion ($s = 0$), or the coupled equations in Eqs. (2.72) and (2.73) for elliptically or circularly polarized motion when $0 < s \leq 1$.

First, the case of linearly polarized driving motion for which $s = 0$ in Eq. (5.1) is considered in Sec. 5.1. The response of the resonator in the

linear case is obtained in Sec. 5.1.1. For excitation near the lowest resonance, the nonlinear wave equation is approximated by an augmented form of the Duffing equation by using a normal mode expansion technique that has been employed previously for nonlinear string vibrations [56] and nonlinear acoustic resonators [57], and an implicit analytical solution is obtained for the amplitude-dependent frequency response of the resonator in Sec. 5.1.2. The augmented Duffing model is applied to the problem of subharmonic generation in Sec. 5.1.3. A resonator driven with elliptically polarized motion ($0 < s \leq 1$) is analyzed in Sec. 5.2, in which a pair of coupled augmented Duffing equations result from the coupled nonlinear shear wave equations. Approximate solutions are presented that demonstrate effects due to the coupling between components of the motion that result from nonlinearity.

5.1 Linearly polarized motion

For $s = 0$ the drive motion and resulting motion of the resonator are linearly polarized. The first of Eqs. (5.1) reduces to $\mathbf{a}(0,t) = a_0 \cos\omega t\, \mathbf{e}_y$, and the equation of motion for the resonator is the nonlinear wave equation for linearly polarized particle motion:

$$\left(1 + t_r \frac{\partial}{\partial t}\right)\left[\frac{\partial^2 u}{\partial t^2} - c_0^2 \frac{\partial^2 u}{\partial x^2} - \frac{2}{3}\beta c_0^2 \frac{\partial}{\partial x}\left(\frac{\partial u}{\partial x}\right)^3\right] = m t_r c_0^2 \frac{\partial^3 u}{\partial x^2 \partial t}, \tag{5.2}$$

where u is the particle displacement in the y direction. In Sec. 5.1.1, an exact solution of Eq. (5.2) is obtained in the linear case for harmonic driving motion. The nonlinear response near the lowest resonance is approximately described in

Sec. 5.1.2 by reducing Eq. (5.2) to an augmented form of the Duffing equation. Subharmonic generation is considered in Sec. 5.1.3.

5.1.1 Linear solution

Without the nonlinear term in Eq. (5.2), the linear solution is found by setting $u = -[\widetilde{a}(x)/\omega^2]e^{j\omega t}$, such that the transverse acceleration at any position x along the resonator is expressed as $a(x,t) = \mathrm{Re}[\widetilde{a}(x)e^{j\omega t}]$, and applying the boundary conditions $\widetilde{a}(0) = a_0$ and $\widetilde{a}\,'(L) = 0$, where the prime indicates a derivative with respect to x. The resulting expression for the acceleration of the free end is

$$\frac{\widetilde{a}(L)}{a_0} = \frac{1}{\cos kL}, \tag{5.3}$$

where the wavenumber k and complex wave speed $\tilde{c}$ are given by

$$k^2 = \frac{\omega^2}{\tilde{c}^2}, \qquad \tilde{c}^2 = c_0^2 \frac{1 + j\omega t_r(1+m)}{1 + j\omega t_r}. \tag{5.4}$$

The complex shear wave speed is related to the complex shear modulus in Eq. (2.52) by the expression $\widetilde{\mu} = \rho\tilde{c}^2$. The linear response given by Eq. (5.3) is plotted versus frequency in Fig. 5.2, showing resonance peaks of the first three modes of the resonator.

The resonance frequencies ω_n are those at which the magnitude of Eq. (5.3) exhibits local maxima. These frequencies may be estimated using the real roots of $\cos k_n L = 0$:

$$k_n = \frac{(2n-1)\pi}{2L}, \qquad n = 1,\, 2,\, 3... \ . \tag{5.5}$$

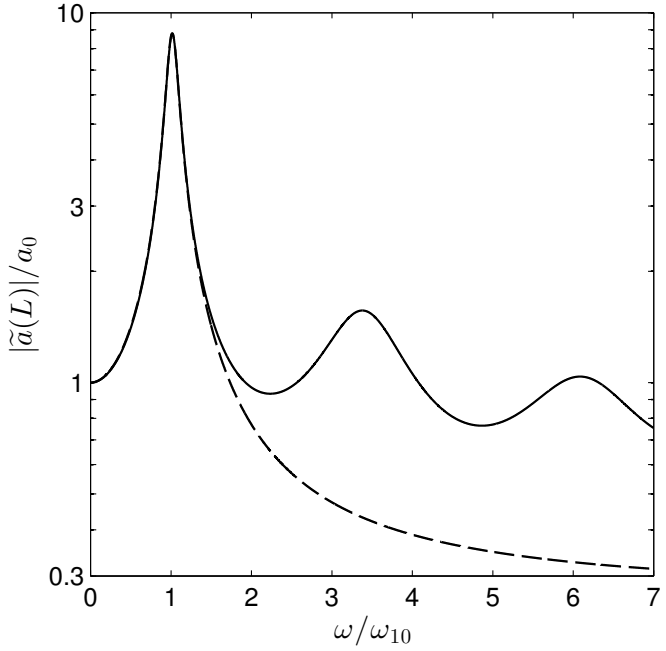

Figure 5.2: Linear response of the resonator showing the first three resonances according to Eq. (5.3) (solid curve) and the response of only the first mode according to Eq. (5.31) (dashed curve).

Since the wave speed in the medium is bounded at low frequencies by c_0 and at high frequencies by $c_\infty = (1+m)^{1/2}c_0$, the n^{th} resonance frequency falls within the range $\omega_{n0} < \omega_n < \omega_{n\infty}$ where

$$\omega_{n0} = c_0 k_n, \tag{5.6}$$

$$\omega_{n\infty} = (1+m)^{1/2} c_0 k_n. \tag{5.7}$$

Modes for which $\omega_n t_r \ll 1$ have resonance frequencies $\omega_n \simeq \omega_{n0}$ and those for which $\omega_n t_r \gg 1$ have $\omega_n \simeq \omega_{n\infty}$. Resonance frequencies estimated in this manner are found to be in good agreement with Eq. (5.3). For example, with the material parameters cited by Andreev et al. [29] for their Resonator I,

$m = 0.68$ and $\omega_{10} t_r = 0.23$, because $\omega_{10} t_r$ is reasonably small compared with unity the first resonance frequency ($n = 1$) is well approximated by Eq. (5.6), $\omega_1/\omega_{10} \simeq 1$. The second resonance ($n = 2$) has $\omega_2 t_r \simeq 0.78$, and $\omega_2/\omega_{10} = 3.38$ lies midway between $\omega_{20}/\omega_{10} = 3.00$ and $\omega_{2\infty}/\omega_{10} = 3.89$.

Energy dissipation in a resonator can be described using the quality factor Q_n of the n^{th} resonance peak, which is defined as the magnitude of the response at the n^{th} resonance frequency ω_n:

$$Q_n = \left| \frac{\widetilde{a}(L)}{a_0} \right|_{\omega=\omega_n} = \frac{1}{\sinh k_n'' L}, \tag{5.8}$$

where

$$k_n'' = \frac{\omega_n}{c_0} \frac{m\omega_n t_r/2}{\sqrt{[1 + (1+m)^2 \omega_n^2 t_r^2][1 + (1+m)\omega_n^2 t_r^2]}} \tag{5.9}$$

is the imaginary part of the first of Eqs. (5.4) evaluated at ω_n. When the relaxation strength is small ($m \ll 1$), Eq. (5.9) reduces to the expression in Eq. (3.11) for the progressive wave attenuation coefficient α, and the quantity $k_n''/(\omega_n/c_0)$ reduces to μ''/μ_0 where the loss modulus μ'' is given in Eq. (2.52). For a given resonance frequency ω_n, k_n'' increases with relaxation time from small values ($\omega_n t_r \ll 1$), achieves a maximum value near $\omega_n t_r = 1$, and then decreases with increasing relaxation time. The hyperbolic sine in Eq. (5.8) is a monotonically increasing function of its argument, therefore the minimum value of Q_n occurs at the maximum value of k_n''. Thus energy dissipation at the n^{th} resonance frequency is maximized when

$$\omega_n t_r = \frac{1}{(1+m)^{3/4}}. \tag{5.10}$$

5.1.2 Augmented Duffing equation

In order to use a modal expansion technique to develop a model equation that describes the nonlinear frequency response of the resonator, the first step is to incorporate the source acceleration into the wave equation by introducing a reference frame that is attached to the resonator at $x = 0$, thereby transforming the boundary conditions so that they are homogeneous. Thus define the relative displacement $U(x,t) = u(x,t) - u_0 \cos \omega t$ and corresponding relative acceleration $A(x,t) = a(x,t) - a_0 \cos \omega t$, in terms of which the equation for conservation of momentum is

$$\frac{\partial^2 U}{\partial t^2} = \frac{1}{\rho}\frac{\partial \sigma}{\partial x} - a_0 \cos \omega t, \tag{5.11}$$

which in combination with Eq. (2.12) yields the following wave equation in U:

$$\left(1 + t_r \frac{\partial}{\partial t}\right)\left[\frac{\partial^2 U}{\partial t^2} - c_0^2 \frac{\partial^2 U}{\partial x^2} - \frac{2}{3}\beta c_0^2 \frac{\partial}{\partial x}\left(\frac{\partial U}{\partial x}\right)^3 + a_0 \cos \omega t\right] = m t_r c_0^2 \frac{\partial^3 U}{\partial x^2 \partial t}. \tag{5.12}$$

In this moving reference frame the source acceleration appears in Eq. (5.12) as a body force, and the boundary conditions become, in place of Eqs. (5.1),

$$U(0,t) = 0, \qquad \frac{\partial U}{\partial x}(L,t) = 0, \tag{5.13}$$

which are homogeneous as desired. Without the nonlinear terms in Eq. (5.12), these boundary conditions lead to the following solution for the acceleration $A(L,t)$ of the free end in the moving reference frame:

$$\frac{\widetilde{A}(L)}{a_0} = \frac{1 - \cos kL}{\cos kL}, \tag{5.14}$$

where $A(x,t) = \mathrm{Re}[\widetilde{A}(x)e^{j\omega t}]$ and k is as defined in the first of Eqs. (5.4). Substitution of $A(x,t) = a(x,t) - a_0 \cos\omega t$ in Eq. (5.14) recovers the solution in the fixed frame, Eq. (5.3).

Equation (5.12) permits an augmented form of the Duffing equation to be developed for modeling the nonlinear amplitude-frequency response of the system when driven near one of the resonance frequencies ω_n. The following normal mode expansion is used to represent the displacement field:

$$U(x,t) = \sum_{n=1}^{\infty} U_n(t) \sin k_n x, \tag{5.15}$$

where k_n is given by Eq. (5.5). Upon substitution in Eq. (5.12), the nonlinear term generates products of the form $U_k U_l U_m$ that account for energy exchange among different modes. Of interest here are drive frequencies only in the neighborhood of the resonance corresponding to one particular mode. A resonator for which the lowest modes exhibit prominent resonance peaks allows for excitation of one of those modes with negligible direct excitation of the other modes. Furthermore, asynchronous modal interaction due to dispersion reduces the amount of energy transferred out of the mode being excited directly. At least for excitation of one of the lowest modes, it is thus sufficient to retain only the nonlinear terms $U_k U_l U_m$ for which k, l and m are all equal to n after substitution of Eq. (5.15) in (5.12). The following approximate relation is then obtained for the modal amplitude U_n:

$$\left(1 + t_r \frac{\partial}{\partial t}\right) \left[\left(\ddot{U}_n + \omega_{n0}^2 U_n\right) \sin k_n x + S_n(x,t) \right] = -m\omega_{n0}^2 t_r \dot{U}_n \sin k_n x, \tag{5.16}$$

where the overdots indicate time derivatives and

$$S_n(x,t) = 2\beta c_0^2 k_n^4 U_n^3(t) \sin k_n x \cos^2 k_n x + a_0 \cos \omega t \tag{5.17}$$

is a source term accounting for the nonlinearity (first term) and the forcing function (second term).

The spatial dependence in Eq. (5.16) is eliminated via multiplication by $\sin k_n x$ and integration over x from 0 to L:

$$\left(1 + t_r \frac{\partial}{\partial t}\right)\left(\ddot{U}_n + \omega_{n0}^2 U_n + \frac{1}{2}\beta c_0^2 k_n^4 U_n^3 + h_n a_0 \cos \omega t\right) = -m\omega_{n0}^2 t_r \dot{U}_n, \tag{5.18}$$

where

$$h_n = \frac{4}{(2n-1)\pi}. \tag{5.19}$$

The orthogonality of $\sin k_n x$ yields the correct contributions to mode n from $S_n(x,t)$. Rearranging Eq. (5.18) and use of the relation $\omega_{n\infty} = (1+m)^{1/2}\omega_{n0}$ yields

$$\begin{aligned}&\left(\ddot{U}_n + \omega_{n0}^2 U_n + \frac{1}{2}\beta c_0^2 k_n^4 U_n^3 + h_n a_0 \cos \omega t\right) \\ &+ t_r \frac{d}{dt}\left(\ddot{U}_n + \omega_{n\infty}^2 U_n + \frac{1}{2}\beta c_0^2 k_n^4 U_n^3 + h_n a_0 \cos \omega t\right) = 0.\end{aligned} \tag{5.20}$$

Each expression in parentheses in Eq. (5.20), if set equal to zero individually, constitutes a lossless Duffing equation,[1] the first expression with natural

[1]The Duffing equation, named after Georg Duffing, is the nonlinear ordinary differential equation of the form $\ddot{x} + c\dot{x} + \alpha x + \beta x^3 = \gamma \cos \omega t$ that is commonly used to describe nonlinear effects in oscillatory systems. See Stoker [58] for an in-depth treatment of the Duffing equation and its solutions for harmonic motions.

frequency ω_{n0} in the linear approximation, and the second with natural frequency $\omega_{n\infty}$. Taken as a whole, Eq. (5.20) is a lossy Duffing-like equation with a damped natural frequency between ω_{n0} and $\omega_{n\infty}$ in the linear approximation, as discussed following Eqs. (5.6) and (5.7).

The desired response at the drive frequency is expressed as

$$U_n = \frac{1}{2}\widetilde{U}_n e^{j\omega t} + \text{c.c.}. \tag{5.21}$$

Time derivatives in Eq. (5.18) can then be replaced with powers of $j\omega$, and with terms at frequency 3ω ignored one obtains $U_n^3 = \frac{3}{8}\widetilde{U}_n|\widetilde{U}_n|^2 e^{j\omega t} + \text{c.c.}$. In terms of the complex acceleration amplitude $\widetilde{A}_n = -\omega^2\widetilde{U}_n$ in the moving reference frame Eq. (5.20) becomes

$$\begin{aligned}&\left(\widetilde{A}_n - \frac{\omega_{n0}^2}{\omega^2}\widetilde{A}_n - \frac{3}{8}\beta\frac{c_0^2k_n^4}{\omega^6}\widetilde{A}_n|\widetilde{A}_n|^2 + h_n a_0\right)\\ &+ j\omega t_r\left(\widetilde{A}_n - \frac{\omega_{n\infty}^2}{\omega^2}\widetilde{A}_n - \frac{3}{8}\beta\frac{c_0^2k_n^4}{\omega^6}\widetilde{A}_n|\widetilde{A}_n|^2 + h_n a_0\right) = 0,\end{aligned} \tag{5.22}$$

which can be rearranged to obtain an implicit expression for $\widetilde{A}_n$,

$$\frac{\widetilde{A}_n}{a_0} = -\frac{(1+j\omega t_r)h_n}{H_{n0} + j\omega t_r H_{n\infty}}, \tag{5.23}$$

where

$$H_{n0} = 1 - \omega_{n0}^2/\omega^2 - \frac{3}{8}\beta c_0^2 k_n^4|\widetilde{A}_n|^2/\omega^6, \tag{5.24}$$

$$H_{n\infty} = 1 - \omega_{n\infty}^2/\omega^2 - \frac{3}{8}\beta c_0^2 k_n^4|\widetilde{A}_n|^2/\omega^6. \tag{5.25}$$

Multiplication of Eq. (5.23) by $\widetilde{A}_n^*$ and further rearrangement yields

$$\left[H_{n0}^2 + (\omega t_r)^2 H_{n\infty}^2\right]|\widetilde{A}_n|^2 = \left[1 + (\omega t_r)^2\right]h_n^2 a_0^2. \tag{5.26}$$

Analytical solutions for $|\widetilde{A}_n|$ are available because Eq. (5.26) is a cubic polynomial in $|\widetilde{A}_n|^2$; alternatively, it is straightforward to solve the equation numerically. Multiple real roots of Eq. (5.26) exist in some regions of the parameter space, so that Eq. (5.23) is a multivalued function of ω in those regions. Physically, a multivalued frequency response function corresponds to *hysteresis* or *jump phenomena*, which are discussed below in relation Fig. 5.3.

Equation (5.15) with modal amplitudes given by Eq. (5.23) with $\beta = 0$ recovers Eq. (5.3) for the linear response. In this case the summation is written as

$$\begin{aligned} \widetilde{a}(L) &= a_0 + \widetilde{A}(L) \\ &= a_0 + \sum_{n=1}^{\infty} \widetilde{A}_n \sin k_n L \\ &= a_0 + \sum_{n=1}^{\infty} (-1)^{n+1} \widetilde{A}_n, \end{aligned} \tag{5.27}$$

and it converges to the linear solution given in Eq. (5.3) with a sufficient number of terms included in the summation.

Attention is now focused on finite-amplitude excitation in the vicinity of the first resonance ($n = 1$), for which one may write

$$\widetilde{A}(L) \simeq \widetilde{A}_1 \sin k_1 L = \widetilde{A}_1, \qquad \omega \simeq \omega_{10}. \tag{5.28}$$

The acceleration $\widetilde{a}$ in the fixed reference frame is found from the acceleration $\widetilde{A}$ in the moving reference frame via the relation $\widetilde{a}(L) = \widetilde{A}(L) + a_0$. Equations (5.23) and (5.28) thus yield

$$\frac{\widetilde{a}(L)}{a_0} = \frac{(H_{10} - h_1) + j\omega t_r \, (H_{1\infty} - h_1)}{H_{10} + j\omega t_r H_{1\infty}}. \tag{5.29}$$

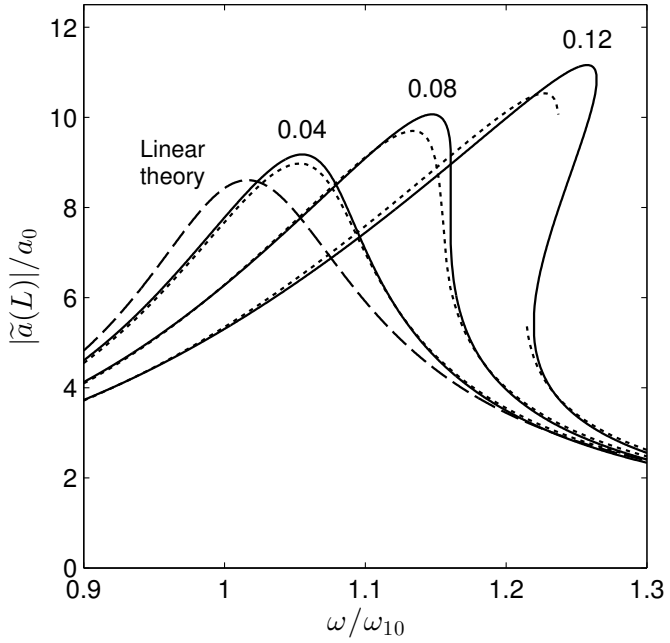

Figure 5.3: Response of the resonator near the lowest resonance: Linear response according to Eq. (5.3) (dashed curve), nonlinear response obained from Eq. (5.30) according to the augmented Duffing model (solid curves), and nonlinear response obtained from direct numerical solution of Eq. (5.2) (dotted curves). Numbers above each pair of curves indicate the acoustic Mach number $\epsilon_0 = a_0/\omega_{10}c_0$ of the source motion at $\omega = \omega_{10}$. Multivalued curves indicate hysteresis.

Multiplication by $\widetilde{a}^*$ then provides the acceleration amplitude $|\widetilde{a}|$ in the fixed frame in terms of the acceleration amplitude $|\widetilde{A}|$ in the moving frame:

$$\frac{|\widetilde{a}(L)|^2}{a_0^2} = \frac{(H_{10} - h_1)^2 + (\omega t_r)^2 (H_{1\infty} - h_1)^2}{H_{10}^2 + (\omega t_r)^2 H_{1\infty}^2}. \tag{5.30}$$

Once $|\widetilde{A}_n|$ is found from Eq. (5.26), Eqs. (5.24) and (5.25) may be evaluated, and the acceleration in the fixed frame is given by Eq. (5.30).

Consider first the linear solution that follows from Eq. (5.30):

$$\frac{|\widetilde{a}(L)|^2}{a_0^2} = \frac{\left(0.273 + \omega_{10}^2/\omega^2\right)^2 + (\omega t_r)^2 \left(0.273 + \omega_{1\infty}^2/\omega^2\right)^2}{(1 - \omega_{10}^2/\omega^2)^2 + (\omega t_r)^2 (1 - \omega_{1\infty}^2/\omega^2)^2}, \qquad \beta = 0, \quad (5.31)$$

where $0.273 = h_1 - 1$. This solution for the first mode is shown as the dashed curve in Fig. 5.2, and it is seen to be in good agreement with the complete linear solution, the solid curve given by Eq. (5.3), in the vicinity of the first resonance.

Nonlinear frequency responses predicted by Eq. (5.30) are shown as solid curves in Fig. 5.3, with linear theory given by Eq. (5.3) shown for reference as the dashed curve. As in Fig. 5.2, material parameters are taken as those cited for Resonator I by Andreev et al. [29]: $m = 0.68$, $\omega_{10} t_r = 0.23$, and $\beta = 2.01$. The number above the frequency response curve indicates the value of the acoustic Mach number $\epsilon_0 = a_0/\omega_{10} c_0$ of the source acceleration at the drive frequency $\omega = \omega_{10}$ for that case. As the source acceleration is increased the effective stiffness of the system increases in accordance with Eq. (2.12), and the resonance curves bend to the right, ultimately becoming multivalued and thus indicating hysteresis or a jump phenomenon. This same behavior was reported by Andreev et al. [29] in experiments performed using a shear-wave resonator with a mass attached at $x = L$.

Jump phenomenon refers to the behavior of a physical system near a frequency $\omega_{\rm vt}^{\pm}$, with $\omega_{\rm vt}^{-} < \omega_{\rm vt}^{+}$, on the frequency response curve at which the tangent to the curve is vertical. The frequency response curve according to Eq. (5.30) is multivalued in the region $\omega_{\rm vt}^{-} < \omega < \omega_{\rm vt}^{+}$. The upper and

lower branch represent steady-state responses that are stable, while the middle branch is an unstable response, e.g., if the resonator in Fig. 5.3 is driven with amplitude $\epsilon_0 = 0.12$ and frequency $\omega_{\rm vt}^- < \omega < \omega_{\rm vt}^+$, the amplitude will tend towards either the upper or lower branch in the steady state, depending on the initial conditions. The amplitude of the response will not tend towards the middle branch unless the necessary initial conditions are specified exactly,[2] and thus the middle branch of the multivalued frequency response curve in Fig. 5.3 cannot be obtained experimentally. If the resonator is initially driven with $\epsilon_0 = 0.12$ at a frequency $\omega < \omega_{\rm vt}^-$ and the frequency is slowly increased, the response follows the upper branch of the tuning curve in the region $\omega_{\rm vt}^- < \omega < \omega_{\rm vt}^+$. Further increase of the frequency past $\omega_{\rm vt}^+$ forces the response to jump down to the only branch of the tuning curve for $\omega > \omega_{\rm vt}^+$. Similarly, if the resonator is initially driven at a frequency $\omega > \omega_{\rm vt}^+$ and the frequency is slowly decreased, the response follows the lower branch of the tuning curve in the region $\omega_{\rm vt}^- < \omega < \omega_{\rm vt}^+$, jumping up once the frequency is decreased below $\omega_{\rm vt}^-$. Jump phenomena are associated with *hysteresis* due to this difference in response when the drive frequency is increased compared to when it is decreased.

The dotted curves in Fig. 5.3 are numerical solutions obtained by solving Eq. (5.2) directly while enforcing the boundary conditions $u(0,t) = -(a_0/\omega^2)\cos\omega t$ and $\partial u/\partial x\,(L,t) = 0$. The broken dotted curve corresponding

[2]See Nayfeh and Mook [59] for a discussion of the stability of steady-state periodic solutions of the Duffing equation

to $\epsilon_0 = 0.12$ indicates that hysteresis was observed in the numerical solutions. The analytical approximation given by Eq. (5.30) is seen to be in qualitative agreement with the full numerical solution in terms of predicting the onset of hysteresis in the vicinity of $\epsilon_0 = 0.08$, and it is in reasonable overall quantitative agreement prior to hysteresis. The overestimation of the resonance peaks by Eq. (5.30) is likely due to ignoring the transfer of energy to higher harmonics and other modes in the analytical approximation.

The numerical solutions in Fig. 5.3 were obtained using a finite-difference scheme that approximates the spatial derivatives in Eq. (5.2) with second-order central differences, then marches forward in time with a first-order Euler method. Relaxation was included using operator splitting, similar to the technique employed by Cleveland et al. [41]. Hysteresis was taken into account by retaining the end state of the simulation at the previous drive frequency for use as the initial conditions at the next drive frequency, the latter being either slightly higher or lower than the previous drive frequency depending on whether the frequency is being swept upwards or downwards, respectively. The steady-state response of the resonator at each drive frequency was decomposed into a Fourier series to extract the component of the response at the drive frequency as required for comparison with Eq. (5.30).

Figure 5.4 illustrates the effect of the relaxation time on the nonlinear response near the lowest resonance. The effect of the relaxation time on the linear frequency response of the lowest mode is to alter the resonance frequency ω_1 and quality factor Q_1. As discussed after Eq. (5.5), the resonance frequency

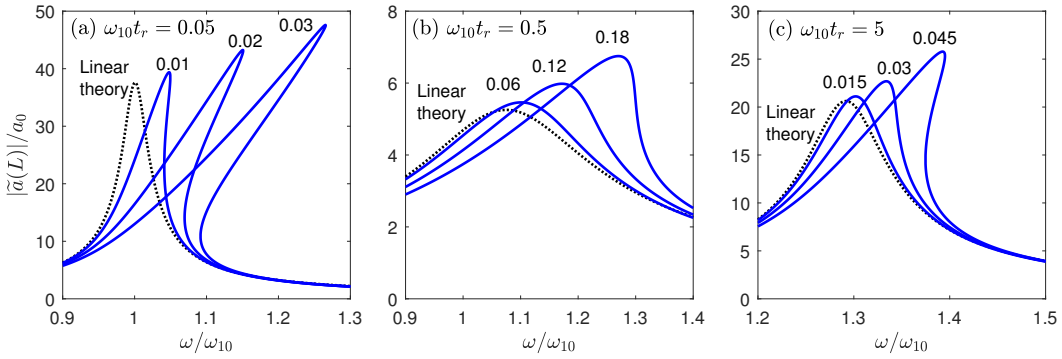

Figure 5.4: Nonlinear frequency response functions for a resonator with $m = 0.68$ and various values of drive amplitude and relaxation time. In all plots the black dashed is the linear response given by Eq. (5.3) and solid blue curves are the nonlinear responses given by Eq. (5.30). Numbers above the nonlinear response curves indicate the acoustic Mach number $\epsilon_0 = a_0/\omega_{10}c_0$ of the source motion at $\omega = \omega_{10}$. Multivalued curves indicate hysteresis.

is bounded by $\omega_{10} = c_0 k_1$ and $\omega_{1\infty} = c_\infty k_1$, and thus for small relaxation times $\omega_1 \simeq \omega_{10}$ and for large relaxation times $\omega_1 \simeq \omega_{1\infty} = \sqrt{1+m}\,\omega_{10}$. Energy dissipation is maximized and the quality factor Q_1 minimized at the relaxation time that satisfies Eq. (5.10).

When the relaxation time is small compared to the resonance frequency [Fig. 5.4(a)], linear theory (dahsed curve) shows that the resonance frequency is very close to ω_{10} and that the quality factor is large ($Q_1 \approx 40$). Because of the sharp resonance peak in this case, significant steepening of the frequency response curve occurs at relatively small drive amplitudes; the tuning curve is multivalued for a drive amplitude corresponding to a Mach number of $\epsilon_0 = a_0/\omega_{10}c_0 = 0.01$ at the base of the resonator, and further steepening of the tuning curve occurs for increasing drive amplitudes. In Fig. 5.4(b) the

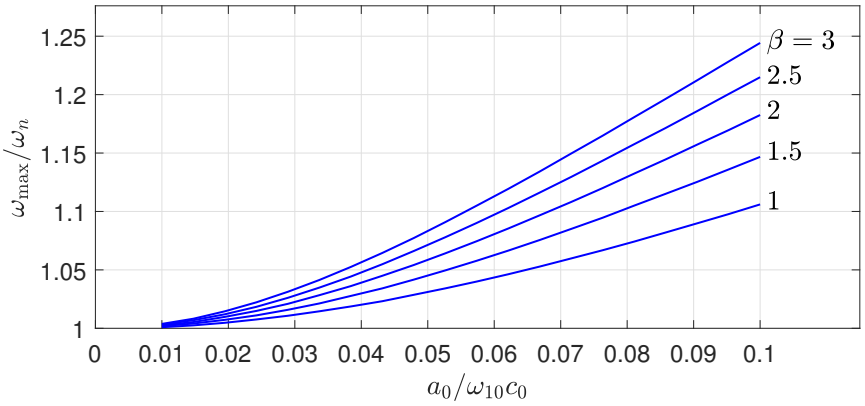

Figure 5.5: Frequency of maximum resonator response as a function of drive amplitude for several values of the coefficient of nonlinearity. Each curve was determined from numerical evaluation of Eq. (5.30) with $m = 0.68$ and $\omega_{10}t_r = 0.23$.

relaxation frequency is given by $\omega_{10}t_r = 0.5$, which is near the critical value $\omega_{10}t_r \approx 0.61$ according to Eq. (5.10). The linear response in this case indicates a resonance frequency slightly greater than ω_{10} and a smaller quality factor of $Q_1 \approx 5.3$. Due to the relatively large damping in this case, large drive amplitudes are necessary in order to see substantial nonlinear effects. The case of a large relaxation time is presented in Fig. 5.4(c): the linear response has a resonance frequency near $\omega_{1\infty} \approx 1.29\,\omega_{10}$ and a quality factor of $Q_1 \approx 20$ that is larger than the intermediate frequency case in Fig. 5.4(b) but smaller than the low frequency case in Fig. 5.4(a). For the quality factor in Fig. 5.4(c), nonlinear effects are evident at moderate drive amplitudes compared to Figs. 5.4(a) and 5.4(b).

The approximate analytical solution for the nonlinear response near the lowest resonance in Eq. (5.29) provides a means for determining the co-

efficient of nonlinearity and viscoelastic parameters from measurement of the response of a shear wave resonator. The viscoelastic parameters m and t_r can be determined from linear measurements by comparing the measured response with Eq. (5.3). See Ref. [28] for a recently reported measurement of the complex modulus of tissue-mimicking gel using a torsional shear wave resonator. Once the linear viscoelastic material parameters are obtained, the coefficient of nonlinearity may be determined by comparison of the measured nonlinear response near the lowest mode with the analytical solution given by Eq. (5.29). For example, the set of curves presented in Fig. 5.5 shows the frequency of maximum response $\omega_{\max}$ of the first mode as a function of drive amplitude for several values of the coefficient of nonlinearity β as determined from numerical evaluation[3] of Eq. (5.30). The frequency of maximum response $\omega_{\max}$ increases approximately with the square of the drive amplitude; a similar dependence was reported by Andreev et al. [29] in their measurements.

5.1.3 Subharmonic generation

In this section, the augmented Duffing model is extended to describe *subharmonic generation*, a commonly observed phenomenon in nonlinear resonant systems. Subharmonic generation is a sustained response at a frequency that is a fraction of the drive frequency. It is commonly observed in systems

[3]The curves in Fig. 5.5 may be determined analytically by differentiating Eq. (5.26) with respect to ω and setting $d|\widetilde{A}|^2/d\omega$ equal to zero, resulting in a polynomial in $\omega_{\max}$. However, the solutions are unwieldy expressions that offer little physical insight, and so the numerically obtained curves in Fig. 5.5 are preferred in this case.

that possess nonlinear restoring forces, and has been studied in the context of nonlinear bubble dynamics [60], microelectromechanical systems [61], and acoustic resonators [62, 63].

Subharmonic generation in a resonator is analogous to parametric amplification or three-wave mixing in nonlinear acoustics [49] and nonlinear optics [64]. It occurs because of nonlinear interaction of motion at the drive frequency with transients that are concentrated near a system resonance. For example, if a resonator with natural frequency ω_0 is in some undriven initial state (not necessarily rest) and is then subjected to a drive frequency $\omega \approx 3\omega_0$, the spectrum of the response near the time that the drive motion began will have two peaks: one near ω_0 that represents the free response (the part of the response associated with the homogeneous solution), and another near ω due to the driven motion (related to the particular solution). If the restoring force in the resonator is linear, the two components of the response are independent of each other. The free response will decay due to whatever losses are inherent to the system, and the forced response will increase to its steady-state value and remain there as $t \to \infty$.

On the other hand, if the restoring force exhibits cubic nonlinearity, as it does for plane shear waves and for the augmented Duffing equation in Eq. (5.20), the free and forced parts of the response are coupled because of the nonlinearity. One combination frequency in this case is $\omega - 2\omega_0 \approx \omega_0$, which provides a means for energy to be continually transferred from the forced response at ω to the free response near ω_0 due to the nonlinear interaction of

the two components of the resonator motion. If the conditions are right, this energy transfer can be maintained out to steady state, and the response at $t \to \infty$ will have components at both the drive frequency ω and the subharmonic $\omega/3$.

Analysis begins with substitution of the expansion given by Eq. (5.15) into the nonlinear wave equation in the moving reference frame given by Eq. (5.12). The drive frequency is $\omega \approx 3\omega_1$ so that the subharmonic is near the lowest resonance frequency ω_1 of the resonator. Because the resonator has also that $\omega_2 \approx 3\omega_1$, the drive motion directly excites motion of resonator at the second mode as well. Therefore the first two terms in Eq. (5.15) must be retained in order to account for motion of the system in the first and second modes. Orthogonality of each mode shape is used as in Sec. 5.1.2 to obtain two coupled augmented Duffing equations:

$$\left(1 + t_r \frac{d}{dt}\right)\left[\ddot{U}_1 + \omega_{10}^2 U_1 + \frac{1}{2}\beta c_0^2 k_1^4 \left(U_1^3 + 3U_1^2 U_2 + 9U_1 U_2^2\right) + h_1 a_0 \cos\omega t\right] = -m t_r \omega_{10}^2 \dot{U}_1, \tag{5.32}$$

$$\left(1 + t_r \frac{d}{dt}\right)\left[\ddot{U}_2 + \omega_{20}^2 U_2 + \frac{1}{2}\beta c_0^2 k_1^4 \left(U_1^3 + 18U_1^2 U_2 + 81U_2^3\right) + h_2 a_0 \cos\omega t\right] = -m t_r \omega_{20}^2 \dot{U}_2, \tag{5.33}$$

where the relation $3k_1 = k_2$ has been used. Steady-state solutions of Eqs. (5.32) and (5.33) are sought that have components at the drive frequency $\omega \approx 3\omega_1$ and at one-third the drive frequency $\omega/3$. Thus a harmonic balance method is employed and the following expressions are assumed for the steady-state

responses of the first and second modes:

$$U_1 = -\frac{1}{2}\frac{\widetilde{A}}{(\omega/3)^2}e^{j\omega t/3} + -\frac{1}{2}\frac{\widetilde{B}_1}{\omega^2}e^{j\omega t} + \text{c.c.}, \tag{5.34}$$

$$U_2 = -\frac{1}{2}\frac{\widetilde{B}_2}{\omega^2}e^{j\omega t} + \text{c.c.} \tag{5.35}$$

The terms in Eq. (5.34) represent the subharmonic response $\widetilde{A}$ and the response of the first mode to the drive frequency $\widetilde{B}_1$, respectively. The second mode response is assumed to consist only of a component at the drive frequency that has complex amplitude $\widetilde{B}_2$.

Substitution of Eqs. (5.34) and (5.35) into Eq. (5.32) and equating terms at $\omega/3$ yields

$$\widetilde{A}\left(G_0 + j\frac{\omega t_r}{3}G_\infty\right) = \left(1 + j\frac{\omega t_r}{3}\right)\frac{243}{8}\frac{\beta c_0^2 k_1^4}{\omega^6}\widetilde{A}^{*2}(\widetilde{B}_1 + \widetilde{B}_2), \tag{5.36}$$

where

$$G_{0,\infty} = 1 - 9\frac{\omega_{1(0,\infty)}^2}{\omega^2} - \frac{1}{2}\frac{\beta c_0^2 k_1^4}{\omega^6}\left(\frac{2187}{4}|\widetilde{A}|^2 + \frac{27}{2}|\widetilde{B}_1 + \widetilde{B}_2|^2 + 27|\widetilde{B}_2|^2\right). \tag{5.37}$$

Similarly, substitution of Eqs. (5.34) and (5.35) into Eq. (5.33) and equating terms at ω yields

$$\begin{aligned}\widetilde{B}_2\left(H_{20} + j\omega t_r H_{2\infty}\right) \\ = -\left(1 + j\omega t_r\right)\left[h_2 a_0 - \frac{1}{2}\frac{\beta c_0^2 k_1^4}{\omega^6}\left(\frac{729}{4}\widetilde{A}^3 + \frac{243}{2}|\widetilde{A}|^2\widetilde{B}_1 + \frac{3}{4}|\widetilde{B}_1|^2\widetilde{B}_1 + \frac{9}{2}\widetilde{B}_1^2\widetilde{B}_2^*\right)\right],\end{aligned} \tag{5.38}$$

where

$$H_{2(0,\infty)} = 1 - \frac{\omega_{2(0,\infty)}^2}{\omega^2} - \frac{1}{2}\frac{\beta c_0^2 k_1^4}{\omega^6}\left(729|\widetilde{A}|^2 + 9|\widetilde{B}_1|^2 + \frac{243}{4}|\widetilde{B}_2|^2\right). \tag{5.39}$$

Finally, the complex amplitude $\widetilde{B}_1$ for the response of the first mode at the drive frequency is assumed to be given by the linear approximation:

$$\frac{\widetilde{B}_1}{a_0} = -h_1 \frac{1 + j\omega t_r}{1 - \omega_{10}^2/\omega^2 + j\omega t_r(1 - \omega_{1\infty}^2/\omega^2)}. \tag{5.40}$$

The subharmonic amplitude $\widetilde{A}$ and the second mode response $\widetilde{B}_2$ are then determined by solving the system of complex-valued algebraic equations in Eqs. (5.36) and (5.38). Equation (5.36) reveals that the trivial solution for which $\widetilde{A} = 0$ and $\widetilde{B}_2 \neq 0$ is a possible steady state solution. Nontrivial solutions of Eqs. (5.36) and (5.38) are determined numerically using `FSOLVE` in Matlab.

Nontrivial solutions of Eqs. (5.36) and (5.38) for the subharmonic amplitude $\widetilde{A}$ are plotted versus frequency in Fig. 5.6 for three cases with various values of t_r, m, and ϵ_0. In all three cases, nontrivial solutions exist only when the drive motion is above a certain frequency that is greater than $3\omega_1$ (corresponding to $\omega/\omega_{10} > 3$ in Fig. 5.6), which is also true of subharmonic generation resulting from the classical Duffing equation [58]. The solid curve, determined from Eqs. (5.36) and (5.38), in each case resembles a droplet in shape, with two nontrivial solutions existing within a certain frequency range. Red squares in Fig. 5.6(a) represent the subharmonic amplitude determined from direct numerical solution of the coupled augmented Duffing equations in Eqs. (5.32) and (5.33). The numerically obtained results lay only on the upper branch of the curve, suggesting that the lower branch represents an unstable response, as does the middle branch of the multivalued part of the frequency response curve presented in Fig. 5.3.

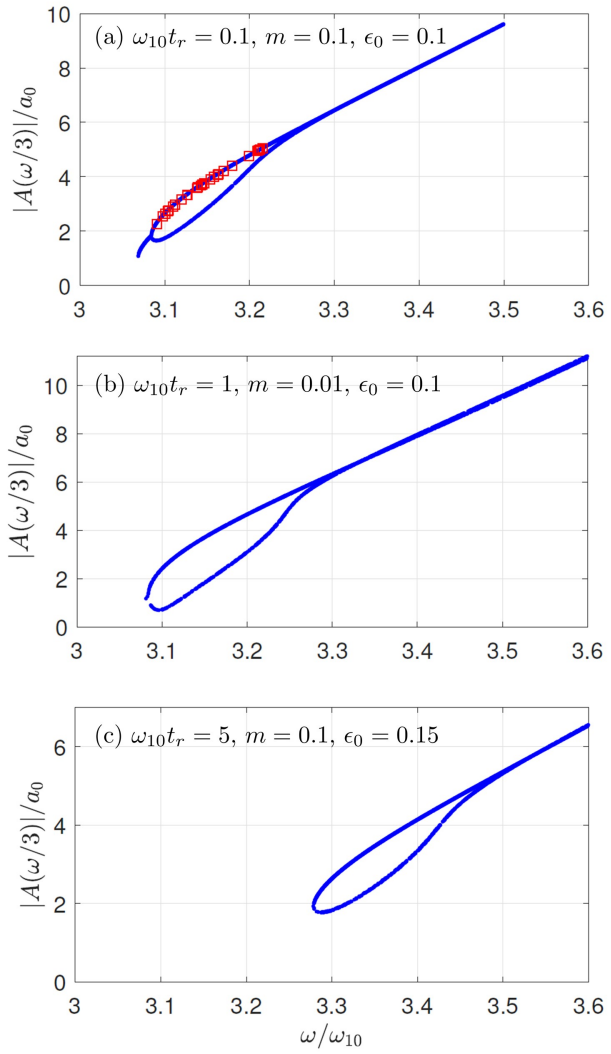

Figure 5.6: Frequency dependence of the subharmonic amplitude as determined from numerical solution of Eqs. (5.36) and (5.38) for cases of low, mid, and high frequency compared to the relaxation frequency. Red squares in (a) represent the subharmonic amplitude in that case determined from direct numerical solution of Eqs. (5.32) and (5.33).

The effect of the relaxation time, as discussed in connection with Fig. 5.4, is to alter the natural frequencies and the quality factors of the resonance peaks. In the context of subharmonic generation, those effects manifest as a shift in the critical frequency above which subharmonic generation can occur and to change the drive amplitude needed to generate the subharmonic. For the small value of the relaxation time in Fig. 5.6(a), subharmonic generation is possible for $\omega/\omega_{10} \gtrsim 3.06$ with $m = 0.1$ and $\epsilon_0 = 0.1$. For the intermediate value of t_r in Fig. 5.6(b), the critical frequency is increased slightly compared to Fig. 5.6(a); nontrivial solutions exist for $\omega/\omega_{10} \gtrsim 3.08$. However, because of the peak in energy dissipation in the first mode near $\omega_1 t_r \approx 1$, the relaxation strength in this case must be much lower ($m = 0.01$) in order for damping to be small enough for subharmonic generation to occur. In Fig. 5.6(c) for the large value of the relaxation time the critical frequency is much higher than in the former two cases; nontrivial solutions exist for $\omega/\omega_{10} \gtrsim 3.28$. Nayfeh and Mook [59] present a good discussion of the influence of damping and drive amplitude on subharmonic generation for the classical Duffing equation.

The response of the resonator at the drive frequency is significantly affected by subharmonic generation. The total response at the drive frequency in the fixed reference frame $\widetilde{a}(\omega) = \widetilde{B}_1 - \widetilde{B}_2 + a_0$ is presented in Fig. 5.7 for both the case in which subharmonic generation occurs and the case in which it does not. Parameters used correspond to those used in Fig. 5.6(a). Because damping is relatively small in this case, the frequency response curve in the absence of subharmonic generation, given by the thin line, is multivalued,

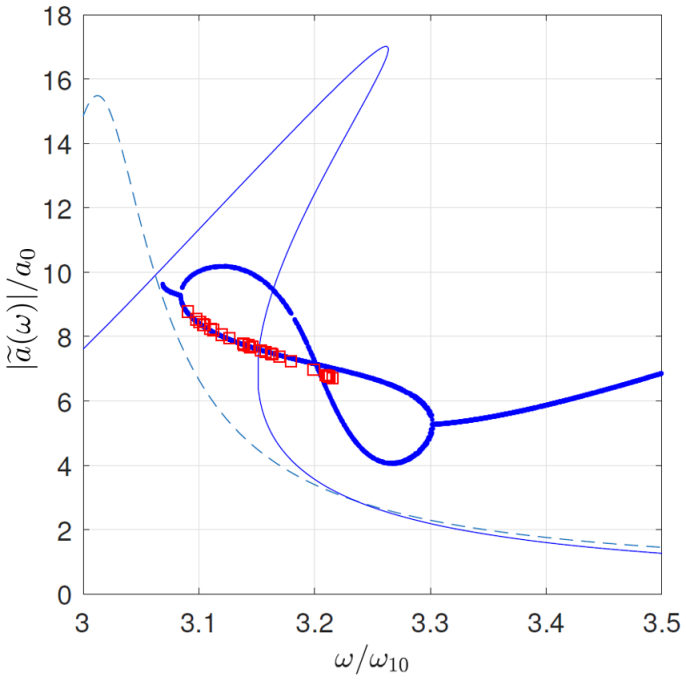

Figure 5.7: Response of the resonator at the drive frequency corresponding to the case presented in Fig. 5.6(a). The dashed curve is linear theory given by Eq. (5.3). The thin solid curve is the nonlinear response without subharmonic generation according to Eq. (5.23). The thick curve and red squares are the nonlinear response at the drive frequency when subharmonic generation occurs, determined by solving either Eqs. (5.36) and (5.38) or Eqs. (5.32) and (5.33), respectively.

indicating hysteresis as for the right-most curve in Fig. 5.3. The thick line represents the response when subharmonic generation occurs. The multivalued "figure 8" shaped curve indicates that multiple nontrivial solutions exist for the response at the drive frequency when subharmonic generation occurs, with the two branches corresponding to those in Fig. 5.6(a). As in Fig. 5.6(a), the red squares correspond to the response at the drive frequency determined from direct numerical simulation of the coupled augmented Duffing equations in

Eqs. (5.32) and (5.33); the numerically obtained results lay only on one branch of curve, suggesting that the other branch represents steady-state responses that are unstable.

Despite agreement between solutions obtained using the harmonic balance method by solving Eqs. (5.36) and (5.38) and solutions obtained by direct numerical solution of the augmented Duffing equations in Eq. (5.32) and (5.33), subharmonic generation has not been observed in numerical solutions of the full nonlinear wave equation given by Eq. (5.2). Good agreement is observed between the augmented Duffing model and the numerical solution of Eq. (5.2) for drive motion near $3\omega_{10}$ when subharmonic generation does not occur. The culprit is most likely the prevalence of the trivial solution of Eq. (5.36). While initial conditions for Eqs. (5.32) and (5.33) were found that result in subharmonic generation, the availability of initial conditions for Eq. (5.2) that result in subharmonic generation seems to be much more limited.

5.2 Elliptically polarized motion

For $s \neq 0$ in Eq. (5.1) the particle motion in the resonator is elliptically polarized. Combination of Eq. (5.11) with Eqs. (2.44) and (2.45) yields coupled nonlinear wave equations in a reference frame attached to the base of the

resonator:

$$\left(1+t_r\frac{\partial}{\partial t}\right)\left\{\frac{\partial^2 U_y}{\partial t^2}-c_0^2\frac{\partial^2 U_y}{\partial x^2}-\frac{2}{3}\beta c_0^2\frac{\partial}{\partial x}\left[\left(\frac{\partial U_y}{\partial x}\right)^3+\frac{\partial U_y}{\partial x}\left(\frac{\partial U_z}{\partial x}\right)^2\right]+a_0\cos\omega t\right\}$$
$$=mt_rc_0^2\frac{\partial^3 U_y}{\partial x^2\partial t} \tag{5.41}$$
$$\left(1+t_r\frac{\partial}{\partial t}\right)\left\{\frac{\partial^2 U_z}{\partial t^2}-c_0^2\frac{\partial^2 U_z}{\partial x^2}-\frac{2}{3}\beta c_0^2\frac{\partial}{\partial x}\left[\left(\frac{\partial U_z}{\partial x}\right)^3+\frac{\partial U_z}{\partial x}\left(\frac{\partial U_y}{\partial x}\right)^2\right]+sa_0\sin\omega t\right\}$$
$$=mt_rc_0^2\frac{\partial^3 U_z}{\partial x^2\partial t}, \tag{5.42}$$

where $U_y(x,t)=u_y(x,t)-u_0\cos\omega t$ and $U_z(x,t)=u_z(x,t)-su_0\sin\omega t$. Coupling between the two components of the transverse particle motion is accounted for by the second terms of the expressions in square brackets on the left-hand sides of Eqs. (5.41) and (5.42).

Only excitation near the lowest resonance frequency is considered here; subscripts corresponding to mode number are thus neglected for the remainder of this section. The fields $U_y(x,t)$ and $U_z(x,t)$ are expressed as modal expansions with only the first term retained:

$$U_y=U_y(t)\sin kx, \qquad U_z=U_z(t)\sin kx, \tag{5.43}$$

where $k=\pi/2L$. Substitution of Eqs. (5.43) into Eqs. (5.41) and (5.42) and elimination of the spatial dependence using orthogonality of $\sin kx$ as in

Sec. 5.1.2 results in a pair of coupled augmented Duffing equations:

$$\left(1+t_r\frac{d}{dt}\right)\left[\ddot{U}_y+\omega_0^2U_y+\tfrac{1}{2}\beta c_0^2k^4(U_y^3+U_yU_z^2)+ha_0\cos\omega t\right]=-m\omega_0^2t_r\dot{U}_y, \tag{5.44}$$

$$\left(1+t_r\frac{d}{dt}\right)\left[\ddot{U}_z+\omega_0^2U_z+\tfrac{1}{2}\beta c_0^2k^4(U_z^3+U_zU_y^2)+sha_0\sin\omega t\right]=-m\omega_0^2t_r\dot{U}_z, \tag{5.45}$$

where $\omega_0 = c_0k$ and $h = 4/\pi$. The response of the resonator at the drive frequency is expressed as $U_{y,z} = -\frac{1}{2}(\widetilde{A}_{y,z}/\omega^2)e^{j\omega t}+\text{c.c.}$, and substitution into Eqs. (5.44) and (5.45) yields

$$(1+j\omega t_r)\left[\widetilde{A}_y\left(1-\frac{\omega_0^2}{\omega^2}\right)-\frac{3}{8}\frac{\beta c_0^2k^4}{\omega^6}\left(|\widetilde{A}_y|^2\widetilde{A}_y+\frac{2}{3}|\widetilde{A}_z|^2\widetilde{A}_y+\frac{1}{3}\widetilde{A}_z^2\widetilde{A}_y^*\right)+ha_0\right]$$
$$=jm\frac{\omega_0^2}{\omega^2}\omega t_r\widetilde{A}_y, \tag{5.46}$$

$$(1+j\omega t_r)\left[\widetilde{A}_z\left(1-\frac{\omega_0^2}{\omega^2}\right)-\frac{3}{8}\frac{\beta c_0^2k^4}{\omega^6}\left(|\widetilde{A}_z|^2\widetilde{A}_z+\frac{2}{3}|\widetilde{A}_y|^2\widetilde{A}_z+\frac{1}{3}\widetilde{A}_y^2\widetilde{A}_z^*\right)-jsha_0\right]$$
$$=jm\frac{\omega_0^2}{\omega^2}\omega t_r\widetilde{A}_z, \tag{5.47}$$

where the superscript * indicates the complex conjugate. A general solution of Eqs. (5.46) and (5.47) is not available. Approximate solutions in limiting cases are obtained in Secs. 5.2.1–5.2.3.

5.2.1 Weakly nonlinear motion

Deviations from the linear response in the case of small but finite driving motions are examined by dividing Eqs. (5.46) and (5.47) by ω_0c_0 and expressing the responses as

$$\widetilde{A}_{y,z}=a_0\left(x_{y,z}^{(0)}+\epsilon_0^2x_{y,z}^{(2)}+\cdots\right),\qquad \epsilon_0\ll 1, \tag{5.48}$$

where $\epsilon_0 = a_0/\omega_0 c_0$ is the acoustic Mach number of the resonator base in the laboratory reference frame. Substitution of Eq. (5.48) into Eqs. (5.46) and (5.47) and equating first-order terms in ϵ_0 yields the linear response:

$$x_y^{(0)} = -h\frac{1 + j\omega t_r}{1 - \omega_0^2/\omega^2 + j\omega t_r\left(1 - \omega_\infty^2/\omega^2\right)}, \tag{5.49}$$

$$x_z^{(0)} = -jsx_y^{(0)}. \tag{5.50}$$

The two components of particle motion are uncoupled in the linear case and the responses are proportional to the drive motion; the factor of $-js$ in the second expression indicates that the minor component $x_z^{(0)}$ lags the major component $x_y^{(0)}$ by $\pi/2$ in phase and is scaled in amplitude by a factor of s. The response of the major component in the linear limit $a_0 x_y^{(0)}$ corresponds to the solution given in Eq. (5.23) with $\beta = 0$.

The nonlinear terms are found by equating coefficients of ϵ_0^3 after substitution of Eq. (5.48) into Eqs. (5.46) and (5.47):

$$x_y^{(2)} = -\frac{3}{8h}\beta\left|x_y^{(0)}\right|^2\left(x_y^{(0)}\right)^2\frac{\omega_0^6}{\omega^6}\left(1 + \frac{s^2}{3}\right), \tag{5.51}$$

$$x_z^{(2)} = js\frac{3}{8h}\beta\left|x_y^{(0)}\right|^2\left(x_y^{(0)}\right)^2\frac{\omega_0^6}{\omega^6}\left(\frac{1}{3} + s^2\right). \tag{5.52}$$

The effect of nonlinearity in this case is to shift the frequency response curves for both components of the motion to slightly higher frequencies, increasing the frequency at which the response is maximum.

An example of the nonlinear coupling of the particle displacement components is an amplitude-dependent phase difference $\Delta\phi$ between the responses,

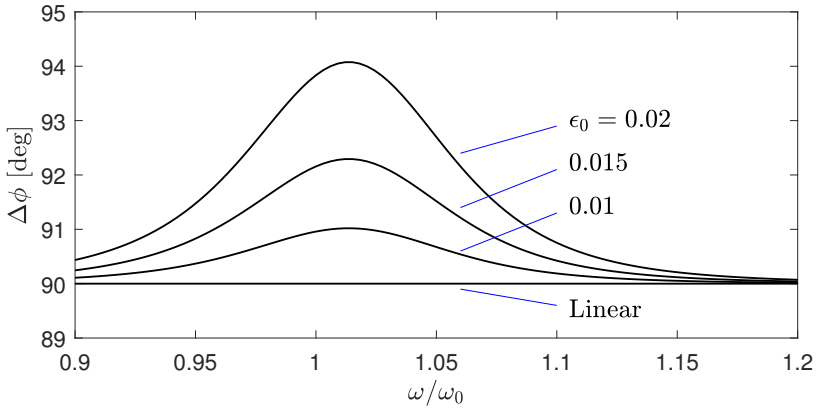

Figure 5.8: Difference in phase between major and minor components in the weakly nonlinear case for several values of the drive amplitude. For each curve $m = 0.68$, $\omega_0 t_r = 0.23$, $\beta = 2$, and $s = 0.5$.

where the difference is $\Delta\phi = \pi/2$ in the linear case. To $O(\epsilon_0^3)$, the phase difference between the major and minor components is

$$\Delta\phi = \angle\widetilde{A}_y - \angle\widetilde{A}_z = \frac{\pi}{2} + \frac{1}{4h}\beta\epsilon_0^2 \left|x_y^{(0)}\right|^3 \frac{\omega_0^6}{\omega^6}(1 - s^2)\sin\phi_0, \tag{5.53}$$

where $\phi_0 = \angle x_y^{(0)}$. The phase difference is proportional to the square of the drive amplitude, and is maximized for $s \ll 1$ and near resonance where $\sin\phi_0 \approx 1$. The frequency dependence of the phase difference $\Delta\phi$ is plotted for several values of drive amplitude ϵ_0 in Fig. 5.8.

While the assumption of weak nonlinearity can be valid in the case of plane progressive waves for source strains up to $\epsilon_0 \simeq 0.1$, the peak strain in a resonator is amplified considerably near resonance. Thus the accuracy of the approximation depends on the sharpness of the lowest resonance peak. For example, the nonlinear response of a resonator with quality factor $Q_1 \simeq 10$ can be approximated by Eq. (5.48) for driving amplitudes up to $\epsilon_0 \simeq 10^{-2}$.

5.2.2 Nearly linearly polarized motion

Another consequence of the coupling between components of the particle motion is a transfer of energy from the major component $\widetilde{A}_y$ to the minor component $\widetilde{A}_z$. This energy transfer can result in a significant amplification of the minor component compared to the linear response, and it is most significant when $s \ll 1$, for which the motion is nearly linearly polarized. In this case the responses are expanded in s as

$$\widetilde{A}_y = \widetilde{A}_L + s\widetilde{A}_y^{(1)} + \cdots, \qquad \widetilde{A}_z = -js\widetilde{A}_z^{(1)} + \cdots, \qquad s \ll 1. \tag{5.54}$$

After substitution of Eqs. (5.54) into Eq. (5.46) and equating terms independent of s, one obtains

$$\widetilde{A}_L = -ha_0 \frac{1 + j\omega t_r}{H_0 + j\omega t_r H_\infty}, \qquad H_{0,\infty} = 1 - \frac{\omega_{0,\infty}^2}{\omega^2} - \frac{3}{8}\frac{\beta c_0^2 k^4}{\omega^6}|\widetilde{A}_L|^2, \tag{5.55}$$

which is the implicit solution for the response of the resonator at the drive frequency to linearly polarized driving motion presented in Eq. (5.23). Equating terms with the factor s reveals that the only solution for $\widetilde{A}_y^{(1)}$ is trivial.

Substitution of Eqs. (5.54) into Eq. (5.47) and equating terms that are first order in s yields

$$\widetilde{A}_z^{(1)}\left(H_0^{(s)} + j\omega t_r H_\infty^{(s)}\right) + (1 + j\omega t_r)\frac{1}{8}\frac{\beta c_0^2 k^4}{\omega^6}\widetilde{A}_L^2\widetilde{A}_z^{(1)*} = -(1 + j\omega t_r)ha_0, \tag{5.56}$$

where

$$H_{0,\infty}^{(s)} = 1 - \omega_{0,\infty}^2/\omega^2 - \frac{1}{4}\frac{\beta c_0^2 k^4}{\omega^6}|\widetilde{A}_L|^2. \tag{5.57}$$

The major and minor components may be expressed in terms of their real and imaginary parts as $\widetilde{A}_L^2 = p_L + jq_L$ and $\widetilde{A}_z^{(1)} = x_z + jy_z$, and then Eq. (5.56) can be written in matrix form:

$$\mathbf{M}\,\mathbf{x} = -ha_0\mathbf{b}, \tag{5.58}$$

where

$$\mathbf{M} = \begin{bmatrix} H_0^{(s)} + \frac{1}{8}\frac{\beta c_0^2 k^4}{\omega^6}(p_L - \omega t_r q_L) & -\omega t_r H_\infty^{(s)} + \frac{1}{8}\frac{\beta c_0^2 k^4}{\omega^6}(q_L + \omega t_r p_L) \\ \omega t_r H_\infty^{(s)} + \frac{1}{8}\frac{\beta c_0^2 k^4}{\omega^6}(q_L + \omega t_r p_L) & H_0^{(s)} + \frac{1}{8}\frac{\beta c_0^2 k^4}{\omega^6}(-p_L + \omega t_r q_L) \end{bmatrix}, \tag{5.59}$$

$$\mathbf{x} = \begin{bmatrix} x_z \\ y_z \end{bmatrix}, \tag{5.60}$$

$$\mathbf{b} = \begin{bmatrix} 1 \\ \omega t_r \end{bmatrix}. \tag{5.61}$$

Equation (5.58) can be inverted analytically or numerically.

Response curves for the major and minor components near the lowest resonance are shown in Fig. 5.9 for $s \ll 1$. As in Figs. 5.3 and 5.4, the frequency response curves bend towards the right as the forcing amplitude increases. Whereas the peak amplitude of the major component response is moderately amplified compared to linear theory by increasing the drive amplitude, the peak amplitude of the minor component is increased significantly. Figure 5.9(e) shows a peak response of the minor component that is double that predicted by linear theory, and Fig. 5.9(f) shows an amplification of almost a factor of four.

Accuracy of the expansions in Eqs. (5.54) depends both on the value of s as well as the amplitude of the driving motion. Comparison of solutions

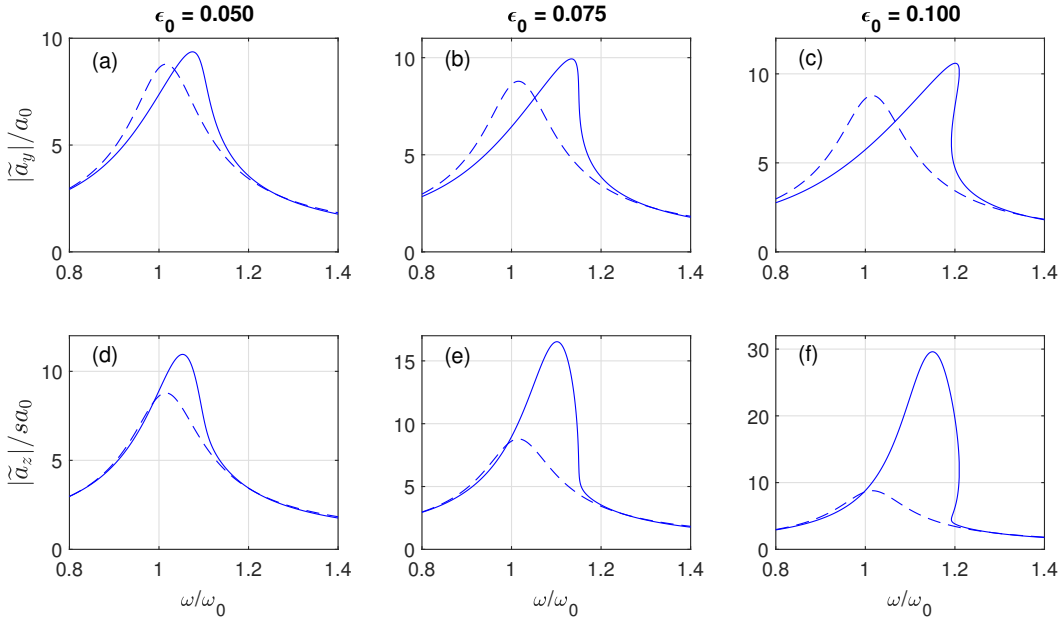

Figure 5.9: Resonator response in the limit of nearly linearly polarized motion ($s \ll 1$). In each plot are the linear (dashed curves) and nonlinear (solid curves) responses in the laboratory frame. In the top row is the response of the major component $\widetilde{a}_y = \widetilde{A}_y + a_0$. The lower row shows the response of the minor component $\widetilde{a}_z = \widetilde{A}_z - jsa_0$. Each column is labeled with the dimensionless drive amplitude $\epsilon_0 = a_0/\omega_0 c_0$. Parameters used are for plastisol [29]: $\beta = 2$, $m = 0.68$, and $\omega_0 t_r = 0.23$.

of Eq. (5.58) with numerical solutions of Eqs. (5.44) and (5.45) reveals that, with parameters for plastisol [29] and for moderate forcing amplitudes near $\epsilon_0 = 0.05$, the approximate solution $\widetilde{A}_z^{(1)}$ is valid up to $s \simeq 0.2$. For a larger drive amplitude of $\epsilon_0 = 0.1$, $\widetilde{A}_z^{(1)}$ is accurate only up to $s \simeq 0.1$.

5.2.3 Nearly circularly polarized motion

Motion of the system that is nearly circularly polarized is approximately described by expanding the response in $e = 1 - s \ll 1$:

$$\widetilde{A}_y = \widetilde{A}_C + e\widetilde{A}_y^{(1)} + \cdots, \qquad \widetilde{A}_z = -j\left(\widetilde{A}_C + e\widetilde{A}_z^{(1)} + \cdots\right), \qquad e \ll 1. \quad (5.62)$$

Substitution of Eqs. (5.62) into either of Eqs. (5.46) or (5.47) and equating terms without a factor of e yields an expression for the response to circularly polarized drive motion:

$$\widetilde{A}_C = -ha_0 \frac{1 + j\omega t_r}{H_0^{(C)} + j\omega t_r H_\infty^{(C)}}, \qquad H_{0,\infty}^{(C)} = 1 - \frac{\omega_{0,\infty}^2}{\omega^2} - \frac{1}{2}\frac{\beta c_0^2 k^4}{\omega^6}|\widetilde{A}_C|^2. \quad (5.63)$$

Equations (5.63) are formally equivalent to Eqs. (5.55) apart from the coefficient 1/2 in the nonlinear term in the former, compared with 3/8 in the latter, indicating that rightward bending of the tuning curve due to nonlinearity is slightly more pronounced for circularly polarized motion than for linear polarization. The next order terms in Eq. (5.62) are found from

$$(1 + j\omega t_r)\left[\widetilde{A}_y^{(1)}\left(1 - \frac{\omega_0^2}{\omega^2} - \frac{\beta c_0^2 k^4}{\omega^6}|\widetilde{A}_C|^2\right) - \frac{\beta c_0^2 k^4}{\omega^6}\widetilde{A}_C^2(\widetilde{A}_y^{(1)*} + \widetilde{A}_z^{(1)*})\right]$$
$$= jm\frac{\omega_0^2}{\omega^2}\omega t_r \widetilde{A}_y^{(1)}, \quad (5.64)$$

$$(1 + j\omega t_r)\left[\widetilde{A}_z^{(1)}\left(1 - \frac{\omega_0^2}{\omega^2} - \frac{\beta c_0^2 k^4}{\omega^6}|\widetilde{A}_C|^2\right) - \frac{\beta c_0^2 k^4}{\omega^6}\widetilde{A}_C^2(\widetilde{A}_y^{(1)*} + \widetilde{A}_z^{(1)*}) + ha_0\right]$$
$$= jm\frac{\omega_0^2}{\omega^2}\omega t_r \widetilde{A}_z^{(1)}, \quad (5.65)$$

or, in matrix form,

$$\left\{\begin{bmatrix}\mathbf{M}_1 & \mathbf{0} \\ \mathbf{0} & \mathbf{M}_1\end{bmatrix} + \begin{bmatrix}\mathbf{M}_2 & \mathbf{M}_2 \\ \mathbf{M}_2 & \mathbf{M}_2\end{bmatrix}\right\}\mathbf{x} = ha_0\mathbf{b}, \quad (5.66)$$

where

$$\mathbf{M}_1 = \begin{bmatrix} H_0^{(e)} & -\omega t_r H_\infty^{(e)} \\ \omega t_r H_\infty^{(e)} & H_0^{(e)} \end{bmatrix}, \tag{5.67}$$

$$\mathbf{M}_2 = -\frac{1}{4}\frac{\beta c_0^2 k_1^4}{\omega^6} \begin{bmatrix} p_C - \omega t_r q_C & q_C + \omega t_r p_C \\ q_C + \omega t_r p_C & -p_C + \omega t_r q_C \end{bmatrix}, \tag{5.68}$$

$$\mathbf{x} = [x_y,\ y_y,\ x_z,\ y_z]^T, \tag{5.69}$$

$$\widetilde{A}_{y,z}^{(1)} = x_{y,z} + j y_{y,z}, \tag{5.70}$$

$$\widetilde{A}_C^2 = p_C + j q_C, \tag{5.71}$$

$$\mathbf{b} = [0,\ 0,\ 1,\ \omega t_r]^T, \tag{5.72}$$

$$H_{0,\infty}^{(e)} = 1 - \frac{\omega_{0,\infty}^2}{\omega^2} - \frac{\beta c_0^2 k_1^4}{\omega^6} |\widetilde{A}_C|^2. \tag{5.73}$$

Equation (5.66) is inverted numerically.

An example frequency response in the case of nearly circularly polarized motion is presented in Fig. 5.10. The dashed curves represent the response in the fixed reference frame in the case of circularly polarized motion $\widetilde{a}_C = \widetilde{A}_C + a_0$. In the nearly circularly polarized case corresponding to the solid curves, the magnitude of the major component $\widetilde{a}_y$ [blue curve in Fig. 5.10(a)] follows closely with that of $\widetilde{a}_C$ except near resonance, where the response is reduced compared to $\widetilde{a}_C$. The magnitude of the minor component $\widetilde{a}_z$ [red curve in Fig. 5.10(b)] lies slightly below $\widetilde{a}_C$ at all frequencies due to the non-zero value of the eccentricity e. The reduction of the magnitude of the major component near resonance indicates that energy is transfered from the major to the minor component at those frequencies, similar to that observed in the case of nearly linearly polarized motion in Sec. 5.2.2.

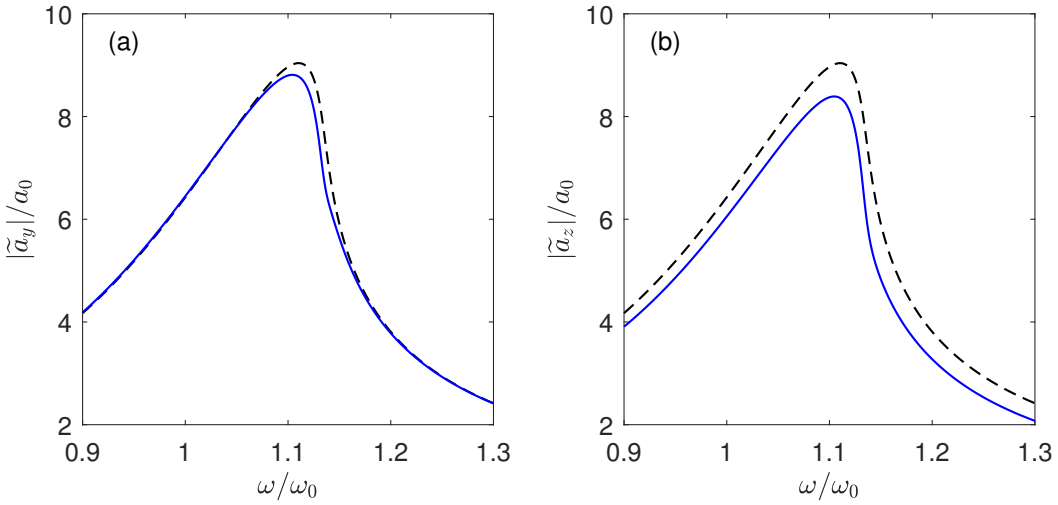

Figure 5.10: Frequency response functions for the major and minor components in the case of nearly circularly polarized motion (solid curves) with $e = 0.1$. In each plot the black dashed curve represents the case of circular polarization $\widetilde{a}_C = \widetilde{A}_C + a_0$. Parameters used are $m = 0.68$, $\omega_0 t_r = 0.23$, $s = 0.9$, $\epsilon_0 = 0.6$, and $\beta = 2$.

Comparison of the response according to the expansion in Eq. (5.62) with numerical solutions of Eqs. (5.41) and (5.42) shows that the expansion is accurate for values of $e \lesssim 0.05$ or, equivalently, in the range $0.95 \lesssim s \leq 1$. Furthermore, for the same drive amplitude, a multivalued tuning curve for circularly polarized motion will have different vertical-tangent frequencies than the corresponding tuning curve in the case of nearly circularly polarized motion. Use of a multivalued frequency response function $\widetilde{A}_C$ in Eq. (5.66) to compute the higher-order terms $\widetilde{A}^{(1)}_{y,z}$ yields singular solutions of Eq. (5.66) because of this discrepancy. Therefore Eq. (5.66) may only be used to compute $\widetilde{A}^{(1)}_{y,z}$ when the frequency response function $\widetilde{A}_C$ is single valued and does not exhibit jump phenomena.

Chapter 6

Summary and Future Directions

This dissertation is an investigation of the interaction between nonlinear elastic and viscoelastic effects in the propagation of plane shear waves. The primary goals were to develop a mathematical description of plane shear wave motion in a nonlinear, relaxing material, and to describe various ways that nonlinearity competes with viscoelasticity during the motion of progressive and standing shear waves. By considering viscoelastic effects due to stress relaxation in particular, we were able to make significant progress analytically, supplemented with several numerically obtained results.

In Chapter 2 the material model that describes shear deformations of a relaxing, elastic material was developed using three separate approaches. Each approach is common to a different field and offers unique insights into the underlying physics of relaxation and nonlinearity. Relations connecting the three approaches to each other were presented. Extensions of the model to multirelaxing media and diffracting shear wave beams were discussed. Finally, nonlinear wave equations were presented that govern the propagation of plane shear waves in a relaxing material. In the case of elliptically polarized shear waves, the two nonlinear wave equations for the components of the transverse

particle motion are coupled as a result of nonlinearity.

Chapter 3 focused on the propagation of progressive plane shear waves. An evolution equation similar to the Burgers equation was derived using the standard transformation of the nonlinear wave equation into a retarded time frame. Several analytical solutions of the evolution equation were derived that demonstrate the influence of relaxation on the nonlinear evolution of a plane shear wave, including an expression for the profile of a steady step shock, a solution for harmonic generation from an initially sinusoidal source, and a weak shock solution for waves at frequencies well above the relaxation frequency.

In Chapter 3 it was revealed by solutions of the evolution equation that energy dissipation due to relaxation is unable to keep waveform steepening in check and prevent initially single-valued time waveforms from developing infinite gradients and ultimately becoming multivalued. In Chapter 4 the evolution equation was transformed into an intrinsic coordinate system, thereby enabling numerical simulation of nonlinear shear waveform evolution in a relaxing medium up to and beyond the point at which overturning occurs. The critical source amplitude above which waveform overturning occurs was determined numerically over a broad range of source frequencies. An interesting result from Chapter 4 is that there exists a critical source amplitude above which waveform overturning will occur regardless of the source frequency, even at frequencies well below the relaxation frequency, where a relaxing material might be expected to behave like a classically viscous medium.

Nonlinear standing shear waves were the topic of Chapter 5, where a

shear wave resonator formed from a nonlinear, relaxing material was analyzed. With the nonlinear wave equation approximated by a modal expansion, the amplitude-dependent frequency response of the resonator was described using one or more ordinary differential equations that are augmented forms of the Duffing equation. For linearly polarized particle motion of the resonator, an implicit analytical expression for the amplitude-dependent frequency response was obtained for the case where the drive frequency is near the lowest resonance. Subharmonic generation was examined for the case where the drive frequency is near the second resonance frequency. Elliptically polarized particle motion of the resonator near the lowest resonance was examined by obtaining approximate solutions of two coupled augmented Duffing equations that demonstrate effects due to the coupling between the transverse displacement components that arises because of nonlinearity. Jump phenomena and hysteresis were observed in all cases for sufficiently large amplitudes of the drive motion.

The availability of analytical solutions of the model equations yields simple means for inferring material parameters from measured data, and they should prove useful for applications in material characterization, such as nonlinear elastography. In each of Chapters 2, 3, and 5, solutions are obtained that may be used for the measurement of viscoelastic and nonlinear material parameters: the rheological application of Sec. 2.3.4, the expression for harmonic generation in radiation from a time-harmonic source given in Sec. 3.4.1, and the amplitude-dependent frequency response of a nonlinear shear wave

resonator derived in Sec. 5.1.2, for example.

The main limitation of this work is its focus on relaxation as the form of viscoelasticity. While stress relaxation has been observed in shear wave motion in a variety of elastic materials (see, e.g., Refs. [27, 28, 29]), and its simple mathematical representation allowed us to make substantial progress analytically, many other manifestations of viscoelasticity have also been observed, such as power-law attenuation (see, e.g., Refs. [51, 52]). Procedures for extending each of the modeling approaches employed in Chapter 2 in order to describe materials that exhibit other types of viscoelasticity (e.g., power-law attenuation or multiple relaxation mechanisms) are discussed in that chapter. Once a stress-strain relation is obtained for the material of interest, the nonlinear shear wave equation and corresponding evolution equation can be obtained for the material following the procedures outlined in Secs. 2.4 and 3.1, respectively. The extent to which analytical progress can be made depends on the form of the resulting wave and evolution equations. For example, a considerable amount of effort has been devoted to the case of linear wave motion with power-law attenuation, for which the loss term is expressed in terms of a fractional derivative [67, 68]. It is reasonable to expect that nonlinear analyses should be worthy of pursuit for arbitrary types of viscoelasticity, for example harmonic generation in the case of weak nonlinearity as carried out in Sec. 3.4.1; see also Blackstock [44]. It is also reasonable to expect that numerical solution of the equations would be possible following the same procedures that were used in Secs. 3.3 and 5.1.2.

Finally, all of the analyses and results contained in this work are restricted to plane shear waves, for which the transverse particle displacement is a function of only one spatial dimension. The restriction to only one-dimensional motion permitted the derivation of relatively simple wave and evolution equations that facilitated investigation of the competition between nonlinearity and viscoelasticity. A similar study of multidimensional motion, such as a diffracting shear wave beam in a relaxing medium, would rely on model equations that are much more complex mathematically; see, e.g., Refs. [15, 16, 17]. Additionally, the lumped-element material representation and the internal variable formulation of the state equation presented in Secs. 2.2.1 and 2.2.2, respectively, are only valid in the one-dimensional case. An extension of the relaxation tensor approach employed in Sec. 2.2.3 is necessary to obtain a stress-strain relation for multidimensional shear deformations in a viscoelastic material.

Appendices

Appendix A

Derivation of Head Shock Integral

Derived here is the integral relation Eq. (3.51) that determines the amplitude of a shock propagating into an undisturbed medium subject to the simple-wave relation Eq. (3.46). The corresponding relation for the evolution of a compressional wave that consists of a head shock propagating into a quiet fluid, for which the nonlinearity is quadratic, was presented by Whitham [46].

A pulse is radiated that is initially described by $Q(\Theta, 0) = F(\Theta)H(\Theta)$ where $H(\Theta)$ is the Heaviside step function. As a result of nonlinear waveform distortion, the initially vertical wave front will become multivalued. The multivalued waveform is described using the parametric solution of Eq. (3.46):

$$Q = F(\Phi), \qquad \Phi = F^{-1}(Q) + ZQ^2. \tag{A.1}$$

The multivalued waveform is corrected using the equal-area rule of weak-shock theory,[1] whereby the areas bounded by the multivalued waveform on either side

Material from this appendix was previously published in J. M. Cormack and M. F. Hamilton, "Plane nonlinear shear waves in relaxing media," *J. Acoust. Soc. Am.* **143**, 1035–1048 (2018), which appears as Ref. [32] in this dissertation. Contributions from JMC include derivation of equations of motion, derivation and validation of solutions, and writing of the article.

[1] Lee-Bapty and Crighton [8] provide several examples and an in-depth discussion of

of the shock arrival time $\Theta_{\rm sh}$ must be equal. Integration over the waveform amplitude Q reveals that the following relation must be satisfied:

$$\int_0^1 \left(-ZQ^2 - \Theta_{\rm sh}\right)\, dQ + \int_{Q_{\rm sh}}^1 \left(\Theta_{\rm sh} - \Theta_F\right)\, dQ = 0, \tag{A.2}$$

where $\Theta_F = F^{-1}(Q) = \Phi - ZF^2$ and $Q_{\rm sh}$ is the value of Q at $\Theta = \Theta_{\rm sh}$. Rearranging yields

$$\Theta_{\rm sh}Q_{\rm sh} + \int_0^1 ZQ^2\, dQ + \int_{Q_{\rm sh}}^1 \left(\Phi - ZF^2\right)\, dF = 0, \tag{A.3}$$

where the definition of Φ given after Eq. (A.2) and the relation $dQ = dF$ have been substituted into the third term in Eq. (A.3). Evaluation of the first integral and the second term in the last integral is straightforward. The remaining integral is evaluated by substituting $dF = F'\, d\Phi$ and then integrating by parts,

$$\int_{Q_{\rm sh}}^1 \Phi\, dF = \int_{\Phi_{\rm sh}}^0 \Phi F'\, d\Phi = (F\Phi)|_{\Phi_{\rm sh}}^0 - \int_{\Phi_{\rm sh}}^0 F(\Phi)\, d\Phi, \tag{A.4}$$

where the integration limits of the integral over Φ correspond to $\Phi = \Phi_{\rm sh}$ at the shock, by definition, and $\Phi = 0$ at the tip of the multivalued waveform where $Q = 1$. Substitution of Eq. (A.4) into Eq. (A.3) yields

$$\Phi_{\rm sh}Q_{\rm sh} - ZQ_{\rm sh}^3 + (\Phi F)|_{\Phi_{\rm sh}}^0 - \int_{\Phi_{\rm sh}}^0 F(\Phi)\, d\Phi + \frac{1}{3}ZQ_{\rm sh}^3 = 0, \tag{A.5}$$

where the relation $\Theta_{\rm sh} = \Phi_{\rm sh} - ZQ_{\rm sh}^2$ has been used. The first and third terms cancel, and rearranging yields Eq. (3.51):

$$ZQ_{\rm sh}^3 = \frac{3}{2}\int_0^{\Phi_{\rm sh}} F(\Phi)\, d\Phi. \tag{A.6}$$

---

weak shock theory and the equal area rule as applied to waves in a medium with cubic nonlinearity.

The integral relation given in Eq. (A.6) is an extension of the corresponding relation obtained by Whitham [46] for the head shock of a compressional wave propagating into a quiet fluid with quadratic nonlinearity. Evolution of a head shock in a medium with n^{th} order nonlinearity is described by the following generalization of Eq. (A.6):

$$ZQ_{\text{sh}}^{n} = \frac{n}{n-1}\int_{0}^{\Phi_{\text{sh}}} F(\Phi)\, d\Phi. \tag{A.7}$$

With $n = 2$, Eq. (A.7) recovers Whitham's head shock integral for a compressional wave with quadratic nonlinearity, and with $n = 3$ Eq. (A.7) reduces to Eq. (A.6) and describes the evolution of a head shock in a shear wave, for which the nonlinearity is cubic.

Appendix B

A Disagreement about the Theory of Sound

The following anecdote is focused on a series of letters published in *Philoshopical Magazine* between 1848 and 1849. The exchange of letters covers disagreement over two fundamental questions that were at the forefront of physical acoustics at that time. The first was a discrepancy between the predicted and measured speed of sound in air, and the second regarded the interpretation of an exact, yet misleadingly simple, solution for propagation of a finite-amplitude plane wave in air. This Appendix is an expansion of a story found in the chapter "History of Nonlinear Acoustics: 1750s–1930s" by D. T. Blackstock, in Hamilton and Blackstock's *Nonlinear Acoustics* [6]. While unrelated to shear wave propagation in relaxing media, it is a relevant precursor to the study presented in Chapter 4 of this dissertation. The account is also quite amusing. Literature that is not cited in the main text of this dissertation are cited as footnotes in this appendix.

B.1 Newtonian sound speed and Laplace's correction

Isaac Newton's prediction in 1686[1] of the speed of sound, $b_0 = \sqrt{p_0/\rho_0}$ where p_0 and ρ_0 are the ambient atmospheric pressure and density, based on the use of Boyle's law for the constitutive relation of air stirred up quite a bit of confusion in the scientific community in the 18th and 19th centuries. Newton's prediction was lower, by about 16%, than the commonly accepted value based on decades of artillery testing, prompting many attempts to explain the discrepancy.

Thermodynamics as a field of research was nonexistent at Newton's time and was only just beginning to develop in the late 18th century. It was Pierre-Simon Laplace who, in 1816, first[2] provided the correct reason for the discrepancy, noting that, in modern terminology, acoustic processes are adiabatic, not isothermal as Newton had presupposed (by no fault of his own): "Since this [heat] diffusion takes place very slowly relative to the velocity of the vibrations, we may suppose without sensible error that during the period of a single vibration the quantity of heat remains the same between two neighboring molecules."

Several decades later in 1847, James P. Joule[3] put Laplace's theory to

[1] I. Newton, *Principia Mathematica* Sec. VIII. Of motion propagated through fluids (1686). Translation by R. B. Lindsay, *Acoustics: Historical and Philisophical Development* (Dowden, Hutchinson & Ross, Stroudsburg, PA, 1972), pp. 75–86.

[2] P.-S. Laplace, "On the velocity of sound through air and through water," *Ann. Chim. Phys.* **3**, 338–241. English translation by Lindsay (1972) pp. 180–182.

[3] J. P. Joule, "On the theoretical velocity of sound," *Phil. Mag. Ser. 3* **31**, 114–115 (1847).

the test and performed the appropriate calculations using recently measured values of the heat capacity of air, and showed that Laplace's prediction for the speed of sound matched almost exactly the measured value. In modern notation the adiabatic sound speed is written as $c_0 = \sqrt{\gamma p_0/\rho_0}$ where γ is the ratio of specific heats, and for air $\gamma = 1.4$.

B.2 "Manifest absurdity"

The thermodynamic explanation was not immediately adopted by all. One amusing exchange of ideas began in March 1848 when Rev. James Challis[4] presented a solution for the three-dimensional wave equation using separation of variables, misinterpreted his expression for the phase velocity, and claimed that he had discovered the reason for Newton's discrepancy without the use of thermodynamics.[5] His conclusion was based on his interpretation that the solution showed that sound is "non-divergent" (i.e., non-diffracting; diffraction theory would not arise for several decades after this exchange).

In the next issue of *Philosophical Magazine*, George B. Airy[6] wrote back

[4]Rev. James Challis (1803–1882) at this time was the Plumian Professor at the University of Cambridge and director of the Cambridge Observatory. He is best known for refining the accuracy of the instrumentation of the observatory, his observations of comets and asteroids, and unfortunately also for barely losing the race to discover the planet Neptune.

[5]J. Challis, "Theoretical determination of the velocity of sound," *Phil. Mag. Ser. 3* **32**, 276–284 (1848).

[6]George Biddel Airy (1801–1892) was at this time the Astronomer Royal (director of the Royal Observatory in Greenwich). His tenure as Astronomer Royal is best known for his organization of the many lunar observations made at the observatory, and for establishing the Prime Meridian to run through Greenwich. He, along with Challis, receives a part of the blame for not discovering Neptune first.

to Challis, correctly interpreting his solution as a plane wave decomposition of the wave field, and pointing out that the phase speed of any plane wave in the expansion is given by Newton's prediction b_0.[7] Airy does not mention Laplace's thermodynamic theory. He also states of the plane waves, again revealing the absence of diffraction theory at this time, that "these waves cannot all originate from one source, and therefore this solution does not relate to the problem of sound."

Challis responded[8] in May 1848 to Airy's interpretation of his solution as a plane-wave expansion by claiming that the existence of plane waves is "manifest absurdity" and "physically impossible", citing the fact that the exact implicit solution of Siméon Poisson for a plane wave of finite amplitude in air,[9] $u = f[x-(c+u)t]$ where u is the particle velocity and f is an arbitrary function, predicts that a plane wave in air will at some point evolve into a waveform for which "the points of no velocity are also points of maximum velocity." Challis was apparently the first to identify the mathematical phenomenon of waveform overturning, but unfortunately concluded that it disqualifies the existence of plane waves altogether. Challis wrote two more letters in July and October of 1848 detailing his thoughts regarding the speed of sound and the (non-) existence of plane and spherical waves in air.

[7] G. B. Airy, "The Astronomer Royal's remarks on Professor Challis's theoretical determination of the velocity of sound," *Phil. Mag. Ser. 3* **32**, 339–343 (1848).

[8] J. Challis, "On the velocity of sound, in reply to the remarks of the Astronomer Royal," *Phil. Mag. Ser. 3* **32**, 494–499 (1848).

[9] S. D. Poisson, "Mémoire sur la théorie du son," *J. l'école Polytech.* **7**, 319–392. Translation of Secs. 23–25 by R. T. Beyer, *Nonlinear Acoustics in Fluids* (Van Nostrand Reinhold, New York, 1974), pp. 23–28.

B.3 Stokes enters the controversy

The most impactful argument in this exchange came in October 1848 with the publication in *Philosophical Magazine* of the groundbreaking letter "On a difficulty in the theory of sound," by George G. Stokes [47],[10] which begins with the amusing statement: "It is not my intention to enter the controversy, but...". The main concern of Stokes in this letter is not the discrepancy with the speed of sound, but is instead with Challis's claim that a plane wave in air is not physically admissible. Stokes correctly interpreted Poisson's implicit solution and identified the consequences of the amplitude-dependent phase speed, sketching for the first time waveform steepening of an initially sinusoidal wave. He then determined the point in the wave field, now referred to as the shock formation distance, at which a vertical tangent forms in the waveform, and points out that the mathematical model upon which Poisson's solution is based can no longer be valid once this occurs.

After ascertaining that the usual differential equations of motion are invalid past the shock formation distance, Stokes speculated about the subsequent motion. He showed that a surface of discontinuity can develop in the waveform, speculated that reflections must occur at the discontinuity, and presented relations for conservation of mass and conservation of momentum

[10] George Gabriel Stokes (1819–1903) made many contributions to the fields of fluid dynamics, optics, and chemistry, to name only a few. He graduated from Pembroke College at the University of Cambridge in 1841 as Senior Wrangler (top undergraduate student in Mathematics) and in 1848 was a fellow of the College. In 1849 he was appointed Lucasian Chair of Mathematics, a position he held until his death. He was 29 years of age during this anecdote.

across a surface of discontinuity. These two relations now make up two-thirds of the famous Rankine-Hugoniot relations for discontinuous motion in gases. Stokes did not derive the third (conservation of energy) as he did not realize that the shock was necessarily a lossy process.[11] Stokes then directly addressed Challis's claims of mathematical prediction versus physical admissibility: "It does not follow that the discontinuous motion considered can ever take place in nature, for we have all along been reasoning on an ideal elastic fluid which does not exist in nature," and concluded by speculating that viscosity would act to limit waveform steepening such that a surface of discontinuity never forms in a real fluid.

Rev. Challis wasted no time in responding: in November 1848 he wrote in another letter[12] that Stokes's claim that a surface of discontinuity can develop in a plane wave in air only proves that plane waves cannot exist. He writes "How then stands the question? According to my reasoning plane-waves are physically impossible; according to Mr. Stokes's, plane-waves are *wholly incompatible with the transmission of articulate and musical sounds* [emphasis is Challis's]. The only conclusion from either result is, that the hypothesis of plane-waves in inadmissible." In other words, Challis claimed that because sound fields from speech and music do not contain surfaces of discontinuity

[11] This was by no fault of his own, as before with Newton, the necessary thermodynamical tools were not available to him at the time. It was not until his famous article in 1870 that Rankine realized that a surface of discontinuity must be accompanied by a change in entropy and therefore energy loss. Thus the famous shock relations bear his name and not Stokes's.

[12] J. Challis, "Further investigation of the nature of aerial vibrations," *Phil. Mag. Ser. 3* **33**, 462–466 (1848).

that such surfaces must not exist at all. Challis continues, "It may, however be urged that spherical waves are possible; and that as these become plane-waves at an infinite distance from the centre, the latter are also physically possible." He then demonstrates that an arbitrary spherically spreading waveform *generates* mass as it propagates, concluding that spherical waves also cannot exist in nature as they violate conservation of mass.[13]

B.4 "An interesting field of inquiry"

Stokes spent his Christmas holiday writing a reply, and on December 23, 1848 submitted another letter.[14] He first addressed Challis's claim that only musical sounds may exist, reminding Challis of the difference between a real fluid and the mathematical model of an ideal fluid: "I was particularly careful to keep purely mathematical questions quite distinct from the physical considerations which followed. ... What signifies it if the *ideal* elastic fluid which forms the basis of our mathematical reasoning be wholly incompetant to transmit such sounds unchanged?" Stokes then recognized that even though the ideal fluid may not be a good model for air when surfaces of discontinuity can develop in the wave field, the model could be useful in the region of propagation before they develop. He stated that, due to spreading and

[13]The other conclusion to draw from Challis's analysis is that spherically spreading waveforms may not be arbitrary, as plane waves may be. See, for example, Landau and Lifshitz, *Fluid Mechanics, 2nd ed.* (Butterworth-Heinemann, Oxford, 1987), Sec. 70.

[14]G. G. Stokes, "On some points in the received theory of sound," *Phil. Mag. Ser. 3* **34**, 52–60 (1849).

thermoviscous losses, "musical sounds" would travel a considerable distance without significant alteration. He also wrote:

> The effect of distance upon the quality of sound ... would form an interesting field of inquiry.

Stokes could not have written more of an understatement; the field of inquiry to which he refers in the above remark is Nonlinear Acoustics itself! The letter concludes with the presentation of no less than four separate arguments against Challis's claim that spherical waves violate conservation of mass.

The quotation above being the apex of the story, we conclude with a summary of the end of the exchange between Challis and Stokes. Challis responded immediately to Stokes's arguments in January 1849,[15] although with a more aggressive tone than before. Challis wrote that he will no longer address Stokes's claims regarding discontinuities in plane waves, "as this difference is not likely to be removed by further mathematical discussion." Moving on to the question of the admissibility of spherical waves, Challis presented a more detailed version of his previous argument, but again ignoring the necessary physical considerations in his derivation that Stokes pointed out in his last letter.

Between February and June of 1849, Stokes and Challis exchanged five more letters arguing over the existence of spherical waves in air, and Challis

[15] J. Challis, "Continuation of researches in the mathematical theory of aerial vibrations," *Phil. Mag. Ser. 3* **34**, 88–98 (1849).

published another continuing his arguments for a hydrodynamical explanation of the sound speed discrepancy. Eventually, Stokes wrote that he will no longer continue to debate either point: "It is not my intention to attack Professor Challis's new views respecting the theoretical velocity of sound; because if Professor Challis and I cannot agree on ... so plain a matter as the theory of spherical waves, I see little chance of our agreeing on the [former] subject."[16]

Airy eventually replied[17] to Challis as well, remarking, "the expression 'a plane wave of air is impossible' stands on precisely the same footing as the expression 'a tide in the Severn is impossible.'" Airy also presented the first derivation for harmonic generation from a time harmonic source using successive approximations in his reply.

The issue of the theoretical velocity of sound arose again a few years later in 1851, though this time it was Professor Richard Potter of University College London who doubted Laplace's theory, and it was William J. R. Rankine of Glasgow University who came to its defense.[18] It was in this letter that Rankine first used the symbol γ to represent the ratio of specific heats, a notation that is commonly used to this day. Two years after that, with new measurements of specific heats and his budding new Mechanical Theory of Heat, Rankine was able to calculate the speed of sound based on Laplace's

[16]G. G. Stokes, "On the theory of sound," *Phil. Mag. Ser. 3* **34**, 501–502 (1849).
[17]G. B. Airy, "The Astronomer Royal on a difficulty in the problem of sound," *Phil. Mag. Ser. 3* **34**, 401–405 (1849).
[18]W. J. M. Rankine, "On Laplace's theory of sound," *Phil. Mag. Ser. 4* **1**, 225–227 (1851).

theory for five gases, demonstrating remarkable agreement with experimental observations in all five cases.[19]

B.5 Summary

On top of being a fun tale, the story above serves as an illustrative example of how a peculiarity encountered in mathematical physics was approached. Challis took the mathematical model of an ideal fluid to give the complete picture of sound in air, thereby concluding that predictions of the model that didn't make physical sense pointed to limitations in nature instead of the model. Stokes, on the other hand, recognized that an ideal fluid is only a modeling tool that cannot be universally applied. Stokes's arguments are reminiscent of George E. P. Box's famous saying, "All models are wrong, but some are useful."

Stokes further recognized the need for a new model to describe the propagation of the wave after the ideal fluid model breaks down. His speculations about conservation of mass and momentum now make up two of the three Rankine-Hugoniot shock relations, which are widely used in gas dynamics to this day. The reduced form of the Rankine-Hugoniot relations in the case of discontinuities with small, but finite, jumps is the foundation of weak shock theory.

[19] W. J. M. Rankine, "Mechanical Theory of Heat.-Velocity of sound in gases," *Phil. Mag. Ser. 4* **5**, 483–486 (1853).

Appendix C

Formulation of the Evolution Equation in Intrinsic Coordinates

Here, basic relations employing the intrinsic coordinates introduced by Hammerton and Crighton [30] are presented. First, a formulation for the transformation of a general evolution equation is derived in Sec. C.1. The evolution equation for plane nonlinear shear waves in a relaxing medium is then transformed in Sec. C.2 by applying the formulation to Eq. (3.19).

C.1 Transformation of a general evolution equation

In reference to the dimensionless physical coordinates in Eq. (3.17), the intrinsic coordinate system consists of the arc length $s(\theta)$ along the waveform from $V(0)$ to $V(\theta)$, and the angle $\psi(\theta)$ of the tangent to the waveform at that point (see Fig. 4.1). The spatial coordinate X is unchanged. Thus the evolution of the waveform is described by $\psi(X, s)$ instead of $V(X, \theta)$. The

Selected material from this appendix was previously published in J. M. Cormack and M. F. Hamilton, "Overturning of nonlinear compressional and shear waves subject to power-law attenuation or relaxation," *Wave Motion* **85**, 18–33 (2019), which appears as Ref. [53] in this dissertation. Contributions from JMC include derivation of transformed equations of motion, numerical solution of those equations, validation of solutions, and writing of the article.

transformation is defined by

$$\psi = \tan^{-1}(\partial V/\partial\theta), \qquad s = \int_0^\theta \sqrt{1 + (\partial V/\partial\theta)^2}\, d\theta\,. \tag{C.1}$$

From these definitions follow the differential relations

$$d\theta = ds\cos\psi, \qquad \frac{\partial}{\partial\theta} = \sec\psi\,\frac{\partial}{\partial s}, \tag{C.2}$$

as well as the inverse transformation

$$V = V_0(X) + \int_0^s \sin\psi\, ds\,, \qquad \theta = \int_0^s \cos\psi\, ds\,, \tag{C.3}$$

where $V_0(X) = V(X, 0)$. For simplicity, it is henceforth assumed here that $V_0(X) = 0$ for all X. If $V_0(X) \neq 0$ an additional term appears in the evolution equation for $\psi(X, s)$ and an additional evolution equation for $V_0(X)$ is required [see Eqs. (3.10) and (3.11) in Ref. [30]].

A general evolution equation has the following form:

$$\frac{\partial V}{\partial X} = G(X,\, \theta,\, V,\, \partial V/\partial\theta, ...), \tag{C.4}$$

where G is a function of the space and time coordinates as well as V and derivatives of V with respect to retarded time θ. From Eq. (C.1) we have $\partial V/\partial\theta = \tan\psi$, and so

$$\frac{\partial}{\partial X}\tan\psi = \frac{\partial G}{\partial\theta}, \tag{C.5}$$

which combined with the second of Eqs. (C.2) yields

$$\frac{\partial\psi}{\partial X} = \frac{\partial G}{\partial\theta}\cos^2\psi = \frac{\partial g}{\partial s}\cos\psi, \tag{C.6}$$

where g is the function G recast in the intrinsic variables. Change in arc length with propagation distance is accounted for by expansion of $\partial\psi/\partial X$ using the chain rule to obtain

$$\left(\frac{\partial\psi}{\partial X}\right)_s + \frac{ds}{dX}\frac{\partial\psi}{\partial s} = \frac{\partial g}{\partial s}\cos\psi, \tag{C.7}$$

where $(\partial\psi/\partial X)_s$ indicates that the derivative is taken with s held constant. This is the case for all occurrences of $\partial\psi/\partial X$ henceforth and in Chapter 4, but the subscript s will be neglected beyond this point. Substituting Eq. (C.4) and the first of Eqs. (C.1) into the spatial derivative of the second of Eqs. (C.1) yields

$$\frac{ds}{dX} = \int_0^s \frac{\partial g}{\partial s}\sin\psi\, ds, \tag{C.8}$$

such that the evolution equation for $\psi(X, s)$ becomes

$$\frac{\partial\psi}{\partial X} = \frac{\partial g}{\partial s}\cos\psi - \frac{\partial\psi}{\partial s}\int_0^s \frac{\partial g}{\partial s}\sin\psi\, ds. \tag{C.9}$$

Once the function G in Eq. (C.4) is identified for the evolution equation of interest, g can be found by direct substitution of Eqs. (C.3). The derivative $\partial g/\partial s$ is evaluated and substituted into Eq. (C.9), which is then simplified to obtain the new evolution equation for $\psi(X, s)$. Waveform evolution is then determined in intrinsic coordinates by solving Eq. (C.9) numerically. Equations (C.3) return the intrinsic-coordinate waveforms $\psi(s)$ to the physical waveforms $V(\theta)$, which are multivalued for $|\psi| > \pi/2$.

C.2 Transformation of Eq. (3.19)

The form of the evolution equation to be used here for plane nonlinear shear waves in a relaxing medium is Eq. (3.19). Comparison with (C.4) shows that in this case

$$G = V^2 \frac{\partial V}{\partial \theta} + D\,H(V), \tag{C.10}$$

where

$$H(V) = \int_{-\infty}^{\theta} e^{-(\theta-\theta')/\theta_r} \frac{\partial^2 V}{\partial \theta'^2}\, d\theta'. \tag{C.11}$$

Use of Eqs. (C.1) and (C.3) gives

$$g = \tan\psi \left(\int_0^s \sin\psi\, ds \right)^2 + Dh(\psi), \tag{C.12}$$

where $h(\psi)$ is the function $H(V)$ recast in the intrinsic variables. The first term on the right-hand side of Eq. (C.9) is

$$\frac{\partial g}{\partial s}\cos\psi = \frac{\partial \psi}{\partial s}\sec\psi \left(\int_0^s \sin\psi\, ds \right)^2 + 2\sin^2\psi \int_0^s \sin\psi\, ds + D\frac{\partial h}{\partial s}\cos\psi, \tag{C.13}$$

and the integral in the second term becomes

$$\begin{aligned} \int_0^s \frac{\partial g}{\partial s}\sin\psi\, ds = \int_0^s & \left[\tan\psi \sec\psi \frac{\partial \psi}{\partial s} \left(\int_0^s \sin\psi(s')\, ds' \right)^2 \right] ds \\ & + 2\int_0^s \left(\tan\psi\, \sin^2\psi \int_0^s \sin\psi(s')\, ds' \right) ds \\ & + D\int_0^s \frac{\partial h}{\partial s}\sin\psi\, ds. \end{aligned} \tag{C.14}$$

The first term on the right-hand side of Eq. (C.13) and the first two terms on the right-hand side of Eq. (C.14) contain tangent and secant terms that

become unbounded if the waveform $|\psi(s)|$ achieves a value of $\pi/2$, indicating that $V(\theta)$ has developed a vertical tangent. The presence of these terms is undesirable if one wishes to simulate multivalued waveforms in $V(X,\theta)$, for which $|\psi| > \pi/2$. Integration of first term on the right-hand side of Eq. (C.14) by parts and substitution of $\sin^2\psi = 1 - \cos^2\psi$ in the second term yields

$$\int_0^s \frac{\partial g}{\partial s}\sin\psi\,ds = \sec\psi\left(\int_0^s \sin\psi\,ds\right)^2 - 2\int_0^s\left(\sin\psi\cos\psi\int_0^s \sin\psi(s')\,ds'\right)ds + D\int_0^s \frac{\partial h}{\partial s}\sin\psi\,ds. \tag{C.15}$$

Substitution of Eqs. (C.13) and (C.15) into Eq. (C.9) results in cancellation of terms involving $\sec\psi$, giving

$$\frac{\partial\psi}{\partial X} = 2\sin^2\psi\int_0^s \sin\psi\,ds + 2\frac{\partial\psi}{\partial s}\int_0^s\left(\sin\psi\cos\psi\int_0^s \sin\psi(s')\,ds'\right)ds + D\left(\frac{\partial h}{\partial s}\cos\psi - \frac{\partial\psi}{\partial s}\int_0^s \frac{\partial h}{\partial s}\sin\psi\,ds\right). \tag{C.16}$$

An alternative form is obtained by integrating the last term by parts, resulting in

$$\frac{\partial\psi}{\partial X} = 2\sin^2\psi\int_0^s \sin\psi\,ds + 2\frac{\partial\psi}{\partial s}\int_0^s\left(\sin\psi\cos\psi\int_0^s \sin\psi(s')\,ds'\right)ds + D\left(\frac{\partial f}{\partial s} + \frac{\partial\psi}{\partial s}\int_0^s f(\psi)\frac{\partial\psi}{\partial s}\,ds\right), \tag{C.17}$$

where $f(\psi) = h\cos\psi$. The form of $f(\psi)$ for a relaxing medium is now developed.

Attenuation and dispersion in an otherwise inviscid, monorelaxing fluid are accounted for by the term given in Eq. (C.11). Factoring out $e^{-\theta/\theta_r}$ and

substituting Eqs. (C.2) and (C.3) along with $\partial^2 V/\partial\theta^2 = (\sec^3\psi)\,\partial\psi/\partial s$ yields

$$h = e^{-\frac{1}{\theta_r}\int_0^s \cos\psi\, ds} \int_{-\infty}^{s} \left(e^{\frac{1}{\theta_r}\int_0^s \cos\psi(s')\, ds'} \frac{\partial\psi}{\partial s'} \sec^2\psi \right) ds'. \tag{C.18}$$

Integrating by parts one obtains

$$h = e^{-\frac{1}{\theta_r}\int_0^s \cos\psi\, ds} \left(e^{\frac{1}{\theta_r}\int_0^s \cos\psi\, ds} \tan\psi - \frac{1}{\theta_r} \int_0^s e^{\frac{1}{\theta_r}\int_0^{s'} \cos\psi\, ds''} \sin\psi(s')\, ds' \right), \tag{C.19}$$

which can be simplified to

$$h = \tan\psi - \frac{1}{\theta_r} e^{-\frac{1}{\theta_r}\int_0^s \cos\psi\, ds} \int_0^s e^{\frac{1}{\theta_r}\int_0^{s'} \cos\psi\, ds''} \sin\psi(s')\, ds', \tag{C.20}$$

or

$$f = \sin\psi - \frac{1}{\theta_r} e^{-\frac{1}{\theta_r}\int_0^s \cos\psi\, ds} \cos\psi \int_0^s e^{\frac{1}{\theta_r}\int_0^{s'} \cos\psi\, ds''} \sin\psi(s')\, ds'. \tag{C.21}$$

Following the discussion after Eq. (C.14), expressions that contain tangent or secant terms are undesirable as they become unbounded as the waveform develops a vertical tangent. Thus the appropriate method for including losses in the intrinsic coordinate formulation is with the evolution equation given by Eq. (C.17) and $f(\psi)$ given by Eq. (C.21).

Appendix D

Overturning of Nonlinear Shear Waves in Media that Exhibit Power-Law Attenuation

Waveform overturning of nonlinear shear waves in media that exhibit power-law attenuation and the accompanying dispersion is the subject of this appendix. The analysis and results parallel the content of Chapter 4 for the overturning of shear waves in a relaxing medium. First, the evolution that describes the propagation of a plane nonlinear shear wave subject to power-law attenuation is presented. The loss term, which is a fractional derivative, is then transformed into intrinsic coordinates. The form of the loss term in intrinsic coordinates demonstrates that overturning may only occur when the attenuation coefficient increases more slowly than linearly with frequency. Numerical results are then presented for the critical source amplitude above which an initially sinusoidal waveform will overturn at a finite distance from the source. Finally, for source amplitudes that exceed the critical value, the distance at which waveform overturning first occurs is determined numerically.

Selected material from this appendix was previously published in J. M. Cormack and M. F. Hamilton, "Overturning of nonlinear compressional and shear waves subject to power-law attenuation or relaxation," *Wave Motion* **85**, 18–33 (2019), which appears as Ref. [53] in this dissertation. Contributions from JMC include derivation of transformed equations

D.1 Basic equations

A nonlinear evolution equation similar to Eq. (3.9) that describes the propagation of a plane nonlinear shear wave in a medium that exhibits power-law attenuation is

$$\frac{\partial v}{\partial x} = \frac{\beta}{c_0^3} v^2 \frac{\partial v}{\partial \tau} - \delta_\nu \frac{\partial^\nu v}{\partial \tau^\nu}\,, \tag{D.1}$$

where c_0 in this case is the shear wave speed in the lossless case, and the last term is a *fractional derivative*.[1] The coefficient δ_ν is a material parameter with units $[T^\nu L^{-1}]$. The parameters δ_ν and ν can be connected to fractional constitutive relations [65]. See the discussion in Sec. 2.3.5 of this dissertation and especially Refs. [38] and [66] for a connection between relaxation and power-law attenuation.

Ignoring the nonlinear term in Eq. (D.1), taking the Fourier transform $\mathcal{F}\{v\} = v_\omega$, and employing the defining relation $\mathcal{F}\{\partial^\nu v/\partial\tau^\nu\} = (j\omega)^\nu \mathcal{F}\{v\}$ for the fractional derivative one obtains

$$\frac{dv_\omega}{dx} + \widetilde{\alpha}_\nu v_\omega = 0, \qquad \widetilde{\alpha}_\nu = (j\omega)^\nu \delta_\nu. \tag{D.2}$$

Inspection of the exponentials of linear solutions of Eq. (D.2) leads to the following expressions for the attenuation coefficient $\alpha(\omega)$ and phase speed $c(\omega)$

---

of motion, numerical solution of those equations, validation of solutions, and writing of the article.

[1] Good references for wave equations that contain fractional derivatives are the books by S. Holm [67] and F. Mainardi [68].

in a medium with power-law attenuation:

$$\alpha(\omega) = \delta_\nu \omega^\nu \cos\left(\frac{\nu\pi}{2}\right), \tag{D.3}$$

$$\frac{1}{c(\omega)} = \frac{1}{c_0} + \delta_\nu \omega^{\nu-1} \sin\left(\frac{\nu\pi}{2}\right). \tag{D.4}$$

The attenuation increases with frequency raised to the power ν, as required, and the phase speed satisfies the Kramers-Kronig relations [69]. It follows from Eq. (D.3) that $\delta_\nu > 0$ is required for $0 \leq \nu < 1$, and $\delta_\nu < 0$ for $1 < \nu < 3$, etc.

At low frequencies corresponding to $\omega t_r \ll 1$, Eqs. (3.11) and (3.12) reduce to $\alpha(\omega) \simeq m\omega^2 t_r/2c_0$ and $c(\omega) \simeq c_0$, respectively; attenuation increases as frequency squared and the phase speed is constant. At high frequencies corresponding to $\omega t_r \gg 1$, Eqs. (3.11) and (3.12) reduce to $\alpha(\omega) \simeq m/2c_0 t_r$ and $c(\omega) \simeq c_0(1 + m/2)$; both attenuation and phase speed are constant with frequency. A relaxing medium thus exhibits two different power-law behaviors. At low frequencies, Eqs. (D.3) and (D.4) with $\nu = 2$ are equivalent to Eqs. (3.11) and (3.12) with $\delta_2 = mt_r/2c_0$. At high frequencies, Eq. (D.3) with $\nu = 0$ is equivalent to (3.11) with $\delta_0 = m/2c_0 t_r$, although the phase speed given by Eq. (3.12) is the high frequency phase speed c_∞, not the low frequency speed as given by Eq. (D.4) with $\nu = 0$.

The dimensionless form of Eq. (D.1) that corresponds to the form of Eq. (3.19) is

$$\frac{\partial V}{\partial X} = V^2 \frac{\partial V}{\partial \theta} - A_\nu \frac{\partial^\nu V}{\partial \theta^\nu}, \tag{D.5}$$

where $A_\nu = \delta_\nu \omega^\nu x_{\rm sh}$. Comparison with (C.4) shows that in this case

$$G_\nu = V^2 \frac{\partial V}{\partial \theta} - A_\nu H_\nu(V), \tag{D.6}$$

where

$$H_\nu(V) = \frac{\partial^\nu V}{\partial \theta^\nu}. \tag{D.7}$$

Transformation of Eq. (D.5) then follows the same procedure as in Sec. C.2, the only difference being the form of $f(\psi)$ corresponding to the fractional loss term in Eq. (D.7). The evolution equation in intrinsic coordinates is

$$\begin{aligned}\frac{\partial \psi}{\partial X} = {} & 2\sin^2\psi \int_0^s \sin\psi \, ds + 2\frac{\partial \psi}{\partial s}\int_0^s \left(\sin\psi\cos\psi \int_0^s \sin\psi(s')\, ds'\right) ds \\ & - A_\nu \left(\frac{\partial f_\nu}{\partial s} + \frac{\partial \psi}{\partial s}\int_0^s f_\nu(\psi)\frac{\partial \psi}{\partial s}\, ds\right),\end{aligned} \tag{D.8}$$

the first two terms of which are identical to those in Eq. (4.3), and the function $f_\nu(\psi)$ that accounts for attenuation and dispersion from power-law attenuation is obtained as follows. Combination of Eqs. (D.7) and (C.1), and the chain rule for fractional derivatives [70],

$$\frac{\partial^\nu}{\partial \theta^\nu} = \left(\frac{ds}{d\theta}\right)^\nu \frac{\partial^\nu}{\partial s^\nu} = (\sec\psi)^\nu \frac{\partial^\nu}{\partial s^\nu}, \qquad 0 \le \nu \le 1, \tag{D.9}$$

leads to

$$h_\nu = (\sec\psi)^\nu \frac{\partial^\nu}{\partial s^\nu}\int_0^s \sin\psi \, ds \qquad 0 \le \nu \le 1 \tag{D.10}$$

$$= (\sec\psi)^{\nu-1} \frac{\partial^{\nu-1}}{\partial s^{\nu-1}} \tan\psi \qquad 1 \le \nu \le 2 \tag{D.11}$$

and

$$f_\nu = (\cos\psi)^{1-\nu} \frac{\partial^\nu}{\partial s^\nu}\int_0^s \sin\psi \, ds \qquad 0 \le \nu \le 1 \tag{D.12}$$

$$= (\cos\psi)^{2-\nu} \frac{\partial^{\nu-1}}{\partial s^{\nu-1}} \tan\psi \qquad 1 \le \nu \le 2\,. \tag{D.13}$$

The purpose of expressing the nonlinear evolution equation in intrinsic coordinates is to enable numerical simulation of solutions for waveforms $V(\theta)$ that contain vertical tangents or are multivalued. As discussed after Eq. (C.14) this means that inclusion of tangent and secant terms in the evolution equation for $\psi(X, s)$ is undesirable. Elimination of the tangent and secant was possible in the terms responsible for waveform steepening in Eqs. (4.3) and (D.8) and for the loss term in Eq. (4.4) that accounts for relaxation, but was not possible for the fractional loss term with exponent in the range $1 < \nu \leq 2$ in Eq. (D.13).

Whereas relaxation on its own is not necessarily sufficient to balance nonlinear and prevent waveform overturning, power laws that have exponent greater than unity are. This observation follows from noting that $f_\nu(\psi)$ for $1 < \nu \leq 2$ in Eq. (D.13) becomes unbounded whereas $f_{\text{rel}}(\psi)$ and $f_\nu(\psi)$ for $0 \leq \nu \leq 1$ in Eqs. (4.4) and (D.12), respectively, remain finite as $|\psi| \to \pi/2$, corresponding to the formation of a vertical tangent in the waveform $V(\theta)$. This conclusion based on the form of $f_\nu(\psi)$ is consistent with a frequency-domain analysis of Kashcheeva et al. [55] demonstrating that pre-existing discontinuities are stable in media with power-law attenuation only for exponents less than unity.

D.2 Critical source amplitude and shock formation distance

Multivalued solutions of Eq. (D.5) are possible for $0 \leq \nu \leq 1$. The critical source amplitude above which an initially sinusoidal waveform will develop

a vertical tangent is characterized by the following dimensionless attenuation coefficient obtained from Eq. (D.3):

$$a = \alpha(\omega) x_{\mathrm{sh}} = A_\nu \cos(\nu\pi/2). \tag{D.14}$$

The parameter a is thus proportional to the attenuation coefficient α and inversely proportional to the source amplitude v_0. The critical value of a below which an initially sinusoidal waveform will develop a vertical tangent is designated $a_{\mathrm{cr}}(\nu)$, such that the critical source amplitude is given by

$$\frac{v_{\mathrm{cr}}}{c_0} = \left[\frac{\alpha(\omega) c_0}{\omega \beta a_{\mathrm{cr}}}\right]^{1/2}. \tag{D.15}$$

The value of a_{cr} may be determined analytically for $\nu = 0$, in which case one obtains $a = A_0$ and Eq. (D.5) has an implicit solution,

$$V = e^{-aX} \sin\left(\theta + \frac{e^{2aX} - 1}{2a} V^2\right), \qquad \nu = 0, \tag{D.16}$$

which develops a vertical tangent at

$$X_{\mathrm{vt}} = -\frac{\ln(1 - 2a)}{2a}. \tag{D.17}$$

From Eq. (D.17) it follows that $a_{\mathrm{cr}}(0) = 1/2$. Waveform overturning is prohibited for $\nu > 1$, so it is concluded that $a_{\mathrm{cr}}(1) = 0$. Values of $a_{\mathrm{cr}}(\nu)$ for $0 < \nu < 1$ are determined by numerical solution of Eq. (4.3) with $f(\psi)$ given by Eq. (D.12). The fractional derivative in Eq. (D.12) is evaluated using the left-sided Caputo definition [71].

The curve $a_{\mathrm{cr}}(\nu)$ is presented in Fig. D.1. Below the curve, the source amplitude is too high for power-law attenuation to balance nonlinearity and

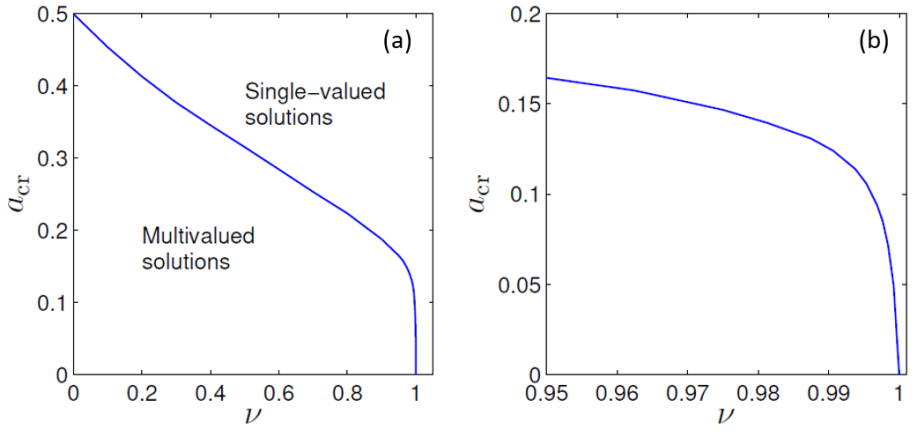

Figure D.1: (a) Critical value of the dimensionless power-law attenuation coefficient $a_{\rm cr}$ below which an initially sinusoidal shear waveform will overturn at a finite distance from the source. (b) Expanded view for values near $\nu = 1$.

a vertical tangent inevitably develops at a finite distance from the source. Above the curve, the initially sinusoidal waveform remains single-valued for all propagation distances. The critical value $a_{\rm cr}(\nu)$ decreases smoothly with increasing ν up until it decreases rapidly to zero as ν approaches unity, as displayed more clearly by the expanded view in Fig. D.1(b). The curve may be approximated in the region $0 \leq \nu \lesssim 0.95$ to within 5% by $a_{\rm cr}(\nu) \simeq 1/2 - 0.40\nu + 0.05\nu^2$.

Values of the shock formation distance $X_{\rm vt} = x_{\rm vt}/x_{\rm sh}$ are shown in Fig. D.2 as a function the attenuation coefficient a in Eq. (D.14) for several values of the exponent ν. The curve corresponding to $\nu = 0$ in Fig. D.2 is given by Eq. (D.17). For larger power-law exponents the shock formation distance increases more quickly with a due to the increased amount of attenuation experienced by nonlinearly generated harmonics. At the point denoted by black

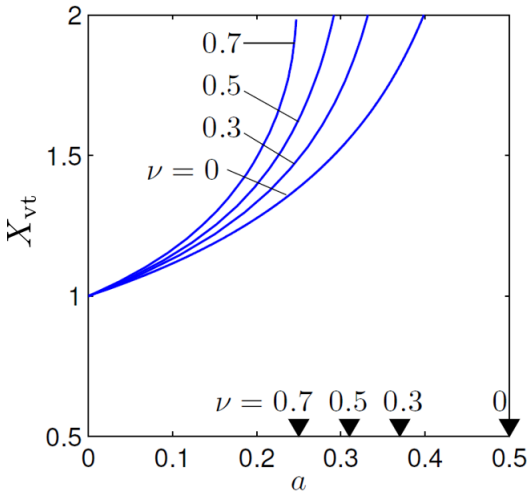

Figure D.2: Propagation distance $X_{\mathrm{vt}} = x_{\mathrm{vt}}/x_{\mathrm{sh}}$ at which an initially sinusoidal shear waveform develops a vertical tangent versus dimensionless attenuation coefficient a in a medium with power-law attenuation for several value of the exponent ν. Triangular markers on the horizontal axis indicate the value of a above which waveform overturning will not occur for the corresponding value of the power-law exponent ν.

triangles on the horizontal axis the shock formation distance is infinite. For values of a larger than that, the initially sinusoidal waveform never develops a vertical tangent, but instead remains single-valued for all distances from the source.

Bibliography

[1] A. P. Sarvazyan, O. V. Rudenko, S. D. Swanson, J. B. Fowlkes, and S. Y. Emelianov, "Shear wave elasticity imaging: a new ultrasonic technology of medical diagnosis," *Ultrasound in Med. and Biol.* **24**, 1419–1435 (1998).

[2] S. Catheline, R. Souchon, M. Rupin, J. Brum, A. H. Dihn, and J.-Y. Chapelon, "Tomography from diffuse waves: Passive shear wave imaging using low frame rate scanners," *Appl. Phys. Letters* **103**, 014101 (2013).

[3] J.-L. Gennisson, M. Rénier, S. Catheline, C. Barrière, J. Bercoff, M. Tanter, and M. Fink, "Acoustoelasticity in soft solids: Assessment of the nonlinear shear modulus with the acoustic radiation force," *J. Acoust. Soc. Am.* **122**, 3211–3219 (2007).

[4] M. Bernal, F. Chammings, M. Couade, J. Bercoff, M. Tanter, and J.-L. Gennisson, "*In vivo* quantification of the nonlinear shear modulus in breast lesions: Feasibility study," *IEEE Trans. Ultrasonics, Ferroelectrics, Freq. Contr.* **63**, 101–109 (2016).

[5] E. L. Carstensen and K. J. Parker, "Physical models of tissue in shear fields," *Ultrasound in Med. and Biol.* **40**, 655–674 (2014).

[6] D. T. Blackstock, "History of Nonlinear Acoustics: 1750s–1930s," in *Nonlinear Acoustics*, edited by M. F. Hamilton and D. T. Blackstock (Acous-

tical Society of America, Melville, 2008), pp. 1–18.

[7] Z. A. Gol'dberg, "Interaction of plane longitudinal and transverse elastic waves," *Sov. Phys. Acoust.* **6**, 306–310 (1961).

[8] I. P. Lee-Bapty and D. G. Crighton, "Nonlinear wave motion governed by the modified Burgers equation," *Phil. Trans. R. Soc. Lond. A* **323**, 173–209 (1987).

[9] K. Naugolnykh and L. Ostrovsky, *Nonlinear Wave Processes in Acoustics* (Cambridge University Press, New York, 1998), pp. 74–77.

[10] V. A. Gusev and Yu. N. Makov, "Spectral representation of solutions of cubically nonlinear evolution equation for the Riemann simple wave," *Acoust. Phys.* **56**, 626–631 (2010).

[11] S. Catheline, J.-L. Gennisson, M. Tanter, and M. Fink, "Observation of shock transverse waves in elastic media," *Phys. Rev. Lett.* **91**, 164301 (2003).

[12] M. F. Hamilton, Yu. A. Ilinskii, and E. A. Zabolotskaya, "Separation of compressibility and shear deformation in the elastic energy density (L)," *J. Acoust. Soc. Am.* **116**, 41–44 (2004).

[13] E. A. Zabolotskaya, M. F. Hamilton, Yu. A. Ilinskii, and G. D. Meegan, "Modeling of nonlinear shear waves in soft solids," *J. Acoust. Soc. Am.* **116**, 2807–2813 (2004).

[14] M. Rénier, J.-L. Gennisson, C. Barriére, D. Royer, and M. Fink, "Fourth-order shear elastic constant assessment in quasi-incompressible soft solids," *Appl. Phys. Lett.* **93**, 101912 (2008).

[15] E. A. Zabolotskaya, "Sound beams in a nonlinear isotropic solid," *Sov. Phys. Acoust.* **32**, 296–299 (1986).

[16] K. S. Spratt, Yu. A. Ilinskii, E. A. Zabolotskaya, and M. F. Hamilton, "Second-harmonic generation in shear wave beams with different polarizations," *Recent Developments in Nonlinear Acoustics,* Proceedings of the 20$^{\text{th}}$ International Symposium on Nonlinear Acoustics, AIP Conf. Proc. Vol. 32, 080007 (2015).

[17] M. S. Wochner, M. F. Hamilton, Yu. A. Ilinskii, and E. A. Zabolotskaya, "Cubic nonlinearity in shear wave beams with different polarizations," *J. Acoust. Soc. Am.* **123**, 2488–2495 (2008).

[18] Lord Rayleigh, "On the cooling of air by radiation and conduction, and on the propagation of sound," *Phil. Mag. Ser. 5* **47**, 308–314 (1899).

[19] A. Einstein, "Schallausbreitung in teilweise dissozierten Gasen," *Sitzber. preussischem Akad. Wiss. Berlin* **24**, 380–385 (1920). English translation: "Sound propagation in partially dissociated gases," in R. B. Lindsay, ed., *Physcal Acoustics,* Vol. 4 in Benchmark Papers in Acoustics series (Dowden, Hutchinson, and Ross, Stroudsberg, 1974), pp. 286–272.

[20] L. I. Mandel'shtam and M. A. Leontovich, "To the theory of absorption of sound in liquids," *Zh. Eksp. Teor. Fiz.* **7**, 438–453 (1937) (in Russian).

[21] L. D. Landau and E. M. Lifshitz, *Fluid Mechanics, 2nd edition* (Butterworth-Heinemann, Oxford, 1987), Sec. 81.

[22] A. L. Polykova, S. I. Soluyan, and R. V. Khokhlov, "Propagation of finite disturbances in a relaxing medium," *Sov. Phys. Acoust.* **8**, 78–82 (1962).

[23] S. I. Soluyan and R. V. Khokhlov, "Finite amplitude acoustic waves in a relaxing medium," *Sov. Phys. Acoust.* **8**, 170–175 (1962).

[24] A. D. Pierce and J. Kang, "Molecular relaxation effects on sonic boom waveforms," *Frontiers of Nonlinear Acoustics: Proceedings of the 12*$^{\text{th}}$ *International Symposium on Nonlinear Acoustics*, edited by M. F. Hamilton and D. T. Blackstock (Elsevier, London, 1990), pp. 165–170.

[25] D. T. Blackstock, *Fundamentals of Physical Acoustics* (Wiley, New York, 2000), Section 9-A and Appendix B.

[26] Y. C. Fung, *Biomechanics: Mechanical Properties of Living Tissues, 2nd ed.* (Springer-Verlag, New York, 1993), pp. 41–46.

[27] P. Asbach, D. Klatt, U. Hamhaber, J. Braun, R. Somasundaram, B. Hamm, and I. Sack, "Assessment of liver viscoelasticity using multifrequency MR elastography," *Magn. Reson. Med.* **60**, 373–379 (2008).

[28] S. S. Yengul, P. E. Barbone, and B. Madore, "Dispersion in tissue-mimicking gels measured with shear wave elastography and torsional vibration rheometry," *Ultrasound in Med. & Biol.* **45**, 586–604 (2019).

[29] V. G. Andreev, T. B. Krit, and O. A. Sapozhnikov, "Shear waves in a resonator with cubic nonlinearity," *Acoust. Phys.* **57**, 779–786 (2011).

[30] P. W. Hammerton and D. G. Crighton, "Overturning of nonlinear acoustic waves. Part 1: A general method," *J. Fluid Mech.* **252**, 585–599 (1993).

[31] P. W. Hammerton and D. G. Crighton, "Overturning of nonlinear acoustic waves. Part 2: Relaxing gas dynamics," *J. Fluid Mech.* **252**, 601–615 (1993).

[32] J. M. Cormack and M. F. Hamilton, "Plane nonlinear shear waves in relaxing media," *J. Acoust. Soc. Am.* **143**, 1035–1048 (2018).

[33] O. V. Rudenko and S. I. Soluyan, *Theoretical Foundations of Nonlinear Acoustics* (Plenum, New York, 1977), pp. 82–83.

[34] M. B. Vinogradova, O. V. Rudenko, and A. P. Sukhorukov, *Theory of Waves* (Nauka, Moscow, 1990, in Russian), pp. 86–90.

[35] R. M. Christensen, *Theory of Viscoelasticity, 2nd ed.* (Dover, New York, 1982), pp. 3–9.

[36] J. F. Kelly and R. J. McGough, "Fractal ladder models and power law wave equations," *J. Acoust. Soc. Am.* **126**, 2027–2081 (2009).

[37] S. Holm, S. P. Näsholm, F. Prieur, and R. Sinkus, "Deriving fractional acoustic wave equations from mechanical and thermal constitutive equations," *Computers and Mathematics with Applications* **66**, 621–629 (2013).

[38] S. P. Näsholm and S. Holm, "On a fractional Zener elastic wave equation," *Fractional Calc. and Appl. Analysis* **16**, 26–50 (2013).

[39] S. Holm and M. B. Holm, "Restrictions on wave equations for passive media," *J. Acoust. Soc. Am.* **142**, 1888–1896 (2017).

[40] S. P. Näsholm and S. Holm, "Linking multiple relaxation, power-law attenuation, and fractional wave equations," *J. Acoust. Soc. Am.* **130**, 3038–3045 (2011).

[41] R. O. Cleveland, M. F. Hamilton, and D. T. Blackstock, "Time-domain modeling of finite-amplitude sound in relaxing fluids," *J. Acoust. Soc. Am.* **99**, 3312–3318 (1996).

[42] D. G. Crighton, "The Taylor internal structure of weak shock waves," *J. Fluid Mech.* **173**, 625–642 (1986).

[43] A. D. Pierce, *Acoustics: An Introduction to Its Physical Principles and Applications* (Acoust. Soc. Am., Woodbury, 1989), p. 592.

[44] D. T. Blackstock, "Generalized Burgers equation for plane waves," *J. Acoust. Soc. Am.* **77**, 2050–2053 (1985).

[45] R. O. Cleveland, "Propagation of sonic booms through a real, stratified atmosphere," Ph.D. dissertation, The University of Texas at Austin, 1995, Chap. 3.

[46] G. B. Whitham, "On the propagation of weak shocks," *J. Fluid Mech.* **1**, 290–318 (1956).

[47] G. G. Stokes, "On a difficulty in the theory of sound," *Phil. Mag. Ser. 3* **223**, 349–356 (1848).

[48] G. I. Taylor, "The conditions necessary for discontinuous motion is gases," *Proc. R. Soc. London, Series A* **84**, 371–377 (1910).

[49] D. T. Blackstock, M. F. Hamilton, and A. D. Pierce, "Progressive Waves in Lossless and Lossy Fluids," in *Nonlinear Acoustics*, edited by M. F. Hamilton and D. T. Blackstock (Acoustical Society of America, Melville, 2008), pp. 81–117.

[50] S. Chatelin, A. Constantinesco, and R. Willinger, "Fifty years of brain tissue mechanical testing: From *in vitro* to *in vivo* investigations," *Biorheology* **47**, 255–276 (2010).

[51] M. W. Urban, J. Chen, and R. L. Ehman, "Comparison of shear velocity dispersion in viscoelastic phantoms measured by ultrasound-based shear wave elastography and magnetic resonance elastography," *2017 IEEE Int. Ultrasonics Symp. (IUS)* (2017).

[52] T. L. Szabo and J. Wu, "A model for longitudinal and shear wave propagation in viscoelastic media," *J. Acoust. Soc. Am.* **107**, 2437–2446 (2000).

[53] J. M. Cormack and M. F. Hamilton, "Overturning of nonlinear compressional and shear waves subject to power-law attenuation or relaxation," *Wave Motion* **85**, 18–33 (2019).

[54] D. G. Crighton and J. F. Scott, "Asymptotic solutions of model equations in nonlinear acoustics," *Phil. Trans. R. Soc. Lond. A* **292**, 101–134 (1979).

[55] S. S. Kashcheeva, O. A. Sapozhnikov, V. A. Khokhlova, M. A. Averkiou, and L. A. Crum, "Nonlinear distortion and attenuation of intense acoustic waves in lossy media obeying a frequency power law," *Acoust. Phys.* **46**, 211–219 (2000).

[56] G. S. Murthy and B. S. Ramakrishna, "Nonlinear character of resonance in stretched strings," *J. Acoust. Soc. Am.* **38**, 461–471 (1965).

[57] M. F. Hamilton, Yu. A. Ilinksii, and E. A. Zabolotskaya, "Linear and nonlinear frequency shifts in acoustical resonators with varying cross sections," *J. Acoust. Soc. Am.* **110**, 109–119 (2001).

[58] J. J. Stoker, *Nonlinear Vibrations* (Interscience, New York, 1950), pp. 81–109.

[59] A. H. Nayfeh and D. T. Mook, *Nonlinear Oscillations* (Wiley-VCH, Weinheim, 2004), pp. 179–183.

[60] W. Lauterborn, "Numerical investigation of nonlinear oscillations of gas bubbles in liquids," *J. Acoust. Soc. Am.* **59**, 283–293 (1976).

[61] E. M. Abdel-Rahman and A. H. Nayfeh, "Secondary resonances of electrically actuated resonant microsensors," *J. Micromech. Microeng.* **13**, 491–501 (2003).

[62] N. Yen, "Subharmonic generation in acoustic systems," Technical Memorandum NR–384–903, No. 65 (Office of Naval Research, Washington, D.C., 1950).

[63] J. H. Cantrell, L. Adler, and W. T. Yost, "Subharmonic generation, chaos, and subharmonic resurrection in an acoustically driven fluid-filled cavity," *Chaos* **25**, 023115 (2015).

[64] R. W. Boyd, *Nonlinear Optics, 3rd Ed.* (Elsevier, New York, 2008), pp. 105–108.

[65] F. Prieur and S. Holm, "Nonlinear acoustic wave equations with fractional loss operators," *J. Acoust. Soc. Am.* **130**, 1125–1132 (2011).

[66] A. I. Nachmann, J. F. Smith III, and R. C. Waag, "An equation for acoustic propagation in inhomogeneous media with relaxation losses," *J. Acoust. Soc. Am.* **83**, 1584–1595 (1990).

[67] S. Holm, *Waves with Power-Law Attenuation* (Springer, New York, 2019).

[68] F. Mainardi, *Fractional Calculus and Waves in Linear Viscoelasticity: An Introduction to Mathematical Models* (Imperial College Press, London, 2010).

[69] K. R. Waters, J. Mobley, and J. G. Miller, "Causality-imposed (Kramers-Kronig) relationships between attenuation and dispersion," *IEEE Trans. on Ultrasound, Ferroelectrics, and Freq. Control* **52**, 822–833 (2005).

[70] G. Jumarie, "On the derivative chain-rules in fractional calculus via fractional difference and their application to systems modelling," *Cent. Eur. J. Phys.* **11**, 617–633 (2013).

[71] E. C. de Oliveira and J. A. T. Machado, "A review of definitions for fractional derivatives and integrals," *Math. Problems in Eng.* Vol. **2014**, Article ID 238459, 6 pages (2014).

Vita

John Michael Napier Cormack was raised in Alfred, New York, where he became fascinated simultaneously by both music and physics. He received a B.S. in Mechanical Engineering in 2014 from the University of Rochester in Rochester, New York. In the summer of 2012 he worked as an intern at Hydroacoustics, Inc. in Henrietta, New York. Beginning in the summer of 2013 and continuing until the fall of 2014 he worked as an undergraduate research assistant with Prof. Sheryl Gracewski in the cochlear mechanics laboratory of Prof. Jong-Hoon Nam. Upon graduation from the University of Rochester, he moved to Austin, Texas at the end of the summer of 2014 to begin work towards a Ph.D. in Mechanical Engineering at The University of Texas at Austin, with a research emphasis on nonlinear acoustics under the supervision of Prof. Mark Hamilton.

Electronic mail: j.m.n.cormack@gmail.com